Design of Smart Shape-memory Polymers for Minimally Invasive Fetal Surgery of Sacrococcygeal Teratoma

（胎児外科治療用デバイスを目指した

スマート形状記憶ポリマーの設計）

AILIFEIRE FULATI

February 2023

Design of Smart Shape-memory Polymers for Minimally Invasive Fetal Surgery of Sacrococcygeal Teratoma

（胎児外科治療用デバイスを目指した
スマート形状記憶ポリマーの設計）

AILIFEIRE FULATI

Doctoral Program in Engineering Sciences
Subprogram in Materials Science and Engineering

Submitted to the
Degree Programs in Pure and Applied Sciences of the
Graduate School of Science and Technology,
in Partial Fulfillment of the Requirements
for the Degree of Doctor of Philosophy in Engineering

at the
University of Tsukuba

Contents

Chapter 1 General Introduction

1.1 Fetal Disease

Congenital anomalies originated in utero before the delivery of the fetus are referred to as fetal diseases. Despite all available therapeutic efforts, a great number of fetal diseases may result in permanent and irreversible organ damage before the delivery of fetus, resulting in fetal demise.[1]

Some of the common fetal diseases includes: congenital cystic adenomatoid malformation, fetal airway obstruction, twin-twin transfusion syndrome, fetal urinary tract obstruction, congenital diaphragmatic hernia, fetal myelomeningocele, and fetal sacrococcygeal teratoma.[2–4]

Most fetal diseases require close monitoring and medications under the supervision of fetal specialists until the delivery, followed by neonatal surgical intervention. However, fetuses with fatal conditions and those with irreversible life-long disabilities require prenatal intervention to allow for survival and appropriate quality of life.[5]

1.2 Fetal Surgery

Fetal surgery refers to the prenatal repair of fetal diseases on a fetus while still inside the uterus, commonly performed between 19 to 28 weeks of gestational age.[6] The goals of fetal surgery are to repair fetal diseases, to improve the surgical outcomes for the fetus, and ultimately improving the quality of life for the family.

The beginning of fetal surgery is believed to be pioneered by Sir William Liley in early 1960s, when he successfully performed the first fetal transfusion on a hydropic fetus without the presence of ultrasonography.[4,7] Since then, with the advancement of fetal imaging tools such as high-resolution ultrasound and magnetic resonance imaging that provided high accuracy for fetal diagnosis, fetal surgery has advanced significantly and became an acknowledged medical specialty.[1,5,8]

Open fetal surgery and fetoscopic surgery are two common representatives of prenatal surgical interventions.

1.2.1 Open fetal surgery

Open fetal surgery was established in the early 1980s by Dr. Harrison at the University of California San Francisco through a maternal laparotomy followed by hysterectomy for the directly exposure to access the fetus.[8,9] After which, the target fetal defect was be repaired. The uterus would be closed after the procedure for

maintaining the fetal development.[9] However, the hysterotomy performed in open fetal surgery could cause an area of weakness that greatly increases the risk of uterine rupture in the future gestational stages. Moreover, the surgical closure of the uterus remains to be under constant tension due to the growth of the fetus. Therefore, one of the key challenges remaining for open fetal surgery is the potential for maternal complications related to uterine scarring and risk of preterm labor due to the preterm premature rupture of membranes.[9–11]

Despite the aforementioned potential risks associated with open fetal surgery, it remains to be one of the gold standards to treat fetal diseases. On the other hand, the search for more minimally invasive procedures to decrease the potential maternal complications and to improve surgical outcomes has become the greatest challenge in the field of fetal surgery.

1.2.2 Fetoscopic surgery

Fetoscopic surgery is a minimally invasive surgical technique that is crucial in ensuring a safe and effective management of fetal development while minimizing the potential risks during the prenatal repair of fetal diseases.

Fetoscope is a specialized endoscopic instrument that was first developed in the 1970s as a tool for diagnosing congenital anomalies, especially to detect external malformations such as spina bifida. Later on, it was utilized for the visualization of the fetus and its surrounding environment in the surgical procedures.

Fetoscopic surgery is a minimally invasive procedure in which ultrasound is used for the real-time guidance into the uterus, providing enhanced surgical accuracy. Additionally, a fetoscope is used with a working channel that could allow for the insertion of small surgical instruments such as catheters, balloons and laser equipment.[7,12] Fetoscopic surgery is commonly used in the prenatal interventions for a variety of fetal diseases such as twin-twin transfusion syndrome, lower urinary tract obstruction, congenital high airway obstruction syndrome, fetal tracheal occlusion, and sacrococcygeal teratoma (SCT).[8,13]

Compared with aforementioned open fetal surgery, the minimally invasive feature of fetoscopic surgery could offers multiple advantages. For instance, fetoscopic surgery could provide far less damage to the maternal abdominal wall and uterus than that of open fetal surgery due to the minimally contained incision and the constrained surgical operations. Therefore, it could reduce a high possibilities of maternal complications,

which could greatly improve the surgical outcome. [5,7,11,14]

Nevertheless, despite such advantages of fetoscopic surgery, there are some crucial drawbacks including the high requirement for surgical expertise, the difficulties in operations owning to the limited surgical vision, and the limited choice for complex surgical operations owning to the small incision and operable surgical angles.

Therefore, advances in novel biomaterials and developments of smart surgical devices are in urgent demand to resolve such difficulties in this nascent surgical field.

1.3 Sacrococcygeal Teratoma

Among the fetal diseases, sacrococcygeal teratoma (SCT) is one of the most common solid tumors in neonates that has an incidence rate of approximately 1:40000 live births.[15–17] The estimated incidence rate of fetal SCT is approximately 1:10000 pregnancies. Thus, fetal SCT is considered one of the most common fetal tumors.[18,19] Fetal SCTs arise from the caudal end, usually located between the anus and coccyx. SCT is believed to be originated from totipotent stem cells from Hensen's node.[17,20,21] Highly vascularized fetal SCTs possess high prenatal morbidities and mortalities mostly owing to the secondary effects such as high-output cardiac failure, hydrops, placentomegaly, polyhydramnios or spontaneous hemorrhage. All of which may lead to preterm labor and fetal demise.[7,16,19,21,22]
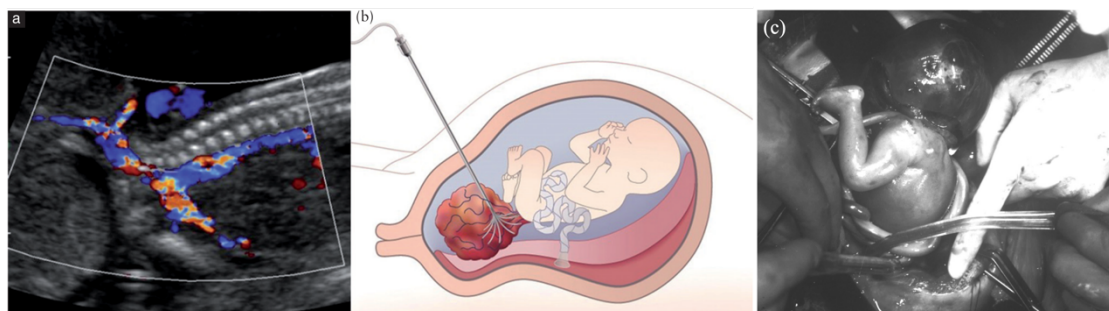
Figure 1.1 (a) Ultrasound image showing a perfusing vessel of a fetal SCT at 26 weeks' gestation. Image adapted from reference[23] with permission. © 2022 Wiley-VCH GmbH. (b) Schematic illustration of placement of the radiofrequency ablation instrument in a SCT case. Image adapted from reference[23] with permission. © 2022 Wiley-VCH GmbH. (c) Sacrococcygeal teratoma during an open fetal surgery. Image adapted from reference[5] with permission. © 2008 SAGE Publications.

In the aforementioned cases, prenatal intervention of the fetal SCTs and their

associated symptoms have been performed at highly specialized fetal centers. As shown in Figure 1.1, the prenatal intervention procedures include vascular occlusion to reduce the vascular supply to fetal SCT, in order to decrease the resulted morbidity and mortality and allow the fetal development to continue. Other approaches include open fetal surgery of fetal SCTs to debulk the tumor, and the fetoscopic laser ablation or radiofrequency ablation of the tumor. However, despite the stringent standards requiring high technical expertise and complex operating conditions, the resulted fetal demise and preterm births due to the regrowth and necrosis of SCTs, as well as bleeding are commonly reported.[17,22,24] Therefore, advancements in novel functional biomaterials capable of resolving these difficulties in the minimally invasive fetal surgeries of SCTs are of considerable significance.

1.4 Shape-memory Polymers

Shape-memory polymers (SMPs) are a representative of smart polymers, otherwise known as stimuli-responsive polymers. SMPs are capable of memorizing and recovering to their permanent original shapes after being fixing into a temporary deformed shape upon exposure to external stimuli, such as heat,[25,26], magnetic field,[27,28] or light.[29,30] Such unique shape-memory properties could induce a variety of motions, from simple shape-memory induced motions like bending, stretching, twisting;[31,32] to complicated combinational motions like shape-memory induced grasping and lifting of a variety of objects.[17,33]

1.4.1 Mechanism for semi-crystalline shape-memory polymers

Poly(ε-caprolactone) (PCL) is a melting temperature (Tm) dependent type of semicrystalline SMP whose Tm is commonly in the vicinity of 60°C.[25]

The shape-memory mechanism for PCL-based semicrystalline SMPs is depicted in Figure 1.2. The crystal regions of semicrystalline SMP will melt upon heating above its Tm. In turn, resulting in an elevated chain mobility. At which point, the SMP can be temporarily deformed upon the application of external stress. Such deformed secondary shape can then be fixed by recrystallizing below its crystallization temperature (Tc) due to the weakening of the chain mobility at low temperature. This process allows the entropic energy of fixed SMP to be stored in the form of elastic potential energy. Then, upon reheating, the stored energy can be released owning to the reactivation of the chain mobility which drives it back to its most energetically stable original shape with highest

entropic state, resulting in the induction of an instantaneous shape-recovery induced contraction force (shape recovery force).[17,34–36]
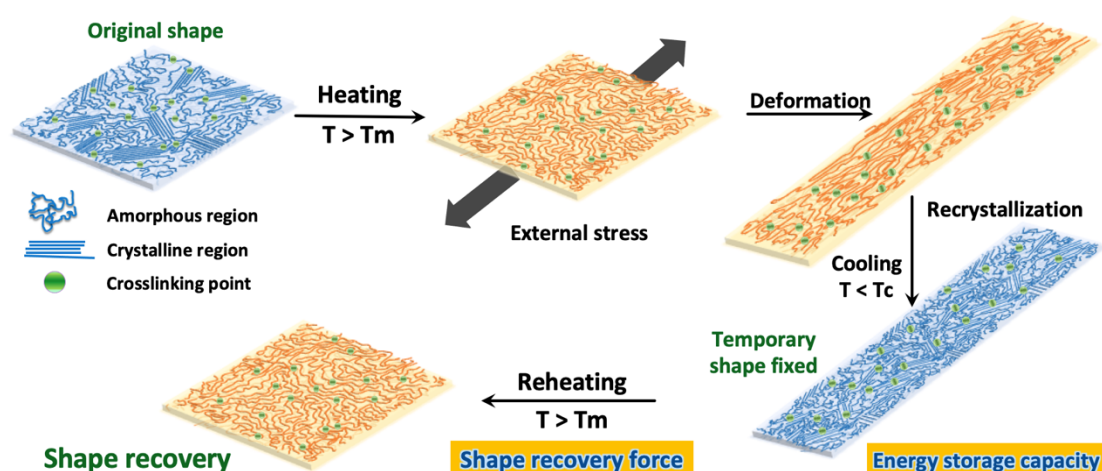
Figure 1.2 Schematic illustration of the brief mechanism of semicrystalline SMPs.

1.4.2 Shape-memory induced motions

Versatile shape-memory induced motions such as bending, twisting and stretching have been intensively studied in the past two decades and demonstrated by multiple different SMPs.[31,32] Besides the reported shape-memory induced simple motions, various complex shape-memory induced dynamic motions have also been reported lately. For instance, a soft multiple-shape-memory polymer-metal composite actuator reported by Shen *et al.*[37] demonstrating complex shape-memory motions such as bending, twisting, and oscillation via electrical and thermal dual stimuli. Furthermore, Zhang *et al.*[33] developed a fast-response, stiffness-tunable actuator with an SMP layer endowing them the function of grabbing and lifting various objects with a wide range of weights, from a rubber ball to a dumbbell. SMPs hold great potential in a variety of applications, including soft actuators, robotics, and biomedical devices owning to such charismatic combinations of shape-memory motions.[17]

Various distinct shape-memory motions have been reported to be utilized as biomedical devices for diverse purposes. For instance, Maitland *et al.*[38] reported an SMP-based intravascular device that was deployed in the blood vessel and twisted into helical shape for the treatment of ischemic stroke. Moreover, similar shape-memory twisting motions have been used for both the embolization of aneurysms and for the retrieval of thrombus as an intravascular thrombectomy device.[39,40] Different than that of the twisting motion above, Baer *et al.*[41] reported an SMP-based expandable vascular stent for the treatment of arterial stenosis. Besides, such controllably expandable SMP

balloon was applied in bone tumor treatment as a bone cement carrier after bone tumor removal.[42] Despite aforementioned appealing shape-memory motions that have probed the feasibility of SMPs in multiple biomedical applications, these SMPs are generally limited by the insufficient physical properties such as mechanical strength, deformability, and maneuverability. Furthermore, correlations between the efficacy of these shape-memory motions and their intrinsic physical and shape-memory properties were yet to be fully understood, which significantly hindered their applicability as biomedical devices.[17]

1.4.3 Applications of shape-memory polymers

SMPs studies have attracted tremendous interest among polymer researchers. Multiple reports have indicated promising future perspectives for SMPs. Especially, with an enhanced understanding of the actuation mechanisms, recent advances have endowed SMPs with versatile potential applications.

Some representatives are demonstrated in Figure 1.3. Sekitani et al.[43] reported a flexible electronic circuits, when fabricated on an SMP film, the circuits are thermally actuated to adapt a helical structure while maintaining the function. Moreover, Liu et al.[44] reported a flexible triboelectric nanogenerator based smart device whose thermally triggered shape transformation could provide adaptive skin compatibility while effectively harvesting mechanical energy as a self-powered mechanosensation sensor and a transformable energy harvester.

More recently, a SMP-based self-deployable system as deployable solar-panel array was reported by Chen et al.[45] They achieved self-deployment features by embedding an SMP within their unit cells, functioning as the rotational hub and as the a substrate, which are expected to be applied into aerospace engineering field. Besides, SMP-based smart textile are reported as well. Roach et al.[46] reported a reversibly actuatable liquid crystal elastomer based fibers. They are fabricated by sewing and loom weaving which gave them breathable pores that could be potentially used as smart clothing. Same year, an SMP-based soft robotics was reported by Zhang et al.[33] that are capable of grasping motion and lift various objects with a variety of shapes weighting from a minimal of less than 10 g to as heavy as 1.5 kg.

In addition to the aforementioned fields, SMPs are widely reported to be applicable in biomedical fields. As early as 2002, Lendlein et al.[47] reported a thermoplastic SMP with self-knotting function when thermally actuated which could potentially be applicable as biodegradable surgical suture for wound closure. Since then, a wide range

of biomedical applications have emerged for SMP-based devices. For instance, a balloon shaped SMP device was reported by Ouchi *et al.*[42] that contains magnetic nanoparticles and anticancer drugs for a synergistic thermo/chemo therapy for osteosarcoma. Moreover, Aoyama *et al.*[48] reported an SMP-based thermoset mask for reusable, shape-adaptive mask for radiotherapy patients. Similarly, Lin *et al.*[49] reported a 4D printed SMP-based occlusion device for atrial septic defect patients. Magnetic nanoparticles are incorporated into the SMP substrate with different device arms for a remotely controllable deployment of the occluder.
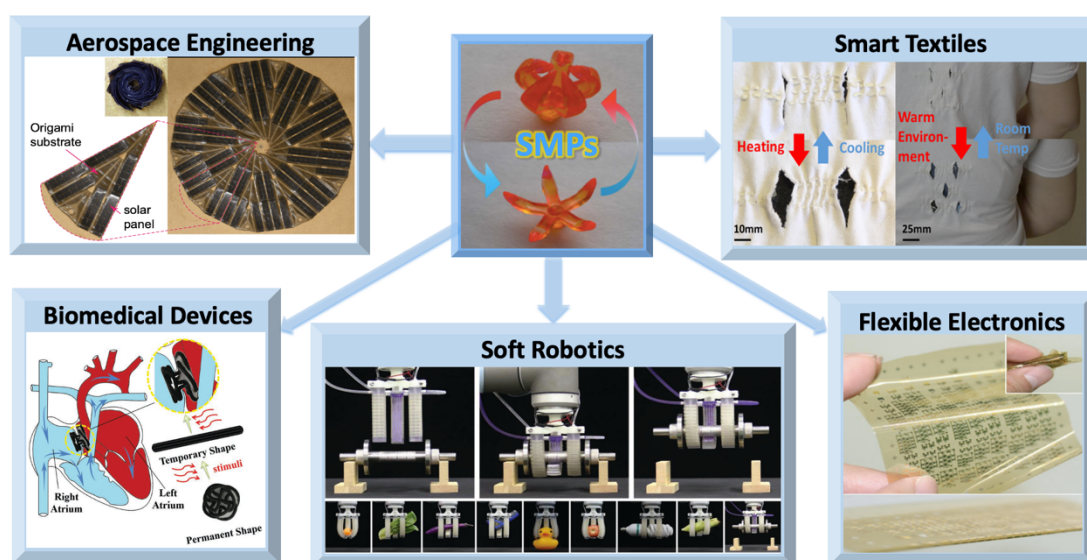
Figure 1.3 Representative potential applications of SMPs reported in different fields such as aerospace engineering, image adapted from reference[45] with permission; biomedical devices, image adapted from reference[49] with permission; soft robotics, image adapted from reference[33] with permission; smart textiles, image adapted from reference[46] with permission; and flexible electronics, image adapted from reference[43] with permission; The 3D printed SMPs gripper image adapted from reference[50] with permission.

1.4.4 Challenges of shape-memory polymers

While the appealing shape-memory motions have explored the feasibility of SMPs in versatile applications in multiple reports, the practical usage of them in reality are still limited to few. It is mostly because despite the charismatic shape-memory behavior, SMPs generally suffer from limitations such as trade-off relationships between inadequate mechanical strength and deformability, inadequate deformability and shape-memory properties, or inadequate shape-memory properties with an increase of

mechanical strength. The general lack of the precise maneuverability caused by such trade-off dilemmas of SMP-based materials have greatly hindered their potentials in practical applications.

1.5 Objectives and Outline

Therefore, the first objective of this PhD research is to conquer existing dilemmas between physical properties of SMPs and to achieve simultaneous realization of strong, tough, ultra-stretchable SMPs with excellent shape-memory properties and strong shape recovery force. Moreover, the second objective of this PhD research is to design a shape-memory polymeric string that can successfully occlude the feeding vessel to fetal SCT via minimally invasive fetoscopic surgery using shape recovery force, ultimately to help save the SCT-carrying fetus safely to term.
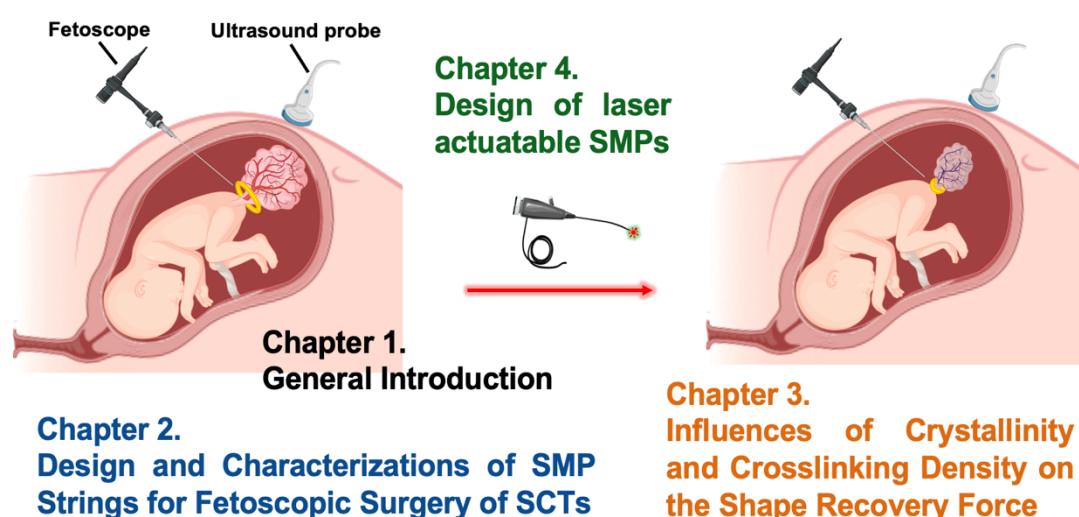
Figure 1.4 Schematic illustration of the design concepts of shape-memory polymers for minimally invasive fetal surgery of sacrococcygeal teratoma and the brief contents of this doctoral dissertation.

In this doctoral dissertation, I proposed a paradigm to design and fabricate a type of smart shape-memory polymer that can provide a novel shape recovery force for the occlusion of feeding vessel in fetoscopic surgeries. The design concepts are presented in Figure 1.4. Required by the minimally invasive fetal surgery of SCT, the SMP string should simultaneously realize high deformability, high strength, appropriate shape transition temperature and speed, as well as high shape recovery force for the occlusion of the feeding vessels to SCTs. In addition, parameters influencing such shape recovery

force was investigated for a better design capability. Furthermore, in-vitro simulation models are designed to evaluate the efficacy for the shape-memory contraction effect and the applicability of such SMP device. Lastly, laser equipment which are commonly used in existing fetoscopic surgeries are considered as a convenient and precise tool for the induction of shape memory motions. Therefore, I researched into laser actuatable SMPs with high shape recovery force for the possible application in minimally invasive fetal surgery of SCTs.

The layout of this doctoral dissertation is described below:

Chapter 1 describes the general introduction and background regarding this PhD research. This chapter provides a literature review regarding fetal diseases, fetal surgeries, sacrococcygeal teratoma and shape-memory polymers as well as their applications and challenges in this research field. The last section describes the motivation, objective, and the outline of this doctoral dissertation.

Chapter 2 describes the design principles and the design of shape-memory polymers with excellent mechanical and shape-memory properties. This chapter provides the design concept, material design, synthesis approach, SMP film fabrication along with relevant polymer, physical and shape-memory characterizations. In addition, this chapter presents the design of in-vitro simulation models for the evaluation of contraction effect of SMP strings in minimally invasive fetal surgery of SCTs. This chapter is adapted from reference[17] with permission, authored by myself doi:10.1002/adhm.202200050. © 2022 Wiley-VCH GmbH

Chapter 3 describes the investigation of the influences of crystallinity and crosslinking density on the shape recovery force in PCL-based semicrystalline shape-memory polymers using shape-memory polymer blend systems. This chapter is adapted from reference[36], doi:10.3390/polym14214740, authored by myself, published by MDPI, 2022.

Chapter 4 describes a simple design of laser actuatable shape-memory polymer composites with high shape recovery force using the SMP designed and fabricated in chapter 2. Results in this chapter belong to a manuscript in submission, authored by myself. Copyright will belong to the publisher upon acceptance.

Finally, a summary of this dissertation is outlined in Chapter 5, highlighting the key results and achievements of this research along with a future perspective of this research.

Reference

[1] J. D. Vrecenak, A. W. Flake, Pediatr. Surg. Int. 2013, 29, 407.

[2] K. D. Wenstrom, S. R. Carr, Obstet. Gynecol. 2014, 124, 817.

[3] N. J. Reedy, K. l. Ford, R. Depp, JOGN Nurs. 1984, 13, 291.

[4] D. L. Farmer, Pediatr. Radiol. 1998, 28, 409.

[5] S. M. Kunisaki, R. W. Jennings, J. Intensive Care Med. 2008, 23, 33.

[6] H. Yamashita, T. Kakimoto, W. Yuan, T. Chib, In Perinatal Mortality, InTech, 2012, p.13.

[7] J. A. Deprest, A. W. Flake, E. Gratacos, Y. Ville, K. Hecher, K. Nicolaides, M. P. Johnson, F. I. Luks, N. S. Adzick, M. R. Harrison, Prenat. Diagn. 2010, 30, 653.

[8] L. L. Evans, M. R. Harrison, Transl. Pediatr. 2021, 10, 1401.

[9] M. Upadhyaya, A. Lander, Surg. 2013, 31, 114.

[10] D. Fan, S. Wu, R. Wang, Y. Huang, Y. Fu, W. Ai, M. Zeng, X. Guo, Z. Liu, Med., 2017, 96, 0.

[11] A. Sacco, L. Van der Veeken, E. Bagshaw, C. Ferguson, T. Van Mieghem, A. L. David, J. Deprest, Prenat. Diagn. 2019, 39, 251.

[12] V. Beck, A. Pexsters, L. Gucciardo, T. van Mieghem, I. Sandaite, S. Rusconi, P. DeKoninck, K. Srisupundit, K. O. Kagan, J. Deprest, Gynecol. Surg. 2010, 7, 113.

[13] W. S. S. Elbanna, I. A. Oun, E. M. A. Ellatif, W. R. Hablas, W. I. El Shaikh, Y. A. Wafa, Open J. Obstet. Gynecol. 2018, 08, 946.

[14] R. M. Antiel, C. A. Collura, A. W. Flake, M. P. Johnson, N. E. Rintoul, J. D. Lantos, F. A. Curlin, J. C. Tilburt, S. D. Brown, C. Feudtner, J. Perinatol. 2017, 37, 994.

[15] R. Swamy, N. Embleton, J. Hale, Prenat. Diagn. 2008, 28, 1048.

[16] J. L. Roybal, J. S. Moldenhauer, N. Khalek, M. W. Bebbington, M. P. Johnson, H. L. Hedrick, N. S. Adzick, A. W. Flake, J. Pediatr. Surg. 2011, 46, 1325.

[17] A. Fulati, K. Uto, M. Iwanaga, M. Watanabe, M. Ebara, Adv. Healthc. Mater. 2022, 11, 2200050.

[18] M. Hambraeus, E. Arnbjörnsson, A. Börjesson, K. Salvesen, L. Hagander, J. Pediatr. Surg. 2016, 51, 481.

[19] S. Hirose, D. L. Farmer, Clin. Perinatol. 2003, 30, 493.

[20] P. Puri, Paediatric Surgery, Second edition (Eds.: Burge, D.; Griffiths, M.; Steinbrecher, H.; Wheeler, R.), CRC Press, 2005.

[21] J. H. Phi, J. Korean Neurosurg. Soc. 2021, 64, 406.

[22] N. Sananes, P. Javadian, I. Schwach Werneck Britto, N. Meyer, A. Koch, A. Gaudineau, R. Favre, R. Ruano, Ultrasound Obstet. Gynecol. 2016, 47, 712.

[23] C. Simonini, B. Strizek, C. Berg, U. Gembruch, A. Mueller, A. Heydweiller, A. Geipel, Prenat. Diagn. 2021, 41, 301.

[24] T. Van Mieghem, A. Al-Ibrahim, J. Deprest, L. Lewi, J. C. Langer, D. Baud, K. O'Brien, R. Beecroft, R. Chaturvedi, E. Jaeggi, J. Fish, G. Ryan, Ultrasound Obstet. Gynecol. 2014, 43, 611.

[25] K. Uto, K. Yamamoto, S. Hirase, T. Aoyagi, J. Control. Release 2006, 110, 408.

[26] M. Ebara, K. Uto, N. Idota, J. M. Hoffman, T. Aoyagi, Adv. Mater. 2012, 24, 273.

[27] K. Uto, M. Ebara, Appl. Sci. 2017, 7, 1203.

[28] R. Mohr, K. Kratz, T. Weigel, M. Lucka-Gabor, M. Moneke, A. Lendlein, Proc. Natl. Acad. Sci. 2006, 103, 3540.

[29] S. Ishii, K. Uto, E. Niiyama, M. Ebara, T. Nagao, ACS Appl. Mater. Interfaces 2016, 8, 5634.

[30] Q. Shou, K. Uto, M. Iwanaga, M. Ebara, T. Aoyagi, Polym. J. 2014, 46, 492.

[31] H. Jiang, S. Kelch, A. Lendlein, Adv. Mater. 2006, 18, 1471.

[32] Y. Li, D. Wang, J. Wen, J. Liu, D. Zhang, J. Li, H. Chu, Adv. Funct. Mater. 2021, 31, 2011259.

[33] Y. Zhang, N. Zhang, H. Hingorani, N. Ding, D. Wang, C. Yuan, B. Zhang, G. Gu, Q. Ge, Adv. Funct. Mater. 2019, 29, 1806698.

[34] Q. Zhao, H. J. Qi, T. Xie, Prog. Polym. Sci. 2015, 49–50, 79.

[35] Y. Xia, Y. He, F. Zhang, Y. Liu, J. Leng, Adv. Mater. 2021, 33, 2000713.

[36] A. Fulati, K. Uto, M. Ebara, Polymers, 2022, 14, 4740.

[37] Q. Shen, S. Trabia, T. Stalbaum, V. Palmre, K. Kim, I.-K. Oh, Sci. Rep. 2016, 6, 24462.

[38] D. J. Maitland, M. F. Metzger, D. Schumann, A. Lee, T. S. Wilson, Lasers Surg. Med. 2002, 30, 1.

[39] W. Small IV, T. S. Wilson, W. J. Benett, J. M. Loge, D. J. Maitland, Opt. Express 2005, 13, 8204.

[40] B. Liu, Z. Xu, H. Gao, C. Fan, G. Ma, D. Zhang, M. Xiao, B. Zhang, Y. Yang, C. Cui, T. Wu, X. Feng, W. Liu, Adv. Funct. Mater. 2020, 30, 1910197.

[41] G. M. Baer, W. Small, T. S. Wilson, W. J. Benett, D. L. Matthews, J. Hartman, D. J. Maitland, Biomed. Eng. Online 2007, 6, 43.

[42] S. Ouchi, E. Niiyama, K. Sugo, K. Uto, S. Takenaka, A. Kikuchi, M. Ebara, Biomater. Sci. 2021, 9, 6957.

[43] T. Sekitani, U. Zschieschang, H. Klauk, T. Someya, Nat. Mater. 2010, 9, 1015.

[44] R. Liu, X. Kuang, J. Deng, Y.-C. Wang, A. C. Wang, W. Ding, Y.-C. Lai, J. Chen, P. Wang, Z. Lin, H. J. Qi, B. Sun, Z. L. Wang, Adv. Mater. 2018, 30, 1705195.

[45] T. Chen, O. R. Bilal, R. Lang, C. Daraio, K. Shea, Phys. Rev. Appl. 2019, 11, 064069.

[46] D. J. Roach, C. Yuan, X. Kuang, V. C.-F. Li, P. Blake, M. L. Romero, I. Hammel, K. Yu, H. J. Qi, ACS Appl. Mater. Interfaces 2019, 11, 19514.

[47] A. Lendlein, R. Langer, Science (80-.). 2002, 296, 1673.

[48] T. Aoyama, K. Uto, H. Shimizu, M. Ebara, T. Kitagawa, H. Tachibana, K. Suzuki, T. Kodaira, Sci. Rep. 2021, 11, 20409.

[49] C. Lin, J. Lv, Y. Li, F. Zhang, J. Li, Y. Liu, L. Liu, J. Leng, Adv. Funct. Mater. 2019, 29, 1906569.

[50] Q. Ge, A. H. Sakhaei, H. Lee, C. K. Dunn, N. X. Fang, M. L. Dunn, Sci. Rep. 2016, 6, 31110.

Chapter 2 Design and Characterizations of Shape-memory Polymers for Fetoscopic Surgery of Sacrococcygeal Teratoma
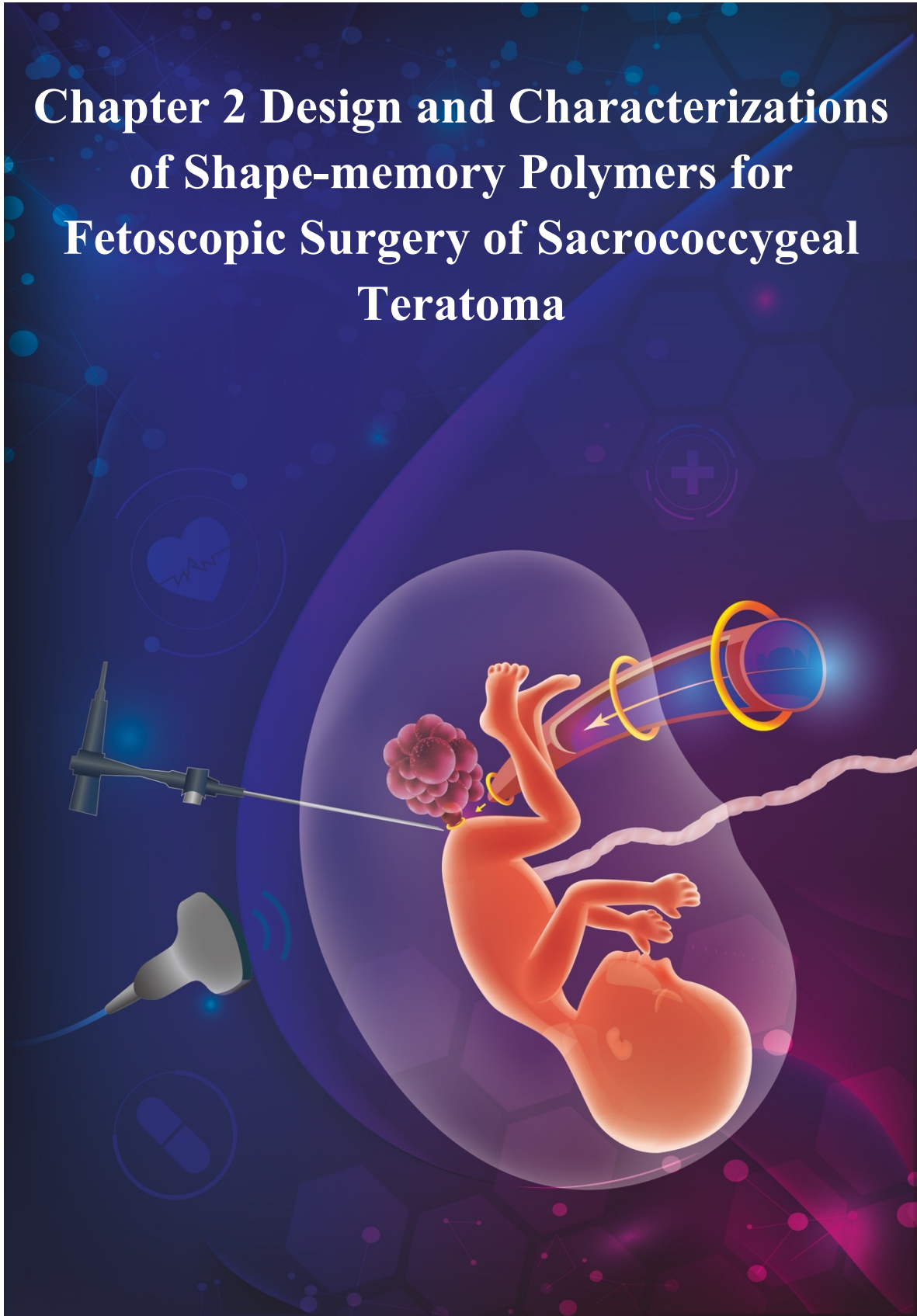
2.1 Abstract

Owning to the charismatic shape-memory characteristics, SMPs have shown great potentials in various biomedical applications. Nevertheless, dilemmas between their physical properties such as high strength, high stretchability, and high toughness; as well as shape-memory properties such as high shape fixity ratio (R_f) and shape recovery ratio (R_r) remained to be a great challenge that need to be conquered which greatly hindered the further application of SMP-based functional materials.

Herein, in this chapter, I present a novel design of a smart shape-memory polymeric string (SMP string) using a facile approach solely with tetra-branched poly(-caprolactone) (4bPCL). Such SMP string simultaneously possess excellent physical properties including high stretchability (up to approximately 1570%), high strength (up to approximately 345 MPa), and high toughness (up to approximately 237.9 MJ m³), while maintaining excellent shape-memory properties including high R_r (averagely above 99.5%) and high R_r (averagely above 99.1%).

Moreover, the aforementioned SMP strings possess highly customizable shape-recovery induced contraction force (shape recovery force) (up to approximately 7.97 N) manipulatable by tuning their energy storage capacities which correlate with the string thicknesses and stretched strains. Furthermore, such SMP string displays a manipulatable shape-memory response time and demonstrates excellent shape recovery-induced contraction effect against the in-vitro teratoma mimicking simulation models.

Therefore, the smart SMP string described in this chapter is envisioned to be applicable in the minimally invasive fetal surgery of SCTs as a smart occluder of the feeding vessel to fetal SCTs that can be used to restrict the blood inflow, in turn, save the fetus.

This chapter is adapted from reference[17] with permission, authored by myself doi:10.1002/adhm.202200050. © 2022 Wiley-VCH GmbH.

2.2 Introduction

SMPs, after temporarily deformed into a secondary shape, are capable of restoring their original shapes when exposed to external stimuli.[51,52] The common SMPs can be categorized by their trigger, such as thermos-responsive SMPs,[25,26] photo-responsive

SMPs,[29,30,53], electric-responsive SMPs.[54,55] Aside from simple trigger, dual or triple triggers of SMPs have drawn extensive interest of researcher as well.[56,57]

Simple motions have been achieved by various SMPs in the past two decades. These simple shape recovery-induced motions include stretching, bending, twisting and etc. have been frequently reported in multiple reports.[31,32] Recent research interest have shifted to complex combinations of shape recovery induced motions for advanced applications such as soft robotics, smart actuators and artificial muscles.

For instance, an SMP-based smart actuator with instant response time, tunable stiffness that demonstrates flexible shape recovery-induced grasping and lifting has been reported by Zhang *et al*.[33] Notably, such complex grasping and lifting motions could be applied to multiple objects from light-weighted ones such as rubber balls, to heavy-weighted objects such as heavy dumbbell. Moreover, besides pure SMP-based materials, SMP-based composites have shown great potential in complex shape recovery-induced motions. A multiple-shape SMP-metal composite-based smart actuator was reported by Shen *et al*.[37] that demonstrates complicated motions such as twisting and oscillation. Such complex motions are achieved by dual triggers including electricity and heat.

In addition to the aforementioned applications, SMP-based materials have been reported in various biomedical fields for different purposes as well. Maitland *et al*.[38] are among the pioneers who have dedicated their efforts into the applications of SMPs as biomedical devices. They reported the use of a laser actuatable SMP as an intravascular device that can be deployed at a temporarily straightened shape in the blood vessels. After which it can be actuated by laser irradiation and be twisted to helical shape for the treatment of ischemic stroke. Similar usage of SMP-based biomedical devices are reported for the retrieval of thrombosis as intravascular thrombectomy devices and for the embolic treatment of aneurysms respectively.[39,40] Besides, various other biomedical applications are reported as well using SMP-based smart devices, such as shape recovery-induced expansion-based vascular stent for treating arterial stenosis,[41] and shape recovery-induced expansion-based smart balloons as bone cement injection carriers after bone tumor removal in osteosarcoma treatment.[42]

Although the appealing SMP-based motions have explored the feasibility of SMPs in versatile applications, they are generally limited by inadequate intrinsic physical properties such as mechanical strength and deformability and shape-memory properties that greatly hindered their practical applications.

On the other hand, SCT, one of the most common fetal tumors [15,16] has a high mortality rate due to multiple complications caused by their large and highly

vascularized features. Among the commonly reported complications, high-output cardiac failure, a symptom mainly caused by vascular-steal phenomenon, is considered highly dangerous which may lead to polyhydramnios, placentomegaly and preterm labor, eventually fetal demise.[7,16,21,58] Therefore, for fetal SCTs, prenatal interventions by fetal surgeries may greatly increase the survival rate of the fetus.

There are a few approaches of prenatal interventions for SCTs, such as open fetal surgery for the reduction of vascular supply to SCT via vascular occlusion. This represents the removal of low-resistance vascular beds of SCTs to continue the fetal development until the delivery of the fetus. In addition, fetoscopic surgery of laser or radiofrequency ablation for fetal SCT patients with early signs of hydrops.

Regardless of the efforts described above, the reported survival rate from both open fetal surgeries and fetoscopic surgeries are approximately 30-50%,[59–61] which make it debatable whether prenatal interventions are indeed beneficial or not, given the maternal risk involved. Among those approaches, fetoscopic surgery was considered one of the most efficient ways to reduce the blood supply to SCTs. However, the imposition of stringent standards revolving high technical expertise and limited operating conditions have resulted in preterm births and fetal demises owing to the regrowth, necrosis, and bleeding of SCTs.[22,24] Therefore, novel functional biomaterials that could resolve such difficulties in this nascent surgical field are of great significance.

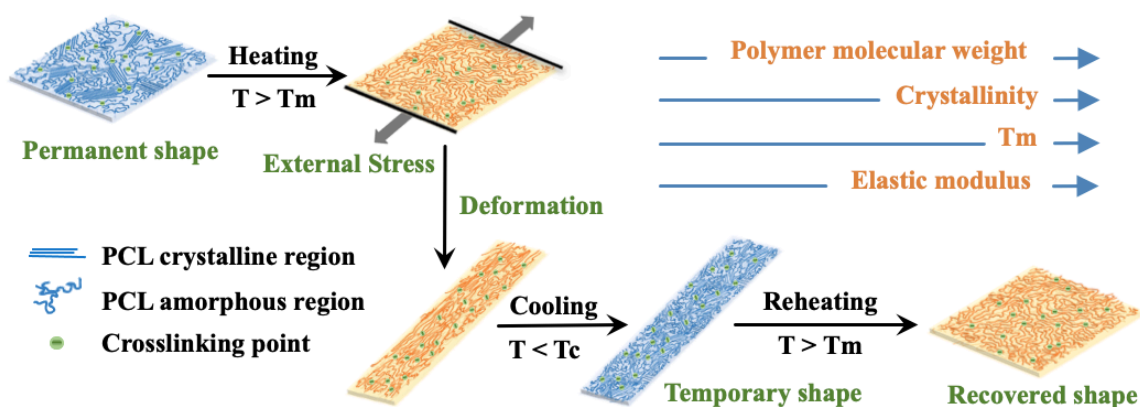**Figure 2.1** Schematic illustrations of the shape-memory mechanism of PCL-based semicrystalline SMPs.

The material used in this chapter is PCL, one of the most intensively studied SMPs in recent years. PCL is a synthetic polyester with excellent non-toxicity and biocompatibility.[62,63] The schematic illustrations of shape-memory mechanism of semicrystalline PCL is shown in Figure 2.1. At ambient temperature, crosslinked shape-

PCL SMP film is semicrystalline with stiff and opaque morphologies. Upon heating above its Tm, the crystal regions of crosslinked PCL film melts, hence, the SMP film becomes soft, transparent, and elastic. At this amorphous state, PCL film can easily be deformed by the addition of external stress to a secondary shape. Such temporary shape can then be fixed upon cooling below its Tc, where the amorphous state recrystallizes back into semicrystalline structure. The shape recovery happens when the aforementioned fixed temporary shape is heated above Tm again, where this temporary shape recovers to the permanent shape due to the entropic change.[17,64]

Compared to linear PCLs, branched PCLs were reported to possess less entanglement and are capable of introducing more functional end groups to provide highly crosslinked polymer networks and diverse functionalities.[65] Thus, as sketched in Scheme 2.1, in this chapter, 4bPCLs were synthesized through ring opening polymerization of ε-caprolactone (CL) and tetra-branched initiator pentaerythritol, for the highly crosslinked polymer networks and enhanced mechanical properties. Then, the hydroxyl end groups were substituted by acryloyl end groups with the addition of acryloyl chloride, forming 4bPCL macromonomer (4bPCL macro). Furthermore, a stably crosslinked SMP film was fabricated with the addition of benzoyl peroxide (BPO) through thermal initiation at 80 ℃.
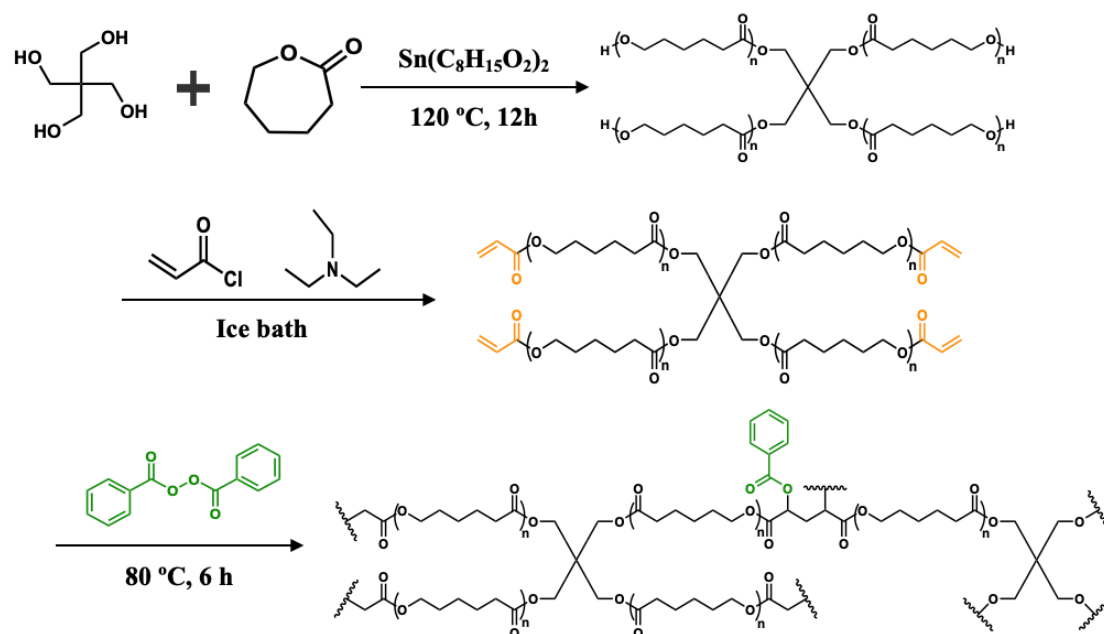
Scheme 2.1 Synthesis scheme of 4bPCLs, the end group substitution of 4bPCLs and further crosslinking reactions.

In addition, in this chapter, the aforementioned synthesis and fabrication of smart SMP strings are envisioned to provide sufficient shape recovery-induced contraction to restrict the blood inflow to SCTs in minimally invasive fetal surgeries. The schematic illustration is presented in Figure 2.2.
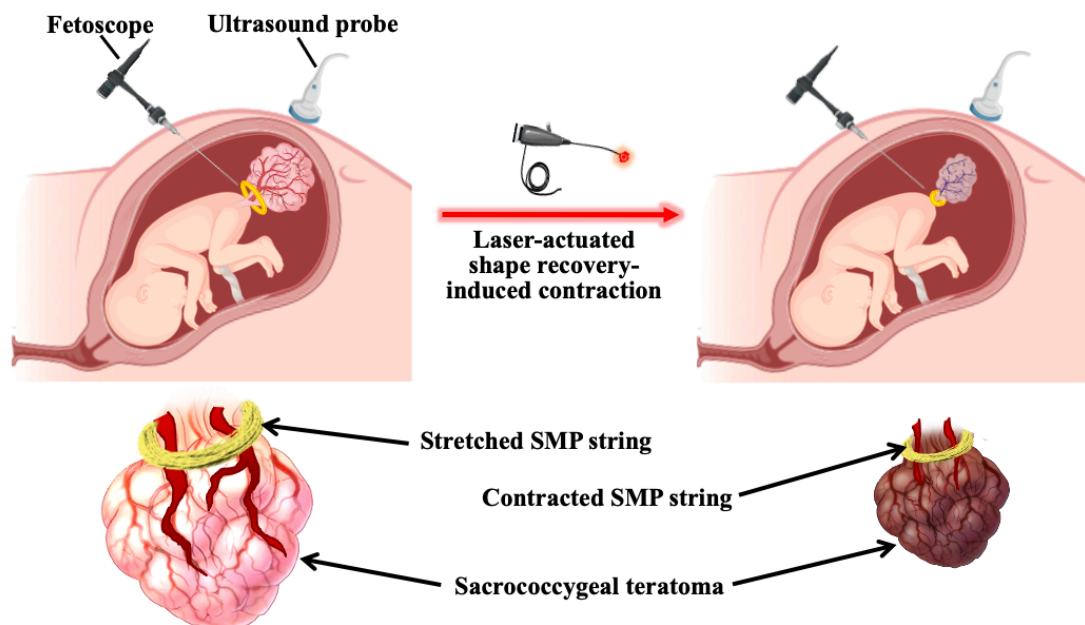
Figure 2.2 Schematic illustrations of the design concept of SMP strings used in minimally invasive fetoscopic surgery of SCT.

As illustrated above, because of the excellent flexibility and high stretchability of the SMP strings, they should be inserted through the fetal trocar during fetoscopic surgery and be trapped onto the SCTs in utero. When actuated by laser irradiation, which is the presumed source for the heat induction in this design, the stretched SMP string can be actuated to recover its original short length, thus, contracting the feeding vessels of SCT. In turn, restrict the blood inflow to SCT and arrest tumor growth until the fetus is safely delivered. In order for such design of smart SMP strings to meet all requirement for fetal surgery of SCTs, correlations between the material design and their performances were evaluated in detail and tested on in-vitro teratoma-mimicking simulation models to confirm the contraction effect and applicability.

2.3 Materials and Methods

2.3.1 Materials

Unless otherwise specified, all reagents were used as received. Pentaerythritol, tin (II) 2-ethylhexanoate, and CL were purchased from Tokyo Chemical Industry Co., Ltd.,

Tokyo, Japan. Triethylamine (TEA), tetrahydrofuran (THF) (super dehydrated), xylene, diethyl ether (super dehydrated), hexane, acryloyl chloride, acetone, chloroform-d ($CDCl_3$) with 0.05 v/v% tetramethylsilane (TMS), and methanol were purchased from Wako Pure Chemical Industries Ltd., Osaka, Japan. BPO and Iron (II-III) oxide nano powder (50-100nm) were purchased from Sigma-Aldrich, MO, USA. BPO was dried prior to use. Porcine blood and porcine carotid were purchased (as abattoir byproduct harvested at slaughterhouse from dead pigs) from Shibaura Zouki, Tokyo, Japan.

2.3.2 Synthesis and characterizations of SMPs

2.3.2.1 Synthesis of 4bPCLs

Initiator, pentaerythritol (1.25 mmol, 168.93 mg) was dehydrated under reduced pressure overnight after placing inside a pre-dried 3-way round-bottom flask (500 mL) prior to use. Monomer, CL (0.5 mol, 52.84 mL), was then added into the flask with dehydrated initiator under flowing nitrogen atmosphere by a glass syringe. A minimal amount (approximately five drops) of tin (II) 2-ethylhexanoate are added by a glass syringe as catalyst. The polymerization was carried out at 120 °C for 12 hours under sealed nitrogen atmosphere. After which, 300 mL of THF was added into the product for dilution. The diluted mixture was then reprecipitated by 1500 mL of hexane/diethyl ether (1:1 v/v%) mixture solvent. The precipitated product was purified by filtration under vacuum and dried overnight. The precipitated product, 4b100PCL, was purified with the aforementioned mixture solvent repeatedly for three to five times to wash off the residual unreacted chemicals and dried with the same approach. The dried 4b100PCL (98.2% yield) was collected and stored for further usage.[17,25]

SMPs with different molecular weights, 4b10PCL and 4b50PCL, were synthesized through the same approach with corresponding molar ratios.

2.3.2.2 Synthesis of 4bPCL macros

The previous obtained 4b100PCL (2.18 mmol, 100.0 g) was dissolved by superdehydrated THF (500mL) in a 500 mL flask by ultrasonication. After it's complete dissolved, an excessive amount of triethylamine (38.6 mmol, 3.91 mL) and acryloyl chloride (20.6 mmol, 1.862 mL) were added to the flask inside an ice bath and reacted for 12 hours in a shaded environment. The resulted product was reprecipitated against 1500 mL of methanol and filtrated to retrieve the precipitates. Such process was repeated three to five times for purification. Afterwards, the 4b100PCL macro was collected after drying under reduced pressure overnight.[17,25]

Similarly, 4b10PCL macro and 4b50PCL macro were synthesized in the same manner with corresponding molar ratios.

2.3.2.3 Characterizations of 4bPCLs and 4bPCL macros

The 4bPCLs and 4bPCL macros were dissolved in CDCl$_3$ with 0.05 v/v% TMS for the determination of their chemical structures by proton nuclear magnetic resonance spectroscopy (^{1}H NMR), JEOL, Tokyo, Japan. Their molecular weights were determined by gel permeation chromatography (GPC), JASCO International, Tokyo, Japan. Polystyrenes (PS) and DMF were used as calibration standards and the elution solvent for GPC measurements.

2.3.3 Fabrications of SMP strings

The crosslinked SMP strings were fabricated through free radical polymerization of the thermal initiator BPO and the previously collected 4bPCL macros. The 4bPCL macros were dissolved in xylene with various polymer concentrations (10 wt%, 20 wt%, 30 wt%, 40 wt% respectively) and various BPO concentrations (2 wt%, 5 wt%, 10 wt% respectively) under ultrasonication. The mixture solutions were sandwiched two glass slides with a Teflon® spacer with a thickness gradient (0.3 mm, 0.5 mm, 1.0 mm, 1.5 mm and 2.0 mm respectively). The reaction was carried out at 80 °C for 6 hours. After which, the crosslinked SMP strings were demolded and washed by acetone exchanged for 3 days to remove the residual chemicals. The purified SMP strings were then washed with methanol for 12 hours and collected after being dried under reduced pressure overnight.

2.3.4 Mechanical characterizations

All mechanical properties of the SMP strings were characterized by a uniaxial tensile tester (EZ-S 500N, Shimadzu, Kyoto, Japan) equipped with a heating chamber (M-600FN, TAITEC, Saitama, Japan) for temperature control. All uniaxial tensile tests were conducted at an elongation rate of 5 mm min^{-1} at 25 °C or 60 °C. All specimens had approximately 4.5-mm width, 30.0-mm length, and 0.3-mm thickness. The elastic modulus of the specimen was calculated from the initial slope of its stress–strain curve. The toughness was calculated from the integrated area under the stress-strain curve until break for each specimen. The energy storage capacity at each stretched strain was defined as the corresponding integrated area under the stress-strain curve at 60°C. All data are presented as mean ± SD, n=5.

Shape recovery-induced contraction force was measured using "hold mode" with the same tensile tester. A heat source of approximately 60 °C was applied onto the specimen at a distance of 10 cm, after held for 20 s under the pre-load of 0.1 N. The recovery-induced contraction force was recorded until heat source was removed. Shape recovery-induced contraction force was defined as the maximum force that was recorded during each process. All data are presented as mean ± SD, n=3.

2.3.5 Thermal characterizations

Thermal properties of the SMP strings were characterized using differential scanning calorimetry (DSC) (7000X, Hitachi High-Tech Science, Japan). All specimens were first equilibrated at 120 °C and cooled to 0 °C. The DSC curves were obtained in the second heating run at a rate of 5 °C min^{-1} for all runs. The degree of crystallinity (χ_c) was calculated using the enthalpy change (ΔH), according to the equation $\chi_c = \Delta H / \Delta H_m$, where ΔH is the specific melting enthalpy for each SMP string, and ΔH_m is the specific melting enthalpy for theoretically 100% crystalline PCL, which is considered as 136 J g^{-1} according to literature.[66]

2.3.6 Shape-memory characterizations

The SMP strings were held at equilibrium at 70 °C (above all specimens' Tm). Then they were stretched to 800% in uniaxial tensile test mode, where the maximum strains were noted as ε_{load}. Afterwards, they were cooled to 0 °C accompanied by the removal of external stress, where the final length was noted as ε. The shape recovery of the SMP string was actuated upon reheating above 70 °C. The shape fixity ratio (R_f) of the SMP string was calculated as $R_f = 100\% \times \varepsilon/\varepsilon_{load}$, and the shape recovery ratio (R_r) of the SMP strings was calculated according to the equation $R_r = 100\% \times (\varepsilon-\varepsilon_{rec})/\varepsilon$, where ε_{rec} represents the recovered strain upon reheating.[67,68] All data are presented as mean ± SD, n=3.

2.3.7 Pressure tests for shape-memory contraction effect

The test system was composed of a pressure sensor (Krone, KDM30, Bluetooth) connected with silicone tubes with hose connectors, a peristaltic pump (Masterflex L/S Precision Variable-Speed Console Drives) providing initial liquid pressure, and a blood reservoir using porcine blood. The Young's modulus of the silicone tube was tested to be 9.1 MPa. For human adult blood pressure mimicking tests, the initial pressure was

adjusted to be relatively constant and set at approximately 16 kPa. SMP strings with a width of 3.5 mm and a length of 20 mm were then tied onto the silicone tube with elongations of 200% and 300% fixed by a square knot. The shape transition was actuated by a heater at approximately 70 °C until the SMP strings were fully contracted. The final pressure was recorded for comparison. All data presented as mean ± SD, n=3. For fetal blood pressure mimicking tests, the initial pressure was manipulated to mimic a heartbeat pattern with a range of 4-8 kPa (30–60 mmHg). SMP strings stretched by 200 % were tied onto the silicone tube and pressure changes were recorded in real time. All tests were performed in triplicates to assess their reproducibility. All data presented as recorded.

2.3.8 Shape-memory contraction effect tests using porcine carotids

Porcine carotids were used to mimic the mechanical properties of teratomas. The SMP strings used in the test were stretched to 200% strain at approximately 70 °C and fixed with a square knot loosely set onto the carotids. A heater set at approximately 70 °C was used to induce heat from a relatively constant distance of 5 cm until full contraction. The test process was video-recorded, and the shape-memory response times were determined from the captured video time frames. A blood leakage test was also conducted using a blood reservoir with porcine carotid and a peristaltic pump operating at a relatively constant pressure of 8 kPa. The blood leakage speed was calculated as the amount of blood leaked in 60 s. All data presented as mean ± SD, n=3. The fabricated size of all SMP strings used in the test was 5 mm in width, 20 mm in length with thickness variances.

2.3.9 Fetal trocar passing through tests

The SMP strings of 2.0 mm thickness along with a 10-Fr fetoscopic cannula sleeve (COOK Medical Corp., U.S.) were used in the tests of the ability of the SMP strings to pass through the endoscopic trocar, method referred to previous report.[69] The SMP strings were tied with a square knot as in the previous contraction tests and inserted through a 10-Fr endoscopic cannula sleeve with the assistance of a plunger. SMP strings were deployed to confirm the intact result. The tests were performed in triplicates to confirm the reproducibility.

2.4 Results and discussions

2.4.1 Design Principles of the SMP Strings

With the aim to utilize the SMP strings in the minimally invasive fetal surgery of SCTs for the contraction of feeding vessels, multiple aspects need to be considered. Excellent mechanical properties such as high strength, toughness and stretchability are essential to the design given the protean sizes and rigidities of the teratoma.

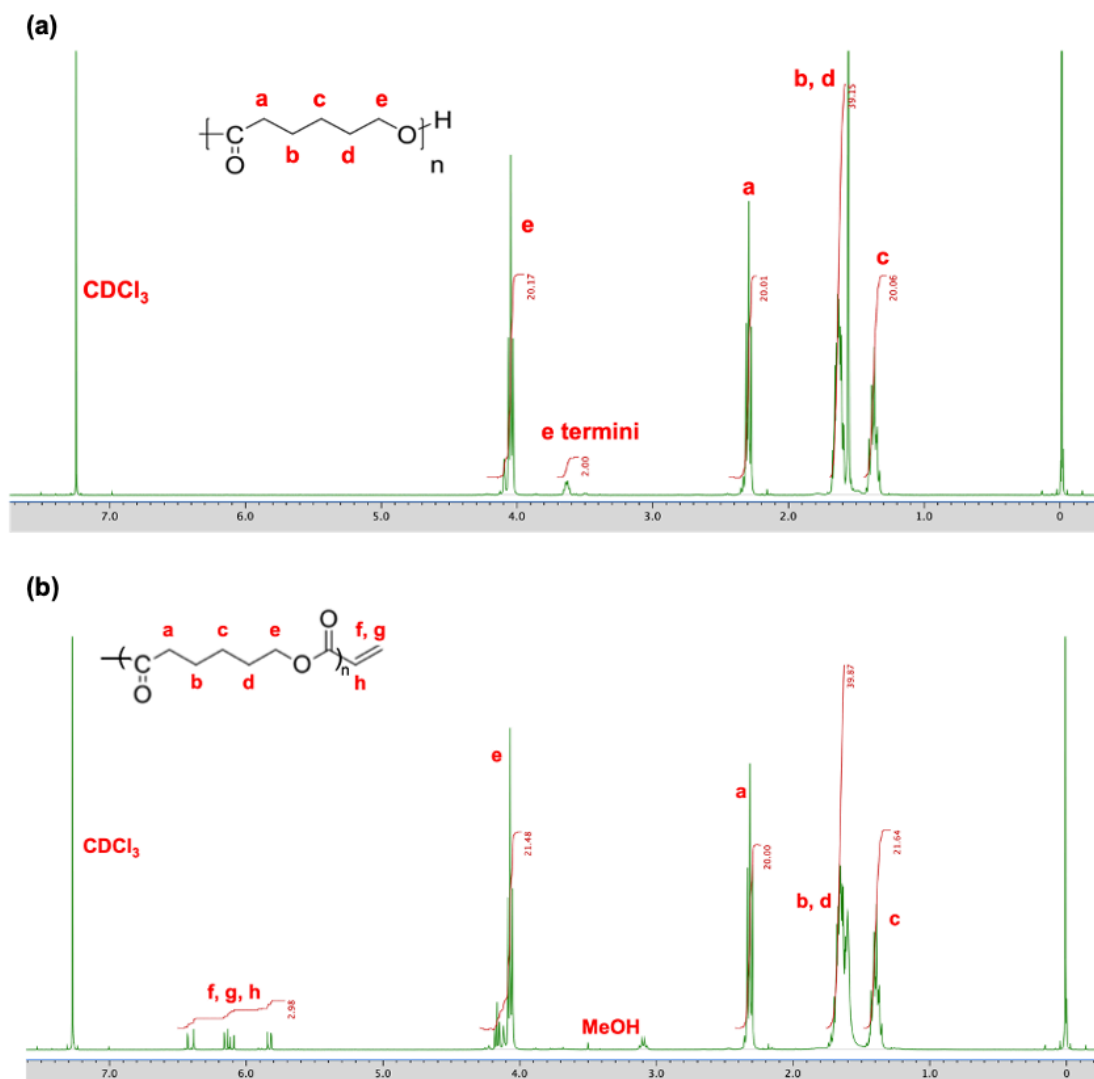**Figure 2.3.** Polymer chemical structure characterizations. (a) Representative ^{1}H-NMR spectra of 4b10PCL. (b) Representative ^{1}H-NMR spectra of 4b10PCL macro.

Furthermore, a proper shape-transition temperature (Tm) is essential for the SMP string design. Surgical equipment such as lasers could be considered for the introduction of the heat actuation. Moreover, the shape-memory response time is crucial

in surgical applications. The shape-memory response times for most PCL-based SMPs are virtually instantaneous, which may result in clinical uncertainties while applying the shape transition, since instant shape-transition may possibly cause damage the surrounding tissues in the operations.[70] Furthermore, a strong shape-memory contraction effect is crucial for the complete obstruction of blood inflow. Therefore, the proposed SMP string design investigated these factors for the aforementioned purpose.

The SMP strings investigated in this study were fabricated through polymerization of the synthesized 4bPCL macro and the thermal initiator BPO. A polymer network composed solely of crosslinked 4bPCL was obtained to retain the advantageous shape-memory properties. Previously, Grosvenor et al. reported that the elongation and tensile strength of PCL increased proportionally with its molecular weight.[71] To substantiate the improved mechanical performance of high molecular weight SMPs, three 4b'X'PCL SMPs were synthesized, with branch chain lengths (X) of 10, 50 and 100 respectively, which was confirmed by ^{1}H NMR (Figure 2.3). The weight-average molecular weights were confirmed by GPC to be in the range of 7.0 – 63.7 kDa and polydispersity between 1.12 to 1.55 (Table 2.1).

Table 2.1. Molecular weights, polydispersity indexes and end group introduction rates of 4b10, 4b50 and 4b100 PCL macromonomers.

Polymer type	Mn (Da) [1]	Mw (Da) [1]	PDI [1]	I.R. [2]
4b10 PCL-macro	6296	7022	1.115	99.3
4b50 PCL-macro	27860	37421	1.343	94.3
4b100 PCL-macro	41126	63661	1.550	95.2

I.R.: End group introduction rate; Mn: number average molecular weight; Mw: weight average molecular weight.

1) Measured by GPC. Solvent: DMF. Standard: PS.

2) Calculated by ^{1}H NMR; solvent: $CDCl_3$

The test results indicated a great enhancement of the mechanical properties (Figure 2.4a) and an accompanying drastic increase in the crystallinity with the increase of the polymer chain length (Figure 2.4b), indicating with the increase of molecular weight, the mobility of each polymer chain and the physical entanglement inside the crosslinked network increases significantly. The increase in crystallinity with the increase in molecular weight gives rise to the desired mechanical performance. Consequently, the 4b100 PCL SMP string with a high molecular weight (long branch chain length) exhibited the highest elastic modulus (approximately 344.9 MPa) and highest

toughness and highest stretchability (approximately 1351%) (Figure 2.4c). Hence, 4b100 PCL was selected as the prime candidate for fabricating the SMP strings. Three different fabrication conditions were investigated as well to obtain highly stretchable and robust SMP strings with excellent shape-memory properties and maneuverability, including different polymer concentrations, thermal initiator (BPO) concentrations, and crosslinking thicknesses.

2.4.2 Physical Characterizations of SMP Strings

Mechanical and thermal properties were investigated to determine the optimum conditions for the maneuverability of 4bPCL-based SMP strings. Results showed that both *Tm* and degree of crystallinity (χ_c) of the SMP strings decreased with regards to polymer concentration. The *Tm* ranged from 56.5 °C for 40 wt% to 67.0 °C for 10 wt%, respectively. The χ_c ranged from 36.4% for 40 wt% to 50.0% for 10 wt%, respectively (Figure 2.5a). A higher polymer concentration provided a denser environment inside the polymer solution, resulting in a higher crosslinking density and a relatively lower crystalline polymer network, both of which reduced the *Tm*. Free polymer chains with certain mobility could contribute to the crystal formation of PCL. SMP strings fabricated with polymer concentrations below 40 wt% showed inhomogeneous morphologies and those above 40 wt% were not successful obtained due to the high viscosity and autonomous crosslinking during the ultrasonication (Figure 2.5b).

In addition, both Tm and χ_c exhibited an increasing trend with increasing BPO concentrations. For 2 wt%, 5 wt%, and 10 wt%. *Tm* were 56.5 °C, 59.8 °C, and 62.9 °C, respectively. Similarly, the χ_c were 36.4 %, 39.2 %, and 42.2 % for BPO concentrations of 2 wt%, 5 wt%, and 10 wt%, respectively (Figure 2.6a). Furthermore, there was a significant downward trend in the average elastic modulus. For 2 wt%, 5 wt%, and 10 wt% BPO concentrations, the elastic moduli were averagely 344.9 MPa, 301.8 MPa and 242.5 MPa, respectively (Figure 2.6b) which were in agreement with previous report.[66] This trend is attributed to the increase in the number of benzoyloxy radicals produced from the thermally induced homolysis of BPO, which resulted in a higher chance of termination of the excessive benzoyloxy radical, thereby interfering with the crosslinking processes and crystal formation. Considering the high elastic modulus and the relatively low *Tm*, the SMP strings fabricated using 4b100 PCL with 40 wt% polymer and 2 wt% BPO concentrations were used for the subsequential investigations.
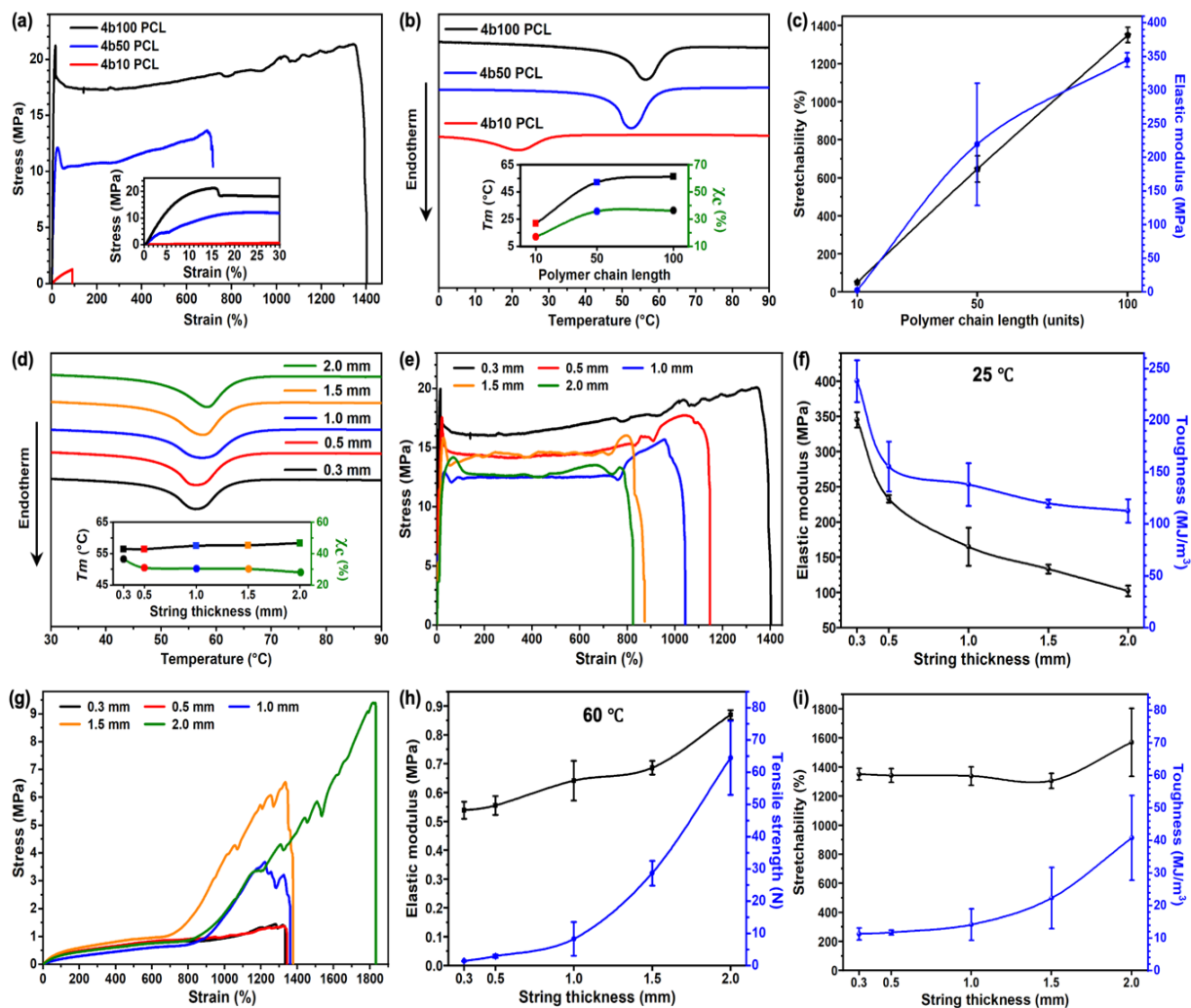
Figure 2.4 Physical characterizations of shape-memory polymeric strings. (a) Tensile stress-strain curves; (b) DSC curves, Tm and crystallinity distributions; (c) stretchability and elastic modulus for SMP strings with different polymer molecular weights. (d) DSC curves, Tm and crystallinity distributions; (e) Tensile stress-strain curves; (f) elastic modulus and toughness of 4b100PCL SMP strings with different crosslinking thicknesses (0.3 mm, 0.5 mm, 1.0 mm, 1.5 mm, and 2.0 mm) at 25 ℃. (g) Tensile stress-strain curves; (h) elastic modulus, tensile strength; (i) stretchability and toughness of 4b100PCL SMP strings with different crosslinking thicknesses at 60 ℃.

Figure 2.5. Physical characterizations of 4b100 PCL SMP strings fabricated by different polymer concentrations. (a) Tm and crystallinity distributions (b) images of SMP strings with different polymer concentrations of 10 wt%, 20 wt%, 30 wt%, 40 wt%.
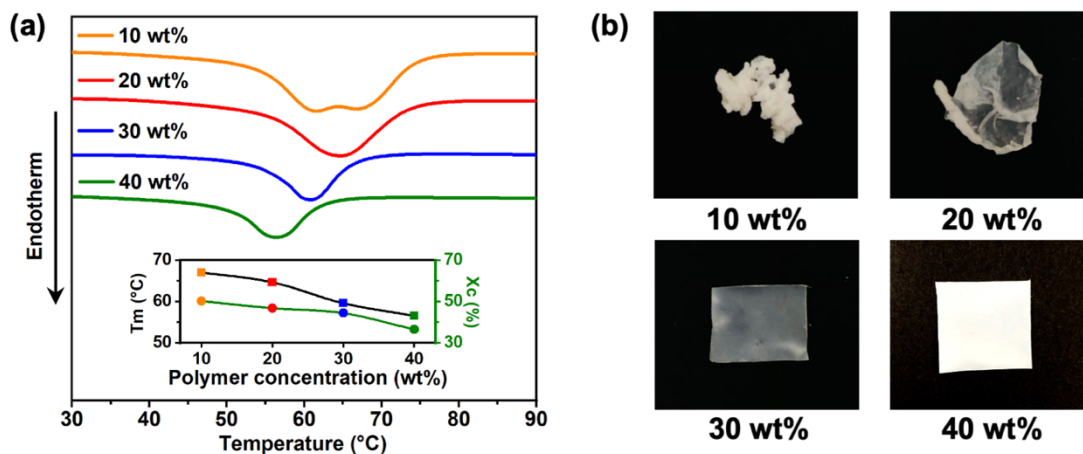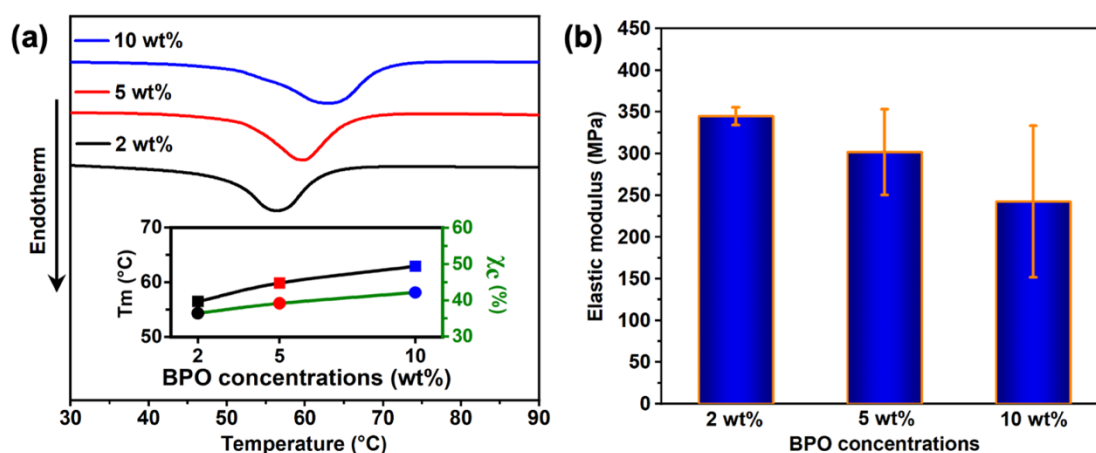

Figure 2.6. Physical characterizations of 4b100 PCL SMP strings fabricated by different BPO concentrations. (a) *Tm* and crystallinity distributions; (b) elastic modulus for SMP strings with different BPO concentrations of 2 wt%, 5 wt% and 10 wt%.

Various crosslinking thicknesses (0.3 mm, 0.5 mm, 1.0 mm, 1.5 mm, and 2.0 mm) of the SMP strings were additionally investigated to assess their maneuverability. Their actual thickness is slightly smaller than the fabricated crosslinking thickness (Figure S5). With increasing thickness, a slight elevation in *Tm* ranging from 56.5 ºC (0.3 mm) to 58.3 ºC (2.0 mm) was observed (Figure 2.4d) most likely caused by the delay of heat penetration due to the geometric differences during the measurements. The typical stress-strain curves of crystallined polymers were observed for SMP strings at 25 ºC with clear yielding points and drawing of chains, due to their semi-crystallined structure below Tm (Figure 2.4e). A slight decrease in the χ_c was observed with increasing

thickness resulting in an exponential decrease of elastic modulus in the range of 102 MPa to 345 MPa, and toughness in the range of 112.6 MJ m^{-3} to 237.9 MJ m^{-3} (Figure 2.4f). Same trend was also confirmed by X-ray diffraction (XRD) patterns of the 4bPCL SMP strings with 0.5 mm, 1.0 mm, 1.5 mm and 2.0 mm (Figure 2.7). The diffraction peaks appeared at $2\theta = 21.6°$, 22.2° and 24.0° which are related to the crystalline planes (110), (111), and (200) of PCL respectively.[72] In addition, exhibited by the stress-strain curves at 60 °C which was above Tm when SMP strings were in amorphous state, clear elastomer-like stress-strain curves with an exponential increase of elastic moduli and tensile strengths were observed in reliance to thickness (Figure 2.4g, h). This result indicates that the amorphous SMP strings at 60 ºC displayed an increase in elastic modulus indicating that without the influence of crystalline phase, the crosslinking density elevated with regards to crosslinking thickness. The increased crosslinking density hindered the crystal formation which was substantiated by the decrease in the χ_c.
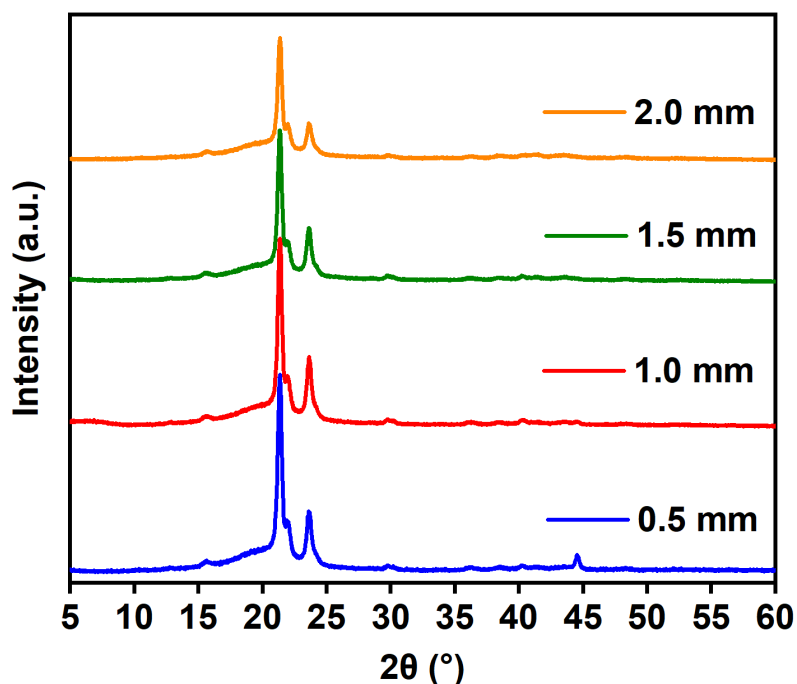
Figure 2.7. XRD patterns of 4bPCL SMP strings with different thickness.

Notably, enhancement of elastic modulus was achieved by various report previously with different approaches, for instance, with the modification of various initiators;[73] composite with various reinforcing materials[72,74] and etc. However, these approaches resulted in the decline of either stretchability, toughness or shape recovery ratio. In this report, an enhancement in the toughness (averagely highest up to 237.9 MJ m^{-3}) and stretchability (averagely highest of which up to 1570% for 2.0 mm) of the

SMP strings was demonstrated (Figure 2.4i) via a simple manipulation of crosslinking thickness. ATR-FTIR results indicated the crosslinking thickness did not affect the chemical structure of 4bPCL-based SMP strings (Figure 2.8). This result could most possibly indicate that the thermal initiation speed of crosslinking varies with the crosslinking thickness, although the polymer concentration and BPO concentration were held constant. It can be surmised that as the thickness increases, the chance for termination of the radical is suppressed due to thermal diffusion, which results in delaying the crosslinking rate and an increased chance of chain elongation. The chain elongation significantly extends the single chain length inside the polymer network. Consequently, more physical entanglement occurs inside the network, leading to a decrease in the chain mobility and weakened mechanical performance below *Tm*. However, the thermal crosslinking process induces certain restrictions on the formation of crystalline regions in the 4bPCL SMP strings. Nonetheless, the *Tm* of the crosslinked 4b100 PCL strings with different thicknesses were all in the vicinity of 56 °C. These temperatures, which are higher than the typical physiological temperatures, can qualify the SMP strings for further application in surgical applications
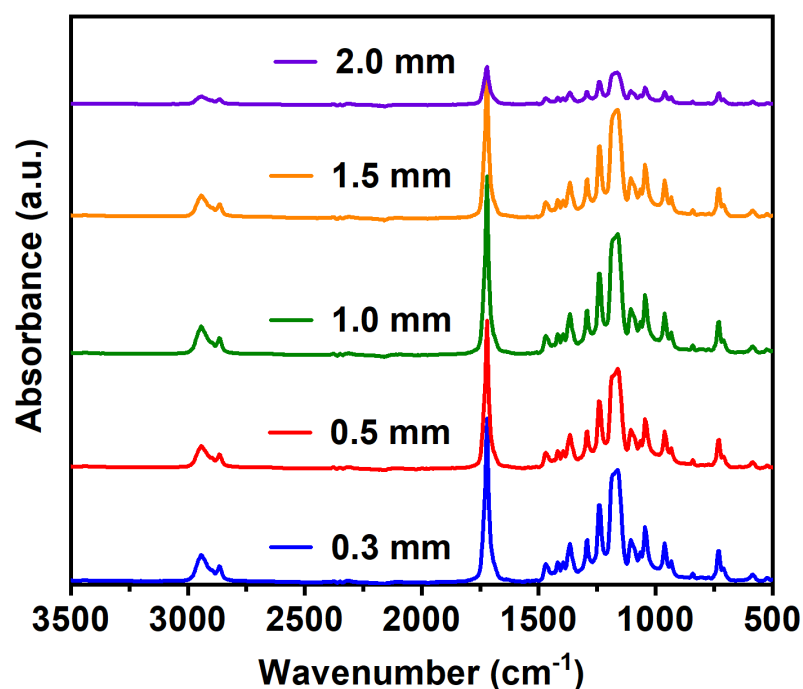

Figure 2.8. ATR-FTIR spectra of 4bPCL SMP strings with different thickness.

2.4.3 Shape-memory Characterizations of SMP Strings

In terms of the manipulation of the contraction motion and its strength in SMP strings, the desirable shape-memory properties including a high shape fixity, shape recoverability as well as a strong shape-memory contraction force capable of restraining

the blood flow are essential. For probing these aspects, SMP strings were fabricated under the aforementioned optimal conditions (4b100 PCL, 40 wt% polymer concentration, 2 wt% BPO concentration) with different string thicknesses. Excellent stretchability, ranging from 1268 % to 1570 % was achieved (exemplary demonstration in Figure 2.9a). With respect to shape-memory properties of the SMP strings, during the shape-memory process elaborated in Figure 2.1a, the rise of temperature above Tm will result in the entropic change, thus increase the chain mobility inside the polymer network. The cooling of the temperature below Tc will provide the fixation of an energetically unstable temporary shape and subsequently store the newfound energy. This energy storage capacity will be released again under the reheating process by overcoming the melting enthalpy of the crystallined region, allowing the induction of macroscopic shape recovery. Therefore, energy storage capacity after heating is crucial for the manipulation of shape-memory properties.[35,64] In this respect, researchers have proposed versatile energy-efficient design principles. Recently, Krajovic et.al., reported a bisurea interaction-based dynamic network for achieving high energy storage capacity achieving above 90% shape recovery ratio (R_r) under deformation up to 200%.[75] For similar purpose, Cooper et.al., reported a strain-induced supramolecular nanostructure achieving a recoverable strain of 300% with an above 90% shape fixity (R_f) and Rr.[76]

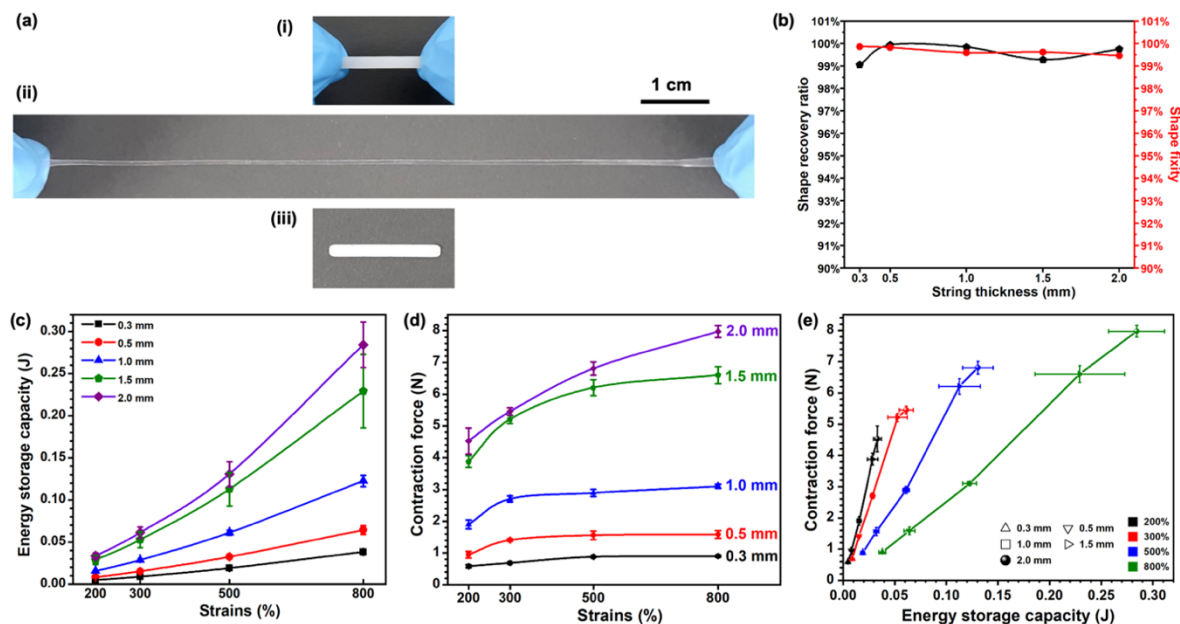**Figure 2.9** Shape-memory properties of the SMP strings. (4b100 PCL, 40 wt% polymer concentration, 2 wt% BPO concentration) (a) Images of SMP string before stretching (i), after stretching (ii) and after shape recovery (iii). (b) Shape recovery ratios and shape fixities of the SMP strings with different thicknesses stretched by 800%. (c) Energy storage capacity; (d) contraction force; (e) contraction force and energy storage

capacity correlations of SMP strings with different thicknesses at various strains of 200%, 300%, 500% and 800%.

In our report, an excellent shape fixity (R_f) and shape recovery ratio (R_r), both of which above 99%, were obtained for all thicknesses at a large deformation of 800% (Figure 2.9b). Assured by this excellent shape fixity and recoverability, the energy storage capacity and shape-memory contraction force were evaluated under the influence of string thickness and various stretched strains, respectively 200%, 300%, 500% and 800%. Results demonstrated that the energy storage capacity of SMP strings at 60 ºC during the deformation demonstrated an upward trend with thicknesses and strains respectively (Figure 2.9c). Shape-memory contraction force results presented a similar exponential increase as energy storage capacity (Figure 2.9d) with different thicknesses (Figure 2.10a) and different strains (Figure 2.10b). Accordingly, shape-memory contraction force showed corresponding tendency to energy storage capacity (Figure 3e). These results indicated that contraction force of the SMP string could be facile-customizable in the range of 0.58 N to 7.97 N, with the simple manipulation of energy storage capacity by adjusting the stretched strains and string thicknesses.
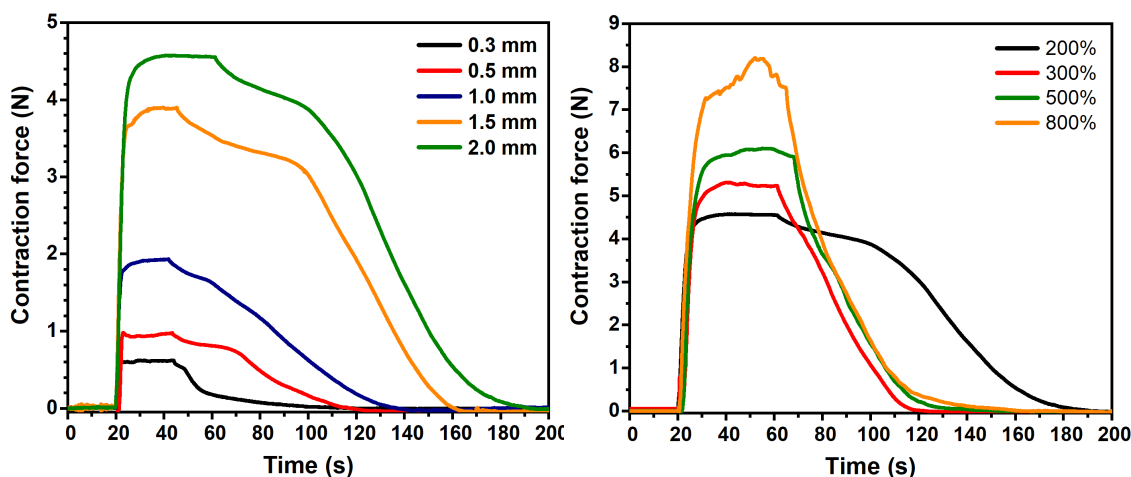
Figure 2.10. Contraction force measurements of (a) 4b100 PCL SMP strings with different thicknesses stretched by 200%, (b) 2.0 mm 4b100 PCL SMP strings stretched by different strains.

2.4.4 Shape-memory Contraction Effect Simulations of SMP Strings

In order to confirm the applicability of the 4b100 PCL SMP strings toward contraction of the blood vessel and their applications in minimally invasive surgeries, we used the fetoscopic surgery of SCT as an exemplary application model. In order to

resolve the difficulties in minimally invasive SCT treatments, the SMP strings are envisioned to occlude the feeding vessel to SCT, in turn arrest the tumor growth. For the in vitro evaluation of such application, a pressure test system was designed and set up (Figure 2.11a). This system comprised of a pressure sensor connected to silicone tubes with a peristaltic pump and a blood reservoir with porcine blood to mimic blood pressure. To probe the ultimate limits of the SMP strings, the initial pressure before contraction was set to be approximately 16 kPa, which was relatively consistent with the average adult systolic blood pressure of close to 120 mmHg. Stretched SMP strings with gradient contraction forces of 0.95 N, 1.90 N, 3.88 N, 4.52 N and 5.46 N (fabrication conditions of which investigated in the last section) were applied onto the silicone tube using a square knot. The final pressure at which the SMP string was fully recovered to original shape was recorded to verify string's shape-memory contraction efficacy. Results indicated that with increased shape-memory contraction forces provided by each SMP strings, acute initial pressures linearly decreased. (Figure 2.11b). This proved that the resistance to the external object during the contraction process of SMP strings increased with the contraction force, ultimately provided a stronger shape-memory contraction effect.
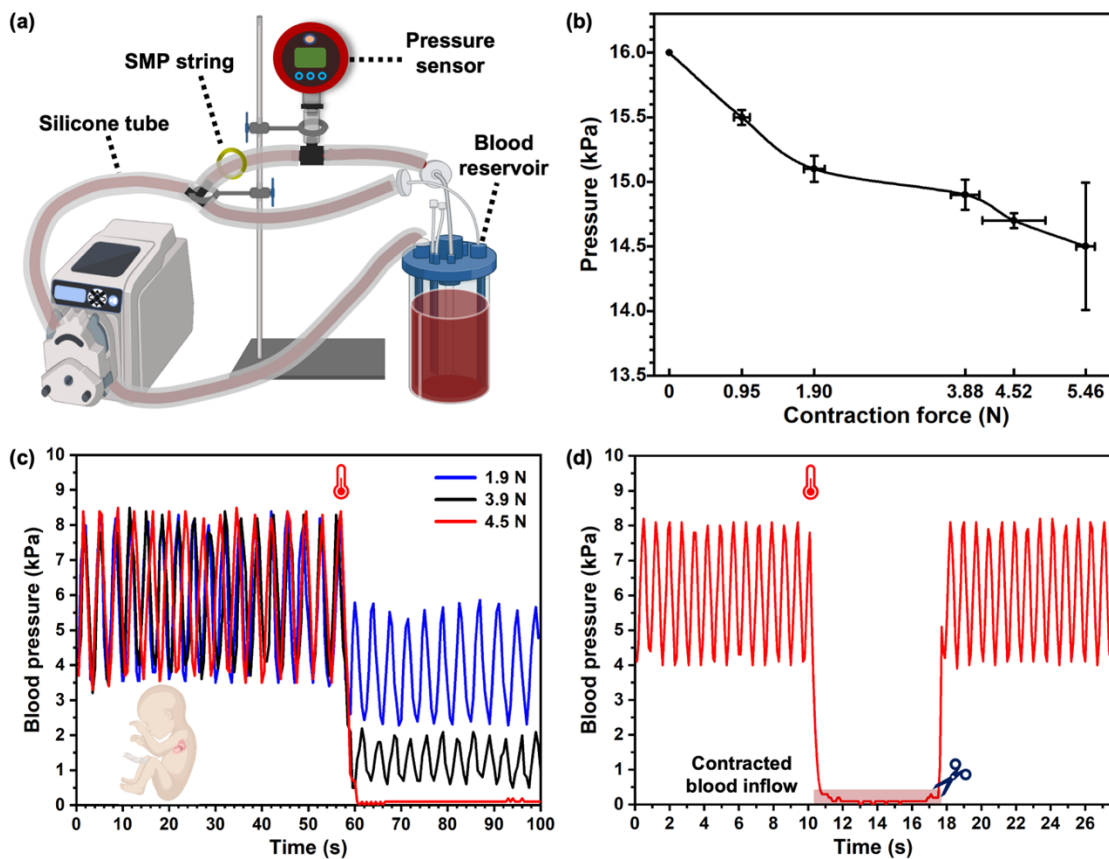

Figure 2.11 Fetal heartbeat pattern mimicking pressure test for the evaluation of shape-memory contraction effect of the SMP strings. (a) Schematic illustration of the design

and setup of the circulatory experimental system. (b) Pressures of the fully contracted silicone tube by SMP strings of different contraction forces. (c) Fetal blood pressure mimicking shape memory contraction process by SMP strings of 1.9 N, 3.9 N and 4.5 N contraction force. (d) Shape memory contraction process by SMP string of 4.5 N contraction force before, after contraction and after SMP string was cut loose.

For the aforementioned purpose of using SMP string in the treatment of fetal SCT, shape-memory contraction effect on fetuses with beating hearts needs to be evaluated on in vitro systems. Therefore, fetal blood pressure-mimicking contraction simulations were conducted. Fetal diastolic and systolic aortic blood pressure are approximately 21 mmHg at 20 weeks' gestation to 29 mmHg at 40 weeks' gestation (diastolic) and 37 mmHg at 20 weeks' gestation to 58 mmHg at 40 weeks' gestation (systolic), respectively.[77] Considering the high-output cardiac situation, fetal blood pressure-mimicking contraction simulations were conducted using an initial pressure of approximately 4 kPa (relatively close to 30 mmHg) and up to 8 kPa (relatively close to 60 mmHg). SMP strings with contraction force below 1.90 N did not exhibit distinguishable pressure changes in this system due to insufficient contraction against the silicone tube. In contrast, the SMP strings with 3.9 N contraction force provided a clear contraction effect against the fetal heartbeat mimicking pattern. Furthermore, SMP string with 4.5 N contraction force was able to achieve complete obstruction, managed to suppress the pressure to zero (Figure 2.11c). After the same kind of SMP string was tested and cut loose after the contraction, the blood pressure returned to the original pressure and pattern, indicating that the complete obstructions of blood flow were entirely attributed to the shape-memory contraction effect of SMP strings (Figure 2.11d).
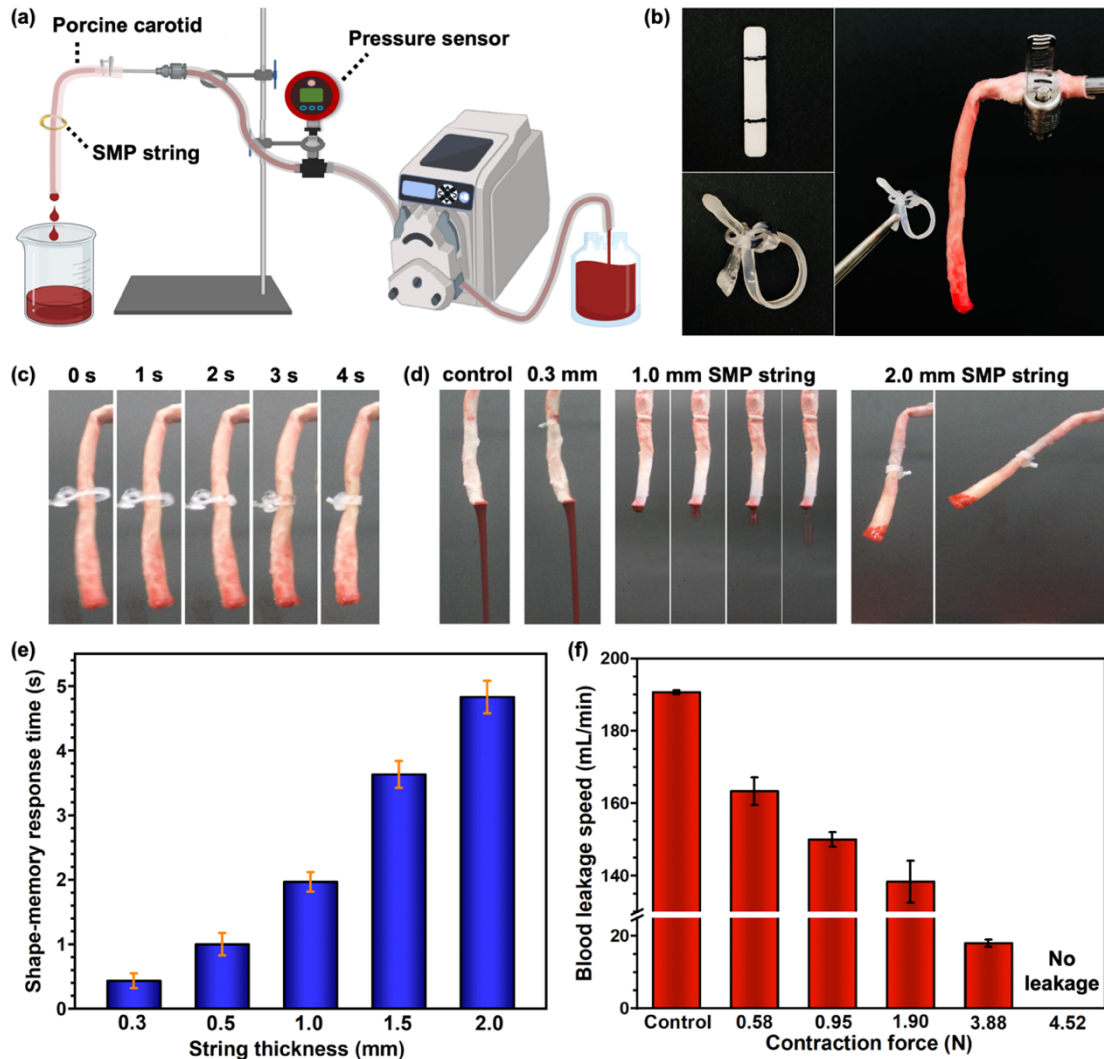
Figure 2.12. Teratoma-mimicking model using porcine carotid for the evaluation of shape-memory contraction effect of SMP strings using porcine carotid. (a) Schematic illustration of the experimental setup for the simulation. (b) Images of the SMP string used in the simulation. (c) Images of the shrinking process for 200% stretched 2.0 mm SMP string on porcine carotid. (d) Images of the blood leakage process using non-contracted control porcine carotid and 0.3 mm, 1.0 mm, and 2.0 mm SMP strings. (e) Shape-memory response time of the SMP strings with different thicknesses. (f) Blood leakage speed through porcine carotid contracted by SMP strings of different contraction forces

Aside from strong shape-memory contraction force to restrict blood inflow to the teratoma, a controllable shape-memory response time is also of great significant to ensure controllability during surgeries. Therefore, in vitro simulations of the shape-memory contraction effect of the SMP string on teratoma-mimicking porcine carotid

models were designed and conducted (Figure 2.12a). The 200% stretched SMP strings were applied to the porcine carotid with a square surgical knot (Figure 2.12b). Manipulation of the shape-memory response time in the range of 0.4 s to 4.8 s was achieved with different string thicknesses, owing to the different heat penetration rates into the SMP strings (Figure 2.12e). The gradual contraction achieved with the 2.0 mm SMP string (Figure 2.12c) could be considered to provide sufficient controllability during clinical operations.
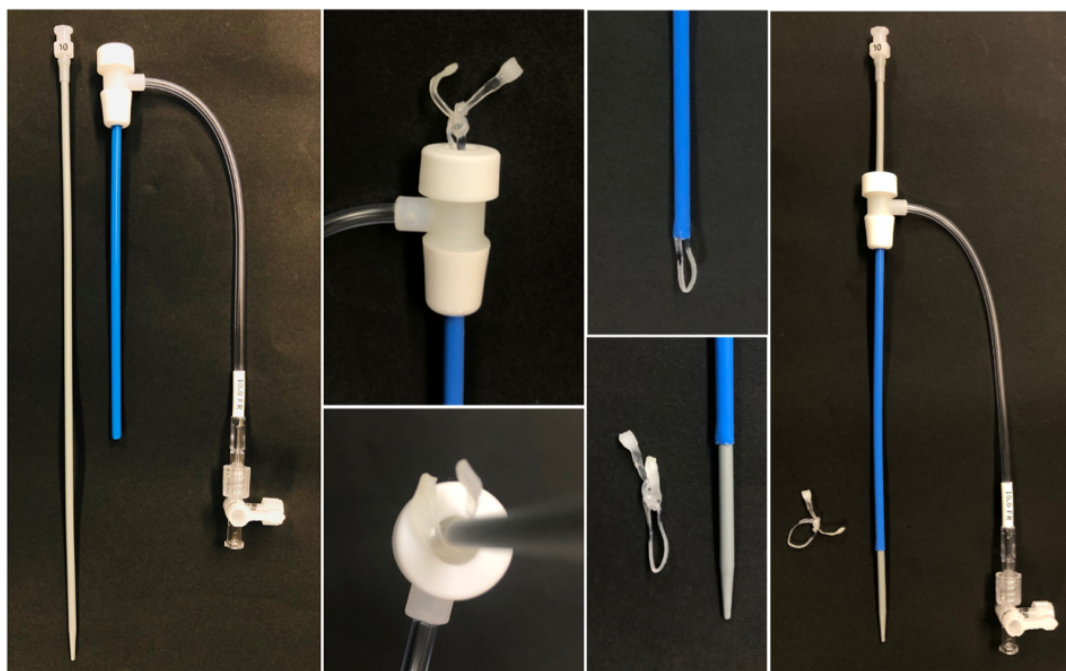
Figure 2.13. Images of the 2.0 mm SMP string (stretched by 200% and tied with a square knot) passed through the 10-Fr fetoscopic cannula sleeve (blue) with the assistance of a plunger (gray).

Shape-memory contraction effect was quantified using the blood leakage speed using an initial blood inflow pressure of 8 kPa, which approximately mimics the fetal systolic aortic pressure under high-output circumstance. The blood leakage speed was proportionally suppressed with an increase of contraction force by SMP strings (Figure 2.12d, f), in consistence with the previous physical characterizations. In particular, as presented in Movie S1, SMP string with a contraction force of 4.52 N successfully obstructed the leakage of blood inflow without rupturing the porcine carotid, resulting in a complete contraction with a maneuverable shape-memory response time.

In addition, the abilities of SMP strings to pass through the fetal trocar was tested using the 2.0 mm SMP string and a 10-Fr fetoscopic cannula sleeve (COOK Medical Corp.).[69,78] The results showed that even the thickest SMP string (2.0 mm), which was

stretched by 200% and tied with a square knot (as used in the abovementioned shape-memory contraction tests) could passed through fetal trocar without any damage to the string (Figure 2.13). However, it was also apparent from the test that the SMP strings with higher thicknesses would not be able to fit into fetal trocar, indicating that the string thickness of 2.0 mm was the limit.

2.5 Conclusions

In this study, we reported a novel design of 4bPCL-based SMP strings with customizable mechanical properties. Among which, stretchability is in the range of 1268% to 1570%; elastic modulus in the range of 102 MPa to 345 MPa; toughness in the range of 112.6 MJ m^{-3} to 237.9 MJ m^{-3}, while maintaining an above 99% R_f and R_r at a large deformation of 800%. Notably, the SMP strings exhibited significantly controllable contraction capabilities with a customizable shape-memory contraction force ranging from 0.58 N to 7.97 N which could be controllable through a facile manipulation of their energy storage capacity; a controllable shape-memory response time (0.4 s – 4.8 s) and demonstrated excellent shape-memory contraction effect against both silicone tubes and porcine carotids. Notably, although the applicability of such shape-memory contraction motion of SMP strings were evaluated and confirmed using fetoscopic surgery of SCT as an exemplary treatment model in this paper, the appealing results could also be utilized in other shape-memory motions such as twisting, bending and expansions. Above all, the SMP strings developed in this study could be very promising in a wide range of future applications such as minimally invasive fetal surgery, treatment of stroke and aneurysm. Additional work is needed to further optimize the detailed operational conditions and to achieve the precise manipulation of such shape-memory contraction effect.

Reference

[1] A. Fulati, K. Uto, M. Iwanaga, M. Watanabe, M. Ebara, Adv. Healthc. Mater. 2022, 11, 2200050.

[2] A. Lendlein, S. Kelch, Angew. Chem. Int. Ed. Engl. 2002, 41, 2034.

[3] W. Miao, W. Zou, Y. Luo, N. Zheng, Q. Zhao, T. Xie, Polym. Chem. 2020, 11, 1369.

[4] K. Uto, K. Yamamoto, S. Hirase, T. Aoyagi, J. Control. Release 2006, 110, 408.

[5] M. Ebara, K. Uto, N. Idota, J. M. Hoffman, T. Aoyagi, Adv. Mater. 2012, 24, 273.

[6] S. Ishii, K. Uto, E. Niiyama, M. Ebara, T. Nagao, ACS Appl. Mater. Interfaces 2016, 8, 5634.

[7] Q. Shou, K. Uto, M. Iwanaga, M. Ebara, T. Aoyagi, Polym. J. 2014, 46, 492.

[8] Z. Li, X. Zhang, S. Wang, Y. Yang, B. Qin, K. Wang, T. Xie, Y. Wei, Y. Ji, Chem. Sci. 2016, 7, 4741.

[9] Y. Liu, H. Lv, X. Lan, J. Leng, S. Du, Compos. Sci. Technol. 2009, 69, 2064.

[10] D. Ren, Y. Chen, S. Yang, H. Li, H. U. Rehman, H. Liu, Macromol. Chem. Phys. 2019, 220, 2.

[11] A. Babaie, M. Rezaei, D. Razzaghi, H. Roghani-Mamaqani, J. Appl. Polym. Sci. 2022, 139, 1.

[12] J. R. Kumpfer, S. J. Rowan, J. Am. Chem. Soc. 2011, 133, 12866.

[13] H. Jiang, S. Kelch, A. Lendlein, Adv. Mater. 2006, 18, 1471.

[14] Y. Li, D. Wang, J. Wen, J. Liu, D. Zhang, J. Li, H. Chu, Adv. Funct. Mater. 2021, 31, 2011259.

[15] Y. Zhang, N. Zhang, H. Hingorani, N. Ding, D. Wang, C. Yuan, B. Zhang, G. Gu, Q. Ge, Adv. Funct. Mater. 2019, 29, 1806698.

[16] Q. Shen, S. Trabia, T. Stalbaum, V. Palmre, K. Kim, I.-K. Oh, Sci. Rep. 2016, 6, 24462.

[17] D. J. Maitland, M. F. Metzger, D. Schumann, A. Lee, T. S. Wilson, Lasers Surg. Med. 2002, 30, 1.

[18] W. Small IV, T. S. Wilson, W. J. Benett, J. M. Loge, D. J. Maitland, Opt. Express 2005, 13, 8204.

[19] B. Liu, Z. Xu, H. Gao, C. Fan, G. Ma, D. Zhang, M. Xiao, B. Zhang, Y. Yang, C. Cui, T. Wu, X. Feng, W. Liu, Adv. Funct. Mater. 2020, 30, 1910197.

[20] G. M. Baer, W. Small, T. S. Wilson, W. J. Benett, D. L. Matthews, J. Hartman, D. J. Maitland, Biomed. Eng. Online 2007, 6, 43.

[21] S. Ouchi, E. Niiyama, K. Sugo, K. Uto, S. Takenaka, A. Kikuchi, M. Ebara, Biomater. Sci. 2021, 9, 6957.

[22] R. Swamy, N. Embleton, J. Hale, Prenat. Diagn. 2008, 28, 1048.

[23] J. L. Roybal, J. S. Moldenhauer, N. Khalek, M. W. Bebbington, M. P. Johnson, H.

L. Hedrick, N. S. Adzick, A. W. Flake, J. Pediatr. Surg. 2011, 46, 1325.

[24] J. A. Deprest, A. W. Flake, E. Gratacos, Y. Ville, K. Hecher, K. Nicolaides, M. P. Johnson, F. I. Luks, N. S. Adzick, M. R. Harrison, Prenat. Diagn. 2010, 30, 653.

[25] J. H. Phi, J. Korean Neurosurg. Soc. 2021, 64, 406.

[26] A. W. Flake, M. R. Harrison, N. S. Adzick, J.-M. Laberge, S. L. Warsof, J. Pediatr. Surg. 1986, 21, 563.

[27] E. Shue, M. Bolouri, E. B. Jelin, L. Vu, B. Bratton, E. Cedars, L. Yoke, F. Byrne, S. Hirose, V. Feldstein, D. Miniati, H. Lee, J. Pediatr. Surg. 2013, 48, 1225.

[28] M. Litwińska, E. Litwińska, K. Janiak, A. Piaseczna-Piotrowska, K. Szaflik, Fetal Diagn. Ther. 2020, 47, 138.

[29] H. L. Hedrick, A. W. Flake, T. M. Crombleholme, L. J. Howell, M. P. Johnson, R. D. Wilson, N. S. Adzick, J. Pediatr. Surg. 2004, 39, 430.

[30] N. Sananes, P. Javadian, I. Schwach Werneck Britto, N. Meyer, A. Koch, A. Gaudineau, R. Favre, R. Ruano, Ultrasound Obstet. Gynecol. 2016, 47, 712.

[31] C. Simonini, B. Strizek, C. Berg, U. Gembruch, A. Mueller, A. Heydweiller, A. Geipel, Prenat. Diagn. 2021, 41, 301.

[32] H. Miyasako, K. Yamamoto, T. Aoyagi, Polym. J. 2008, 40, 806.

[33] T. Muroya, K. Yamamoto, T. Aoyagi, Polym. Degrad. Stab. 2009, 94, 285.

[34] A. Lendlein, O. E. C. Gould, Nat. Rev. Mater. 2019, 4, 116.

[35] Y. Ren, Z. Wei, X. Leng, T. Wu, Y. Bian, Y. Li, J. Phys. Chem. B 2016, 120, 4078.

[36] C. Han, X. Ran, X. Su, K. Zhang, N. Liu, L. Dong, Polym. Int. 2007, 56, 593.

[37] T. Xie, Nature 2010, 464, 267.

[38] W. Miao, W. Zou, B. Jin, C. Ni, N. Zheng, Q. Zhao, T. Xie, Nat. Commun. 2020, 11, 4257.

[39] M. Watanabe, H. Li, M. Yamamoto, J. Horinaka, Y. Tabata, A. W. Flake, J. Biomed. Mater. Res. Part B Appl. Biomater. 2021, 109, 921.

[40] D. Ibrahim, E. Ho, S. A. Scherl, C. M. Sullivan, J. Pediatr. Surg. 2003, 38, 248.

[41] M. Grosvenor, Int. J. Pharm. 1996, 135, 103.

[42] A. Babaie, M. Rezaei, R. L. M. Sofla, J. Mech. Behav. Biomed. Mater. 2019, 96, 53.

[43] Przybysz, Hejna, Haponiuk, Formela, Polymers (Basel). 2019, 11, 1101.

[44] B. Lepoittevin, M. Devalckenaere, N. Pantoustier, M. Alexandre, D. Kubies, C. Calberg, R. Jérôme, P. Dubois, Polymer (Guildf). 2002, 43, 4017.

[45] Y. Xia, Y. He, F. Zhang, Y. Liu, J. Leng, Adv. Mater. 2021, 33, 2000713.

[46] D. M. Krajovic, M. Anthamatten, ACS Appl. Polym. Mater. 2021, 3, 2082.

[47] C. B. Cooper, S. Nikzad, H. Yan, Y. Ochiai, J.-C. Lai, Z. Yu, G. Chen, J. Kang, Z. Bao, ACS Cent. Sci. 2021, 7, 1657.

[48] P. C. Struijk, V. J. Mathews, T. Loupas, P. A. Stewart, E. B. Clark, E. A. P. P. Steegers, J. W. Wladimiroff, Ultrasound Obstet. Gynecol. 2008, 32, 673.

[49] P. Klaritsch, K. Albert, T. Van Mieghem, L. Gucciardo, E. Done', B. Bynens, J. Deprest, BJOG An Int. J. Obstet. Gynaecol. 2009, 116, 188.

Chapter 3 Influences of Crystallinity and Crosslinking Density on the Shape Recovery Force

3.1 Abstract

Shape-memory polymers (SMPs) show great potential in various emerging applications, such as artificial muscles, soft actuators, and biomedical devices, owing to their unique shape recovery-induced contraction force (shape recovery force). However, the factors influencing this force remain unclear. Herein, we designed a simple shape-memory polymer blends (SMPBs) using a series of tetra-branched poly(ε-caprolactone) (4bPCL)-based SMPs with long and short branch-chain lengths that demonstrate decreased crystallinity and increased crosslinking density gradients. The resultant polymer blends possessed mechanical properties manipulable in a wide range in accordance with crystallinity gradient, such as stretchability (50.5% –1419.5%) and toughness (0.62 MJ m^{-3} –130.4 MJ m^{-3}), while maintaining excellent shape-memory properties. The experimental results show that crosslinking density affected the shape recovery force, which correlates to the SMPs' energy storage capacity. Such a polymer blending system could provide new insights on how crystallinity and crosslinking density affect macroscopic thermal and mechanical properties as well as the shape recovery force of SMP networks, improving design capability for future applications.

3.2 Introduction

SMPs are representative smart polymers and have been extensively studied in the past few decades owing to their unique capability of recovering their permanent original shapes from a temporarily fixed shape when actuated by various external stimuli, such as heat,[26,42,47] light,[29,30] and laser.[39,41] Tremendous efforts have been dedicated to exploring this unique shape-memory property and its induced shape-memory motions, such as bending, stretching, lifting, and grasping, in vast applications, including soft robotics, artificial muscles, actuators and biomedical devices.[33,79–83] While the appealing shape-memory motions explored so far have shown great potential, the feasibility of SMPs in practical applications suffers from various limitations, such as inadequate deformability, maneuverability, and shape recovery force.

Wang et al.[84] reported a PCL-based photo-responsive SMP with polydopamine nanospheres as photothermal filler. The proposed artificial muscle-mimicking motions was achieved by the shape-recovery-induced contraction motion, which was demonstrated by lifting a weight. Similarly, Li et al.[32] reported an SMP capable of

mechanical bearing achieved by solvent-induced shape recovery force, which is applicable for soft robotics, sensors and etc. Kumar et al.[85] demonstrated an SMP-based smart compression device that utilizes the shape recovery-induced contraction force for the treatment of chronic venous disorder. In our previous study, we designed a novel shape-memory string capable of occluding the feeding vessels of fetal tumors in minimally invasive fetoscopic surgery contributed by the laser-actuatable shape-memory contraction.[17] The aforementioned shape recovery force is a pivotal function of SMPs, which are commonly utilized in wide range of applications. However, aside from demonstrations of such motion, such as weight lifting[81] and muscle-mimicking contractions, the shape recovery force and its influential factors have not yet been systematically investigated.

PCL is a semicrystalline SMP with a melting temperature (Tm) in the vicinity of 60°C. Figure 3.1(a) showed a schematic illustration of the shape-memory mechanism for PCL-based SMPs. When heat above its Tm is applied upon the semicrystalline SMP, accompanied by melting of the crystal regions, the molecular mobility of the chains will increase. At this time, the SMP can be deformed by the application of external stress. Upon cooling below its crystallization temperature (Tc), the recrystallization process can contribute to the weakening of the chain mobility, which enables the storage of entropic energy in the SMP in the form of elastic potential energy. After which, the stored energy can be released upon reheating, which reactivates the chain mobility and drives it back into its original shape, which is the highest entropic state.[34,35]

Extensive research has shown that the semicrystalline feature of PCL contributes to a tunable mechanical property, which is greatly dependent on its crystallinity. Several attempts have been made to substantiate the crystallinity effect on mechanical properties. Miyasako et al.[86] reported a copolymer of ε-caprolactone (CL) and lactic acid, which endowed a drastic decrease in crystallinity due to the increased lactic acid ratio in the copolymers. The resultant copolymer exhibited weakened shape-memory characteristics. A similar copolymerization approach has been utilized by multiple recent studies, such as Xu et al.[87] reported a copolymer of CL and n-butyl acrylate that demonstrated decreased crystallinity. A simple alternative approach would be blending PCL with other polymers with low crystallinity to tune the crystallinity of the polymer network. Chen et al.[88] blended PCL with poly(L-lactide), and the resultant polymer blends showed crystallinity-dependent mechanical properties as well. We have reported a polymer blending approach of tuning the crystallinity using a polymer blend of tetra-branched and linear PCL.[25] Needless to concern the immiscibility when blending with

other types of polymers, this blending approach achieved successful tuning of the crystallinity and obtained the design capability of polymer blends with a Tm between 30.7°C and 42.7°C without the loss of shape-memory characteristics.
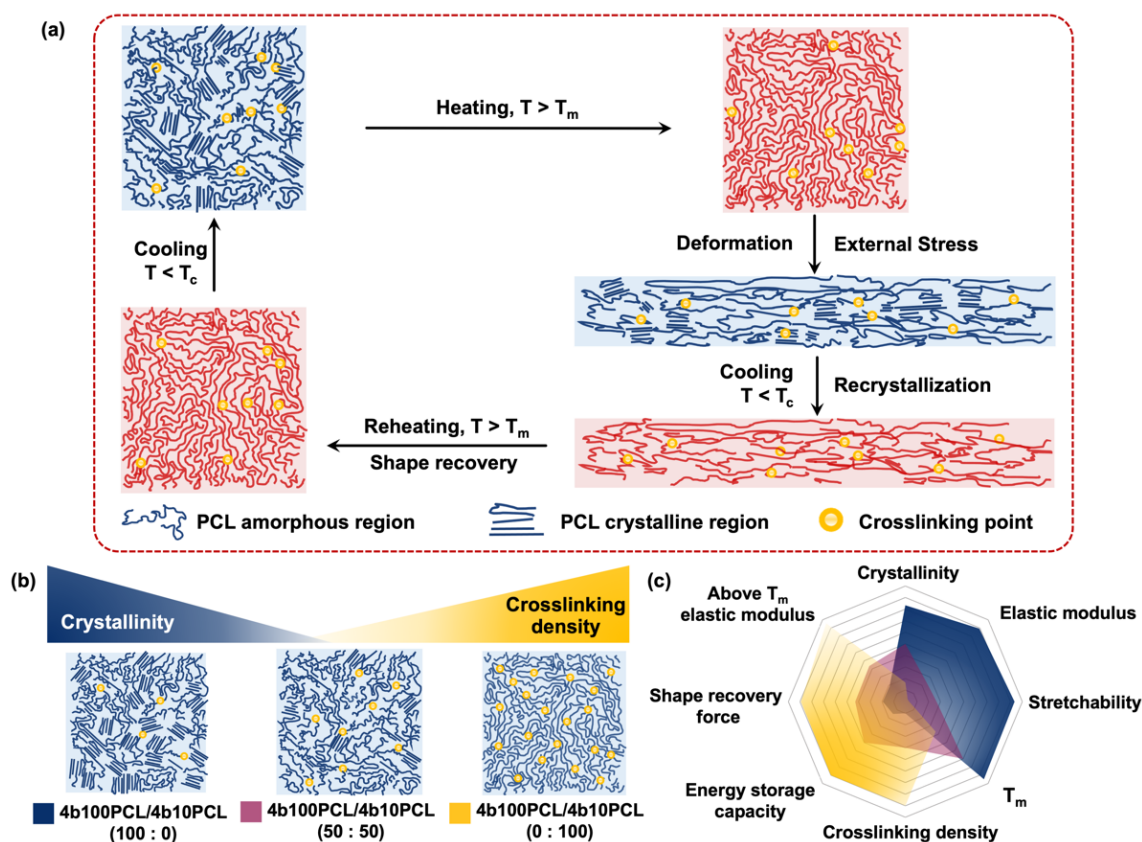

Figure 3.1 Schematic illustrations of (**a**) Shape-memory mechanism for semicrystalline PCL-based SMPs. (**b**) Decreased crystallinity gradient and increased crosslinking density gradient in 4b100PCL/4b10PCL SMPB achieved by the manipulation of amorphous 4b10PCL ratios. (**c**) Comparison of major physical properties and their expected correlations with crystallinity and crosslinking density in 4b100PCL/4b10PCL SMPBs. Different 4b100PCL/4b10PCL ratios are indicated by different colors.

Herein, we designed and fabricated a series of SMPBs using semicrystalline PCL-based SMPs that can provide clear crystallinity and crosslinking density gradients (Figure 3.1b). Tetra-branched PCL (4bPCL) has been reported to possess less entanglement and provide better crosslinking efficiency compared to linear PCL. Therefore, a stable thermally crosslinked polymer blend network was obtained by simply blending two types of 4bPCL macromonomers with long (high crystallinity) and short (low crystallinity) chain length, thermally initiated by benzoyl peroxide (BPO) and the acryloyl end group on a PCL macromonomer. Low molecular weight 4b10PCL

is theoretically amorphous after crosslinking resulted by the short chain length between crosslinking points, which can contribute to a higher crosslinking density and usually results in difficulty forming crystal regions.[89] Contrarily, high molecular weight 4b100PCL is highly crystalline and possesses excellent mechanical properties, as reported in our previous study.[17] By simply blending different ratios of amorphous 4b10PCL with highly crystalline 4b100PCL, we could obtain a series of polymer blends that could help distinguish the influence of crystallinity and crosslinking density on macroscopic thermal, mechanical, and shape-memory properties such as elastic modulus, stretchability, Tm, and shape recovery force, as shown in Figure3.1(c). With a better understanding of the influences of crystallinity and crosslinking density on the shape recovery force of semicrystalline SMPs, we can expect great convenience and precision in the future design of soft robotics, actuators, and biomedical devices.

3.3 Materials and Methods

3.3.1 Materials

Unless otherwise specified, all reagents were used as received. Pentaerythritol, tin (II) 2-ethylhexanoate, TEA and CL were purchased from Tokyo Chemical Industry Co., Ltd., Tokyo, Japan. THF (super dehydrated), xylene, hexane, diethyl ether (super dehydrated), acryloyl chloride, acetone, $CDCl_3$ with 0.05 v/v% TMS, and methanol were purchased from Wako Pure Chemical Industries Ltd., Osaka, Japan. BPO was purchased from Sigma-Aldrich, MO, USA, and dried prior to use.

3.3.2 Synthesis and characterizations of SMPs

3.3.2.1 Synthesis of 4bPCLs

Initiator, pentaerythritol (1.25 mmol, 168.93 mg) was pre-dried overnight after placing inside a 500mL flask prior to use. Monomer, CL (0.5 mol, 52.84 mL), was then added into the flask with dehydrated initiator under flowing nitrogen atmosphere by a glass syringe with a catalytic level of tin (II) 2-ethylhexanoate. The polymerization was carried out at 120 °C for 12 hours under nitrogen atmosphere. After which, 300 mL of THF was added into the product for dilution. The diluted mixture was then reprecipitated by 1500 mL of hexane/diethyl ether (1:1 v/v%) mixture solvent. The precipitated product was purified by filtration under vacuum and dried overnight under reduced pressure. The precipitate, 4b100PCL, was purified with the aforementioned mixture solvent repeatedly for 3 to 5 times to wash off the residual unreacted chemicals

and dried with the same approach. The dried 4b100PCL (98.2% yield) was collected and stored for further usage.[17,25]

The 4b10PCL (97.9% yield) was synthesized using the same approach with CL (0.5 mol, 52.84 mL) and pentaerythritol (12.5 mmol, 1.69 g).

3.3.2.2 Synthesis of 4bPCL macros

The previous obtained 4b100PCL (2.18 mmol, 100.0 g) was dissolved by superdehydrated THF (500mL) in a 500 mL flask by ultrasonication. After it's complete dissolved, an excessive amount of TEA (38.6 mmol, 3.91 mL) and acryloyl chloride (20.6 mmol, 1.862 mL) were added to the flask inside an ice bath and reacted for 12 hours in a shaded environment. The resulted product was reprecipitated against 1500 mL of methanol and filtrated to retrieve the precipitates. Such process was repeated three to five times for purification. Afterwards, the 4b100PCL macro was collected after drying under reduced pressure overnight.[17,25]

Similarly, 4b10PCL macro was synthesized with corresponding molar ratios.

3.3.2.3 Characterizations of 4bPCLs and 4bPCL macros

Chemical structures, degrees of polymerizations of 4bPCLs and 4bPCL macros, the end group introduction rate (I.R.) of 4bPCL macros were determined by ^{1}H NMR, JEOL, Tokyo, Japan, in CDCl$_3$ with 0.05 v/v% TMS. Their molecular weights were determined by GPC, JASCO International, Tokyo, Japan using PS as calibration standards and DMF as the elution solvent.

The results of molecular weight, polydispersity index (PDI), and I.R. of the 4b10PCL macro and 4b100PCL macro are summarized in Table 3.1.

Table 3.1. Molecular weights, polydispersity indexes and end group introduction rates of 4b10PCL and 4b100PCL macromonomers.

Polymer type	Mn (Da) [1]	Mw (Da) [1]	PDI [1]	I.R. (%) [2]
4b10 PCL-macro	6296	7022	1.115	99.3
4b100 PCL-macro	41126	63661	1.550	95.2

1) Measured by GPC. Solvent: DMF. Calibration standards: PS.

2) Calculated by ^{1}H NMR; solvent: CDCl$_3$

3.3.3 Fabrication of SMPB films

The crosslinked SMPB films were fabricated through free radical polymerization

of the thermal initiator BPO and the previously collected 4bPCL macros. The 4bPCL macros (500.0 mg) were dissolved in xylene with a polymer concentration of 40 wt% to polymer, and a BPO concentration of 5 wt% under ultrasonication. The mixture solutions were casted between two glass slides with a Teflon® spacer with a thickness of 0.3 mm. The reaction was carried out at 80 °C for 6 hours. After which, the crosslinked SMPB films were demolded and washed by acetone exchanged for 2 days to remove the residual chemicals. The obtained SMPB films were then washed with methanol for 12 hours and dried under reduced pressure overnight. Afterwards, the SMPB films were annealed at 60°C oven for 10 min and collected after cooling down at room temperature.[17,36]

3.3.4 Swelling ratio measurements

The crosslinked cylindrical samples were prepared by the film fabrication conditions above using a 0.3-mm-diameter capillary tubes as molds corresponding to the 0.3-mm Teflon spacer for the SMPB films. The SMPB capillary tubes were swelled in THF solutions for 48 h to reach the equilibrium state. Diameters of the SMPB capillary tubes after swollen were measured by laser scanning microscope (VK-X1000, Keyence Co.,) at five different spots on each film. The swelling ratio (Q) of each sample was estimated by its volumetric change according to the equation $Q = (L_s/L_0)^3$, where L_s and L_0 are the diameters of the specimen at the equilibrium swollen state and the initial diameter of the specimen, respectively. The reproducibility of the test was confirmed by a minimum of three samples from each condition.

3.3.5 Thermal characterizations

Thermal properties of the SMP strings were characterized using differential scanning calorimetry (DSC) (7000X, Hitachi High-Tech Science, Japan). All specimens were first equilibrated at 100°C and then cooled to -30°C. The DSC curves were obtained in the second heating run at a rate of 5 °C min^{-1} for all runs. The degree of crystallinity (χ_c) was calculated using the enthalpy change (ΔH), according to the equation $\chi_c = \Delta H / \Delta H_m$, where ΔH is the specific melting enthalpy for each SMPB blend films and ΔH_m is the specific melting enthalpy for theoretically 100% crystalline PCL, which is considered as 136 J g^{-1} according to literature.[74]

3.3.6 Mechanical characterizations

All mechanical properties of the SMPB films were characterized by a uniaxial tensile tester (EZ-S 500N, Shimadzu, Kyoto, Japan) equipped with a heating chamber (M-600FN, TAITEC, Saitama, Japan) for temperature control. All uniaxial tensile tests were conducted at an elongation rate of 5 mm min^{-1} at 25 °C or 60 °C. All specimens had approximately 4.5-mm width, 30.0-mm length, and 0.3-mm thickness. The elastic modulus of the specimen was calculated from the initial slope of its stress–strain curve. The toughness was calculated from the integrated area under the stress-strain curve until break for each specimen. The energy storage capacity at each stretched strain was defined as the corresponding integrated area under the stress-strain curve at 60°C. All data are presented as mean ± SD, n=3.

Shape recovery-induced contraction force was measured using "hold mode" with the same tensile tester. A heat source of approximately 60 °C was applied onto the specimen at a distance of 10 cm, after held for 20 s under the pre-load of 0.1 N. The recovery-induced contraction force was recorded until heat source was removed. Shape recovery-induced contraction force was defined as the maximum force that was recorded during each process. All data are presented as mean ± SD, n=3.

3.3.7 Shape-memory characterizations

The 4b100PCL/4b10PCL SMPB films were first equilibrated at 70°C and stretched to 800% strain (within the maximum deformation range for 4b100PCL/4b10PCL SMPB films with 0–30 w.t.% of 4b10PCL ratios). Then they were cooled at 0°C, accompanied by the removal of the external stress. Shape recovery was actuated by reheating upon 70°C (above all sample's Tm). The shape fixity ratios (R_f) of all 4b100PCL/4b10PCL SMPB films were calculated according to the equation R_f= 100% × ε/$ε_{load}$, where $ε_{load}$ represents the initial stretched strain and ε represents the fixed strain after removing the external stress. The shape recovery ratios (R_r) of the 4b10/4b100 SMPB films were calculated according to the equation R_r = 100% × (ε-$ε_{rec}$)/ε, where $ε_{rec}$ represents the recovered strain.[52]

The shape recovery force was measured using a strain-controlled Dynamic Mechanical Analyzer (ARES G2, TA Instruments) with a designated program. The 4b100PCL/4b10PCL SMPB films were equilibrated at X°C (each SMPB film's Tm + 10°C) at the speed of 10°C min^{-1}. Then annealed for 2 mins, and stretched to various strains (50%, 100%, 200%, 300%, 500%, and 800% for each SMPB films within their deformation ranges at a speed of 1 mm min^{-1}. All specimens were then cooled down to Y°C (each SMPB film's Tc –20°C) at the speed of 10°C min^{-1}, held at equilibrium for 5 min before reheating to X°C at the maximum speed. The shape recovery force was

recorded as the induced instantaneous force upon reheating process. A minimum of three samples from each condition were tested to confirm the reproducibility.

3.4 Results and discussions

3.4.1 Thermal properties of SMPBs

The thermal properties of semicrystalline polymers have been reported to be greatly influenced by their crystallinity. For the substantiation of the crystallinity effect of the 4b100PCL/4b10PCL SMPBs, their thermal properties were evaluated by DSC. The endothermic melting peaks of 4b100PCL/4b10PCL SMPB films in Figure 3.2a demonstrated a clear decreasing peak positions with the increase of the 4b10PCL ratios. The same decreasing positions were observed at the exothermic crystallization peaks in Figure 3.2(b). The T_m, T_c, melting enthalpy (ΔH_m), crystallization enthalpy (ΔH_c) and calculated degree of crystallinity (χ_c) are summarized in Table 3.2.
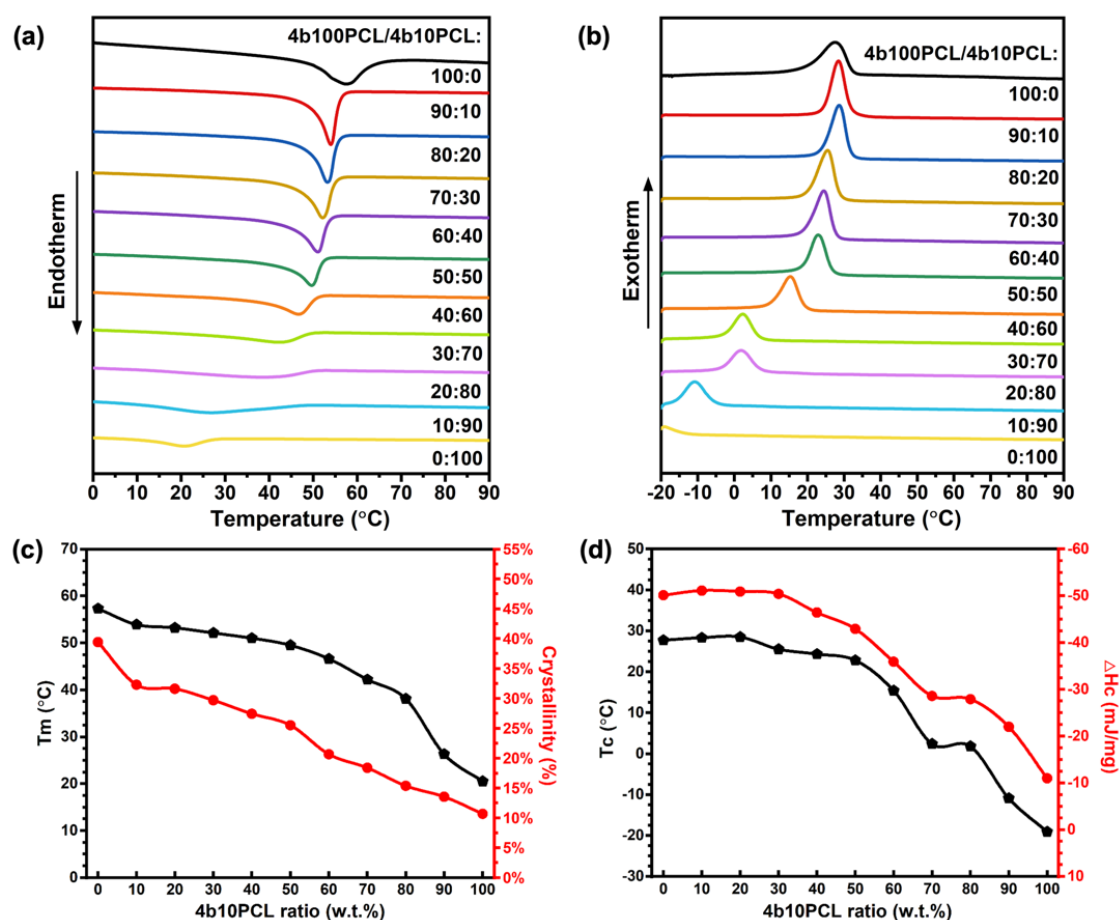

Figure 3.2 Thermal properties of 4b100PCL/4b10PCL SMPBs prepared with different 4b10PCL ratios. (**a**) DSC melting curves, (**b**) DSC crystallization curves, (c) melting temperature and crystallinity, (d) crystallization temperature and ΔHc of the

4b100PCL/4b10PCL polymer blends.

The Tm and Tc of the crosslinked 4b100PCL homopolymer were 57.3°C and 27.7°C, respectively, while the crosslinked 4b10PCL homopolymer is theoretically amorphous and showed a shallow melting peak at around 20.5°C and a crystallization peak at around -19.1°C. Figure 3.2c and Figure 3.2d demonstrates that the increasing blending ratios of amorphous 4b10PCL can be attributed to a clear decreasing tendency of crystallinity from 39.41–10.66%. Consequently, Tm and Tc both showed excellent maneuverability with a large design capability (20.5–57.3°C for Tm and -19.1–27.7°C for Tc), which proves the crystallinity-dominant effect on thermal properties of the polymer blending systems, which is consistent with previous literature.[89,90]

Table 3.2. Thermal properties of 4b100PCL/4b10PCL SMPBs

Sample names	Tm (ºC)	Tc (ºC)	ΔH_m (mJ/mg)	ΔH_c (mJ/mg)	χ_c (%)
4b100PCL/4b10PCL_100:0	57.3	27.7	53.6	-50.1	39.4
4b100PCL/4b10PCL_90:10	53.9	28.3	43.9	-51.1	32.2
4b100PCL/4b10PCL_80:20	53.2	28.5	43	-50.9	31.6
4b100PCL/4b10PCL_70:30	52.1	25.5	40.4	-50.4	29.7
4b100PCL/4b10PCL_60:40	51	24.3	37.3	-46.4	27.4
4b100PCL/4b10PCL_50:50	49.5	22.8	34.7	-42.9	25.5
4b100PCL/4b10PCL_40:60	46.6	15.4	28.1	-35.9	20.6
4b100PCL/4b10PCL_30:70	42.2	2.4	25	-28.6	18.3
4b100PCL/4b10PCL_20:80	38.1	1.8	20.9	-27.9	15.3
4b100PCL/4b10PCL_10:90	26.3	-10.9	18.4	-22	13.5
4b100PCL/4b10PCL_0:100	20.5	-19.1	14.5	-11	10.6

Similar results were substantiated by the X-ray diffraction (XRD) patterns of the 4b100PCL/4b10PCL SMPBs (Figure. 3.3). Two distinct diffraction peaks were observed for all blend polymer samples at $2\theta = 21.6°$ and $2\theta = 23.8°$, which respectively correspond to the (110) and (200) planes of orthorhombic crystalline structures of PCL.[72] The decreasing peak areas under the XRD patterns of the 4b100PCL/4b10PCL SMPBs substantiated the decreasing crystallinity gradient of the 4b100PCL/4b10PCL SMPBs.
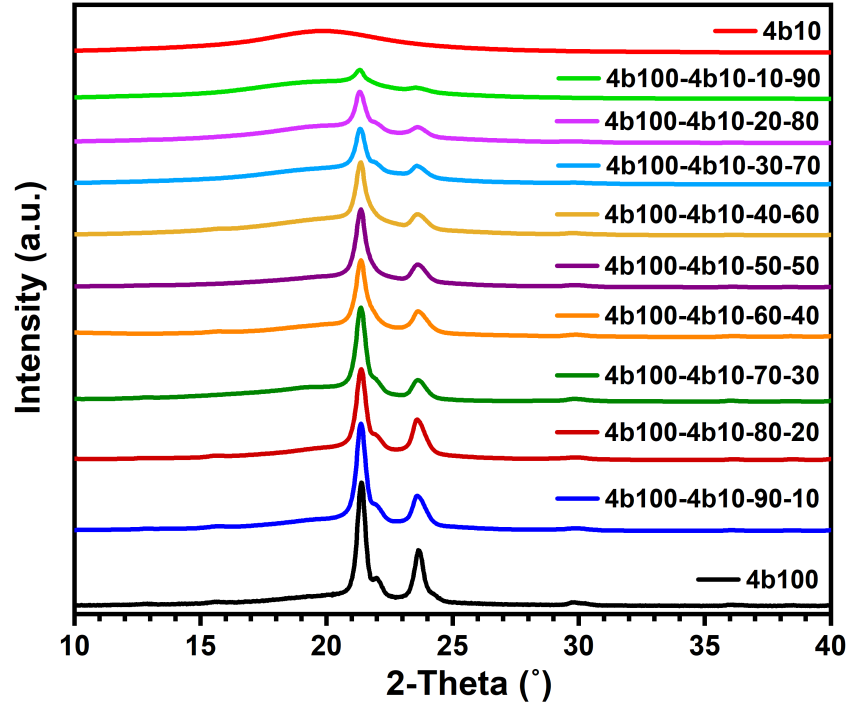
Figure 3.3. XRD patterns of 4b100PCL/4b10PCL SMPB films.

3.4.2 Mechanical Properties of SMPBs

A number of mechanical properties, including elastic modulus at room temperature and toughness, are crucial for the practical application of semicrystalline SMPs in a variety of fields. In these polymer blending systems, various mechanical properties were investigated to determine the influences of crystallinity and crosslinking density. Figure 3.4(a) provides a brief schematic illustration of the decreasing crystallinity gradient of the 4b100PCL/4b10PCL SMPBs. As substantiated in the previous section, the increase of the short chain amorphous 4b10PCL ratio could have led to the hindrance in forming the crystal region, resulting in the clear decreasing crystallinity gradient in the polymer blending systems. The correlations between this crystallinity change and the mechanical properties were investigated by uniaxial tensile tests.

The elastic moduli, toughness, and stress–strain curves of the 4b100PCL/4b10PCL SMPBs in the uniaxial tensile test at room temperature are shown in Figure 3.4(b) and Figure 3.4(c). The related data are summarized in Table 3.3. The results revealed a drastic decrease in elastic modulus as well as toughness at room temperature, which correspond to the decline in the degree of crystallinity. Compared to the elastic modulus of the 4b100PCL homopolymer (approximately 250.4 MPa), that of the 4b10PCL homopolymer was extremely low (2.6 MPa) due to its amorphous

feature. This proved that crystallinity is the dominant factor in determining the stiffness and toughness of the semicrystalline SMPs. In addition, the decrease in crystallinity resulted in the decline in strain at the break of the SMPBs, as depicted in the typical stress–strain curves of the 4b100PCL/4b10PCL SMPB films in Figure 3.4d. Moreover, the 4b100PCL/4b10PCL SMPB films with 0–50 w.t.% of 4b10PCL ratios all presented a typical stress–strain curve of thermoplastic polymer with a clear yielding point, necking feature, and a hardening process, which accord with the previous literature.[72] Furthermore, the 4b100PCL/4b10PCL SMPB films with 60–90 w.t.% of 4b10PCL ratios presented highly crosslinked rubber-like tensile features with relatively short strains at break, in accordance with the 4b10PCL homopolymer.
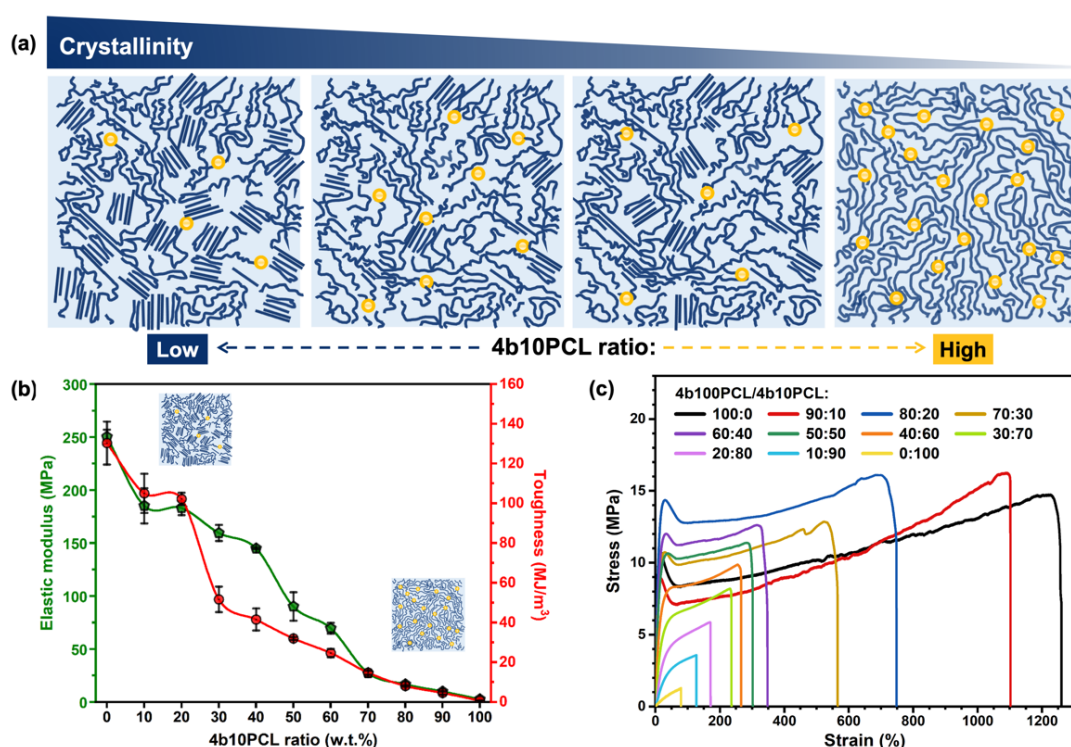

Figure 3.4 Crystallinity dominant effect on the mechanical properties of 4b100PCL/4b10PCL SMPBs at 20°C. (**a**) Schematic illustrations of the decreasing crystallinity of the 4b100PCL/4b10PCL SMPBs with the increase of the amorphous 4b10PCL ratio, (**b**) Elastic modulus and toughness, and (**c**) stress–strain curves of the 4b100PCL/4b10PCL SMPBs with gradient 4b10PCL ratios.

In addition to the mechanical properties at room temperature investigated above, which were proven to be mainly dominated by the crystallinity of the polymer blending systems, the mechanical properties above Tm were of great significance. These include the elastic modulus and stretchability at 60°C, at which temperature the influence of

crystallinity is expected to be omitted due to the elimination of crystal regions above all samples' Tm.

Table 3.3. Mechanical properties of 4b100PCL/4b10PCL SMPBs in the uniaxial tensile test at room temperature.

Sample names	Elastic modulus (MPa)	Toughness (MJ/m^3)	Strain at break (%)
4b100PCL/4b10PCL_100:0	250.4	130.4	1003.6
4b100PCL/4b10PCL_90:10	185.1	105.0	952.6
4b100PCL/4b10PCL_80:20	183.0	102.2	872.0
4b100PCL/4b10PCL_70:30	159.5	51.6	549.2
4b100PCL/4b10PCL_60:40	144.9	41.5	359.5
4b100PCL/4b10PCL_50:50	90.2	32.0	315.3
4b100PCL/4b10PCL_40:60	69.6	24.7	283.9
4b100PCL/4b10PCL_30:70	27.3	14.7	245.5
4b100PCL/4b10PCL_20:80	16.6	8.1	197.9
4b100PCL/4b10PCL_10:90	9.9	4.5	151.6
4b100PCL/4b10PCL_0:100	2.6	0.6	86.5

As briefly sketched in Figure 3.5(a), the shorter-branched feature represents 4b10PCL, and the longer one represents 4b100PCL. The incorporation of short-chain 4b10PCL with crosslinkable end groups is thought to contribute to a highly crosslinked polymer network. Thus, with the increase of the incorporation amount of 4b10PCL, it is inferred that the 4b100PCL/4b10PCL SMPBs possess an enhanced crosslinking density. The swelling ratios of the 4b100PCL/4b10PCL SMPB films were measured in THF, a good solvent for PCL, for 48 h (until equilibrium) to confirm the hypothesized increase in the crosslinking density gradient of the aforementioned systems. As shown in Figure 3.5(b), owing to the increase in crosslinking density, the swelling ratio showed a decreasing tendency with regards to the 4b10PCL ratios, which is in accordance with the previous hypothesis.

For further confirmation of the increasing crosslinking density gradient of the blend polymer systems, the above Tm mechanical properties were investigated using uniaxial tensile tests at 60°C. The elastic moduli and stretchability of the 4b100PCL/4b10PCL SMPBs are shown in Figure 3.5(c), and related data are

summarized in Table 3.4. The typical stress–strain curves of the 4b100PCL/4b10PCL SMPBs are compared in Figure 3.5(d), and the stress–strain curves of the 4b100PCL/4b10PCL polymer blend films with 50–100 w.t.% of 4b10PCL ratios are shown in Figure 3.5(e). A drastic decline in the stretchability of the blend polymers from 1419.5% for 4b100PCL to merely 50.5% for 4b10PCL was observed. When increasing the low molecular weight 4b10PCL ratios in the 4b100PCL/4b10PCL SMPBs, the chain length between crosslinking points drastically decreases, resulting in an elevated crosslinking density and an extensive decline in chain mobility which led to this almost a 30-fold difference in stretchability. Based on the same grounds, a steady inclining tendency of the elastic modulus at 60°C from approximately 0.58 MPa for 4b100PCL to around 2.05 MPa for 4b10PCL was found, which was attributed to the highly crosslinked polymer network.
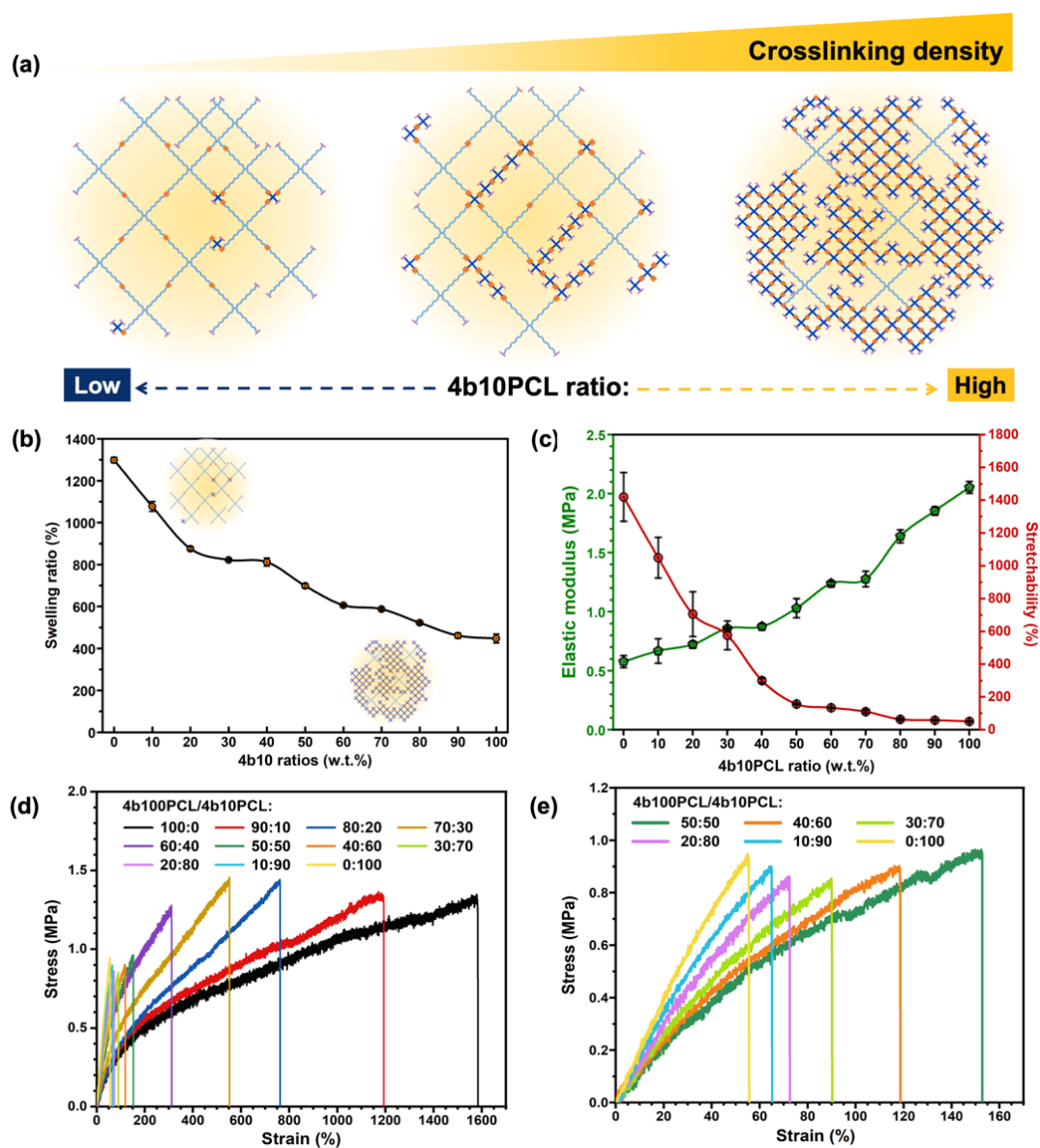
Figure 3.5 Crosslinking density dominant effect on the mechanical properties of 4b100PCL/4b10PCL SMPBs at 60°C. (**a**) Schematic illustrations of increasing crosslinking densities of the 4b100PCL/4b10PCL SMPBs with the increase of the short-chained 4b10PCL ratios, (**b**) swelling ratios measured at room temperature, (**c**) elastic modulus and stretchability, (**d**) stress–strain curves of the 4b100PCL/4b10PCL polymer blends with gradient 4b10PCL ratios. and (**e**) zoomed in stress–strain curves of the 4b100PCL/4b10PCL SMPBs with 0–50 w.t.% of 4b10PCL ratios.

Table 3.4. Mechanical properties of 4b100PCL/4b10PCL SMPBs in the uniaxial tensile test at 60ºC.

Sample name	Elastic modulus (MPa)	Stretchability (%)
4b100PCL/4b10PCL_100:0	0.5772	1419.5
4b100PCL/4b10PCL_90:10	0.6677	1049.0
4b100PCL/4b10PCL_80:20	0.7221	705.3
4b100PCL/4b10PCL_70:30	0.8579	576.1
4b100PCL/4b10PCL_60:40	0.8740	299.6
4b100PCL/4b10PCL_50:50	1.0302	156.3
4b100PCL/4b10PCL_40:60	1.2391	133.6
4b100PCL/4b10PCL_30:70	1.2766	110.0
4b100PCL/4b10PCL_20:80	1.6381	63.2
4b100PCL/4b10PCL_10:90	1.8530	57.5
4b100PCL/4b10PCL_0:100	2.0528	50.5

3.4.3 Shape-memory Properties of SMPBs

The crystallinity and crosslinking density effects on macroscopic thermal and mechanical properties were probed in the previous sections. The ultimate purpose of understanding the correlations of the aforementioned parameters and their influences on the shape recovery force are discussed in this section. During the shape-memory cycle, after deformation upon heating, the recrystallization process can provide fixation of the temporary secondary shape due to the weakening of the chain mobility. In turn, the entropic energy that was endowed during the heating and deformation process can be stored inside the SMPs in the form of elastic potential energy. The amount of the energy stored inside, called the energy storage capacity, can be released upon the

reactivation of chain mobility during the reheating, which could be the main driving force of the shape recovery force. Therefore, the energy storage capacity and shape recovery force of the 4b100PCL/4b10PCL polymer blending systems were investigated to obtain a better understanding of their correlations and dominant influential factors.
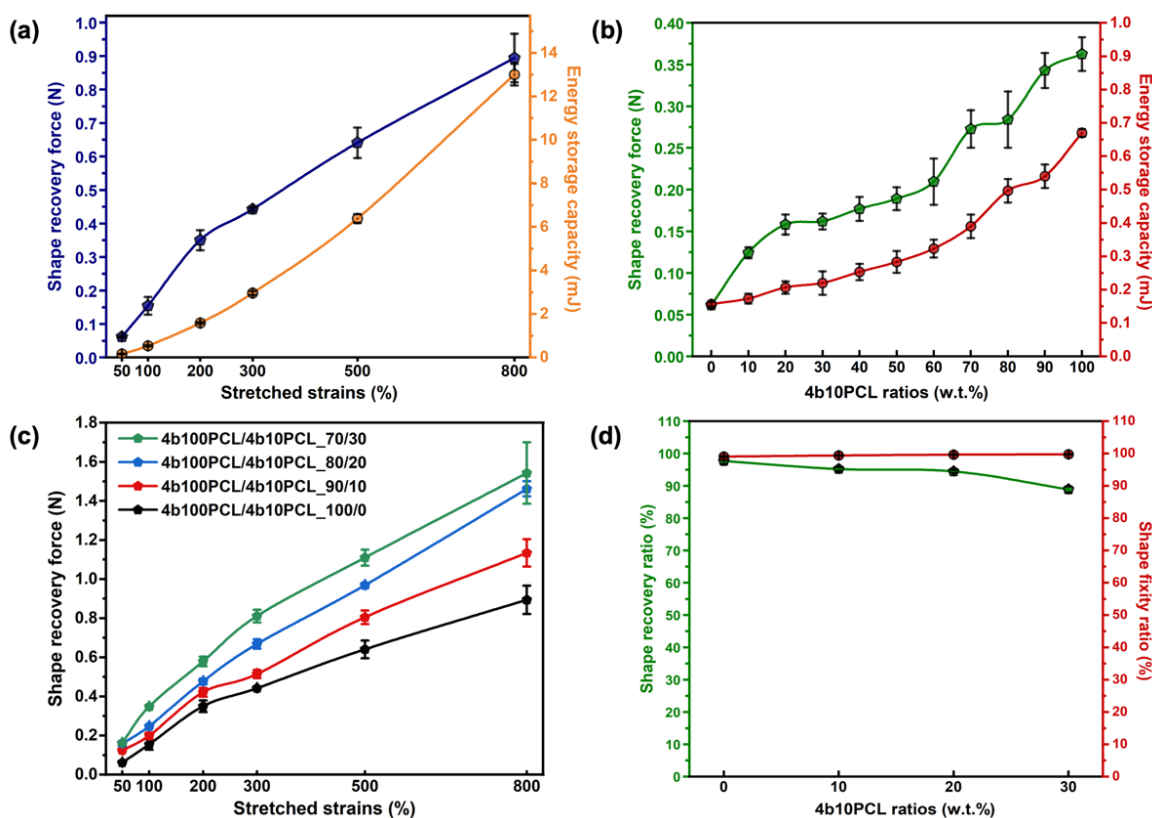

Figure 3.6. Shape-memory properties, shape recovery forces, and their correlations with the energy storage capacities of the 4b100PCL/4b10PCL SMPBs. Shape recovery force and energy storage capacities of (**a**) 4b100PCL at different stretched strains and (**b**) 4b100PCL/4b10PCL SMPBs with gradient 4b10PCL ratios at 50% stretched strain. (**c**) Shape recovery forces of 4b100PCL/4b10PCL SMPBs with 0–30 w.t.% of 4b10PCL ratios at different stretched strains. (**d**) Shape recovery ratios and shape fixity ratios of 4b100PCL/4b10PCL SMPBs with 0–30 w.t.% of 4b10PCL ratios at a large deformation of 800%.

In our previous study, we reported that the increase in stretched strains could give rise to a stronger shape recovery force and better contraction effect.[17] For support of this conclusion, the shape recovery forces and energy storage capacities at different stretched strains of 4b100PCL are depicted in Figure 3.6(a). The shape recovery force of the 4b100PCL homopolymer greatly enhanced from 0.061 N at 50% strain to 0.894

N at 800% strain. These results are in accordance with the previous conclusion that an almost linear enhancement in shape recovery force that correlates with the energy storage capacity in response to the increase of the stretched strains occurs.[17,91] Moreover, evidence suggests that crosslinking density is among the most important factors for tuning the shape-memory properties.[52] On this basis, due to the poor stretchability of 4b10PCL SMP film, the investigation of the influential effect was conducted by comparing the shape recovery forces and energy storage capacities of 4b100PCL/4b10PCL SMPB films stretched at 50% strain. Figure 3.6(b) shows a clear inclining correlation of both shape recovery force and energy storage capacity with regards to the increasing 4b10PCL ratio, which corresponds with the crosslinking density gradient. On this basis, we could conclude that shape recovery force was mainly dominated by the crosslinking density instead of the degree of crystallinity in the polymer blending system when stretched at the same strains. For further confirmation of this preliminary result, the shape recovery forces of 4b100PCL/4b10PCL SMPBs with 0–30 w.t.% of 4b10PCL ratios at a small strain of 50% to a large deformation of 800% were measured (Figure 3.6c). The summarized results also demonstrated a clear strain-dependent enhancement of the shape recovery force. Furthermore, the shape recovery forces were all gradually elevated with regards to the 4b10PCL ratios at every strain, which proved the dominance of the crosslinking density effect in such property. Large deformations like 800% have been commonly reported to greatly deteriorate shape-memory properties. Therefore, the shape fixity and shape recovery ratios of the 4b100PCL/4b10PCL SMPBs with 0–30 w.t.% of 4b10PCL ratios stretched at 800% are shown in Figure 3.6(d). The results showed that all samples possessed excellent shape fixities above 99.00%. A slight increase from 99.05% shape fixity for 4b100PCL to 99.73% for the 4b100PCL/4b10PCL_70/30 SMPBs was observed. Contrarily, the shape recovery ratio decreased from 97.67% for 4b100PCL to 88.89% for the 4b100PCL/4b10PCL_70/30 SMPBs. The changes in shape-memory properties were most likely due to the highly crosslinked polymer network at large deformations resulting in an alignment in the crystal region during recrystallization, which contributes to a relatively better fixation and energy storage and slightly weakened recovery due to the decrease in total crystallinity. However, the shape-memory properties were still excellent despite the large deformation. Therefore, a simple manipulation of SMPB system using minor amount of short-chain 4b10PCL can enhance the shape recovery force by approximately 166% (0.061 N for 4b100PCL homopolymer and 0.162 N for 4b100PCL/4b10PCL_70/30 SMPB at 50% stretched strains) without compromising much of shape-memory performance.

3.5 Conclusions

In this chapter, we designed a simple polymer blending system using a series of 4bPCL-based SMPs with long and short branch chain lengths that demonstrate decreased crystallinity and increased crosslinking density gradients. The influences of crystallinity and crosslinking density on the polymer blends were investigated, and result confirmed the crystallinity dominant effect on thermal properties and mechanical properties at room temperature, such as elastic modulus, stretchability, and toughness. The crosslinking density dominant effect was shown in the mechanical properties at 60°C at the shape recovery force of the SMPBs. With the understanding gained from this study, we could achieve a series of polymer blending systems with highly manipulable mechanical properties covering a wide range, such as stretchability (50.5– 1419.5%) and toughness (0.62–130.4 MJ m^{-3}), while maintaining excellent shape-memory properties even at a large deformation of 800%. Although the shape recovery force was proven to be dominated by the crosslinking density of the polymer network, the stretchability was also decreased in response to the decreased chain length between crosslinking points due to the elevated crosslinking density. Therefore, balanced manipulation between crystallinity and crosslinking density in the polymer network of SMPs is required for the design of an appropriate range for the shape recovery force. The elucidation of the factors influencing each property gained from this study is expected to contribute to better design of semicrystalline SMP networks, in turn providing great potential for future applications in soft robotics, actuators, and biomedical devices.

Reference

[1] A. Fulati, K. Uto, M. Ebara, Polymers. 2022, 14, 4740.

[2] A. Lendlein, R. Langer, Science. 2002, 296, 1673.

[3] M. Ebara, K. Uto, N. Idota, J. M. Hoffman, T. Aoyagi, Adv. Mater. 2012, 24, 273.

[4] S. Ouchi, E. Niiyama, K. Sugo, K. Uto, S. Takenaka, A. Kikuchi, M. Ebara, Biomater. Sci. 2021, 9, 6957.

[5] S. Ishii, K. Uto, E. Niiyama, M. Ebara, T. Nagao, ACS Appl. Mater. Interfaces 2016, 8, 5634.

[6] Q. Shou, K. Uto, M. Iwanaga, M. Ebara, T. Aoyagi, Polym. J. 2014, 46, 492.

[7] G. M. Baer, W. Small, T. S. Wilson, W. J. Benett, D. L. Matthews, J. Hartman, D. J. Maitland, Biomed. Eng. Online 2007, 6, 43.

[8] W. Small IV, T. S. Wilson, W. J. Benett, J. M. Loge, D. J. Maitland, Opt. Express 2005, 13, 8204.

[9] I. Yungerman, I. Starodumov, A. Fulati, K. Uto, M. Ebara, Y. Moskovitz, J. Phys. Chem. B 2022, 126, 3961.

[10] D. Schönfeld, D. Chalissery, F. Wenz, M. Specht, C. Eberl, T. Pretsch, Molecules 2021, 26, DOI 10.3390/molecules26030522.

[11] J. J. Song, H. H. Chang, H. E. Naguib, Eur. Polym. J. 2015, 67, 186.

[12] B. Q. Y. Chan, Z. W. K. Low, S. J. W. Heng, S. Y. Chan, C. Owh, X. J. Loh, ACS Appl. Mater. Interfaces 2016, 8, 10070.

[13] Y. Zhang, N. Zhang, H. Hingorani, N. Ding, D. Wang, C. Yuan, B. Zhang, G. Gu, Q. Ge, Adv. Funct. Mater. 2019, 29, 1806698.

[14] J. Wang, Z. Tu, H. Zhang, M.-M. Wang, W. Liu, J.-P. Qu, Macromolecules 2022, 55, 3986.

[15] K. Wang, X. X. Zhu, ACS Biomater. Sci. Eng. 2018, 4, 3099.

[16] Y. Li, D. Wang, J. Wen, J. Liu, D. Zhang, J. Li, H. Chu, Adv. Funct. Mater. 2021, 31, 2011259.

[17] B. Kumar, J. Hu, N. Pan, Biomaterials 2016, 75, 174.

[18] A. Fulati, K. Uto, M. Iwanaga, M. Watanabe, M. Ebara, Adv. Healthc. Mater. 2022, 11, 2200050.

[19] Q. Zhao, H. J. Qi, T. Xie, Prog. Polym. Sci. 2015, 49–50, 79.

[20] Y. Xia, Y. He, F. Zhang, Y. Liu, J. Leng, Adv. Mater. 2021, 33, 2000713.

[21] H. Miyasako, K. Yamamoto, A. Nakao, T. Aoyagi, Macromol. Biosci. 2007, 7, 76.

[22] Z.-Y. Xu, L. Li, L.-Y. Shi, K.-K. Yang, Y.-Z. Wang, Macromolecules 2022, 55, 5104.

[23] J. Chen, C. Deng, R. Hong, Q. Fu, J. Zhang, J. Polym. Res. 2020, 27, 221.

[24] K. Uto, K. Yamamoto, S. Hirase, T. Aoyagi, J. Control. Release 2006, 110, 408.

[25] I. Sedov, T. Magsumov, A. Abdullin, E. Yarko, T. Mukhametzyanov, A. Klimovitsky, C. Schick, Polymers (Basel). 2018, 10, 902.

[26] B. Lepoittevin, M. Devalckenaere, N. Pantoustier, M. Alexandre, D. Kubies, C. Calberg, R. Jérôme, P. Dubois, Polymer (Guildf). 2002, 43, 4017.

[27] W. Miao, W. Zou, Y. Luo, N. Zheng, Q. Zhao, T. Xie, Polym. Chem. 2020, 11, 1369.

[28] E. D. Rodriguez, X. Luo, P. T. Mather, ACS Appl. Mater. Interfaces 2011, 3, 152.

[29] A. Babaie, M. Rezaei, R. L. M. Sofla, J. Mech. Behav. Biomed. Mater. 2019, 96, 53.

[30] M. Baniasadi, M.-A. Maleki-Bigdeli, M. Baghani, Smart Mater. Struct. 2020, 29, 055011.

Chapter 4 Design of Laser Actuatable Shape-memory Polymers

4.1 Abstract

Laser actuatable shape-memory polymers (SMPs) exhibit great potential in various emerging applications, such as artificial muscles, soft actuators, especially biomedical field, owing to their remote controllability because of the convenience of indirect heating. We have designed and fabricated a series of laser actuatable SMP composites by incorporating magnetic nanoparticles (MNPs) into poly(ε-caprolactone) (PCL)-based semicrystalline SMP networks. Compared with other photothermal fillers, MPNs can be well dispersed in with the SMP networks, providing excellent photothermal effect because of their strong absorption of laser. The variation in temperature of the PCL/MNPs composites can be correlated with the incorporation amount of MNPs as well as the irradiation energy. These SMP composites showed excellent mechanical and shape memory properties under stress-free condition when the near-infrared (NIR) light is irradiated. The generated heat is larger for composites irradiated with a higher laser energy or with a higher incorporation amount of MNPs. Even the minimal incorporation amount could still induce enough heat for the actuation of the SMP composite. An artificial muscle mimicking weight-lifting test is designed and the liftable weight with high shape recovery ratios generated by these SMP composites are proven to be sufficient. The use of biodegradable polyesters and biocompatible MNPs makes such SMP composites potentially useful as biomedical devices.

4.2 Introduction

SMPs possess the capacity to spontaneously transform from a temporary shape to a permanent shape upon exposure to a variety of external stimuli such as heat,[2–4] light,[5,6] laser,[7,8] and magnetic field.[9,10] They have been widely used in many fields, such as actuators,[11] soft robotics,[12,13] and biomedical applications.[1,4] SMPs are particularly important in biomedical fields, such as embolization device,[14,15] implantable stents,[16,17] and intelligent sutures.[2] SMP-based biomedical devices are especially compatible with minimally invasive surgeries to solve the aforementioned shortcomings owning to the remote actuatable characteristics.

SMP-based biomedical devices induced by direct heating are always limited by

the applicable choices of external heating sources. In such case, remotely controllable, indirect heating source such as laser, remains to be an ideal actuation approach. Besides, near-infrared (NIR) light is with a wavelength length of 700-900 nm. NIR laser is reported to have strong penetrating capabilities in tissues compared to visible light.[18] Therefore, NIR is a common choice for the laser actuation of SMP-based materials.

A variety of thermally responsive SMPs have been reported as laser actuatable SMPs using photothermal conversion source. Versatile photothermal fillers have been loaded into thermally responsive SMPs to convert optical energy into heat and actuate the shape recovery process. For instance, Dai et al.[19] reported an SMP capable of selective actuation by NIR irradiation using a PCL-based polymer with polydopamine nanoparticles as photothermal filler. Similarly, Ward et al.[20] demonstrated a polyurethane-based laser actuatable SMP with gold nanorod as photothermal source. In our previous study, we utilized gold nanorod as photothermal filler for PCL-based laser actuatable SMPs as well.[6] However, in these approaches, due to the less-than ideal dispersibility of the aforementioned photothermal fillers, all of them requires additional modification before the incorporation of the SMPs to avoid poor dispersity in the SMP substrate.

On the other hand, MNPs have become ubiquitous in biomedical applications such as therapeutic microbots,[21] hyperthermia therapy for cancer,[22,23] and SARS-CoV-2 detection strips[24] owning to their great colloidal stability, biocompatibility and thermal property.[25] In our lab, we have developed a MNPs-incorporating linear PCL-based SMP for simultaneous thermo-chemotherapy. The film morphology exhibited excellent dispersion feature of MNPs inside PCL-based SMP films. An elevation in temperature up to 57 °C was obtained by the application of alternating magnetic field on linear PCL-film containing a large amount of MNPs of 46.1 wt%.[1,4]

Herein, we designed and fabricated a series of PCL/MNPs composite films using semicrystalline 4bPCLs that possessed excellent physical and shape-memory properties in the previous studies,[1,26] and MNPs as photothermal source for laser actuation. By simple incorporation of different ratios of MNPs inside PCL-based SMPs, we could obtain a series of laser actuatable SMP composites that possess excellent mechanical properties, shape-memory properties and strong shape recovery force that are selectively actuatable by laser irradiation. This simple yet universal design of laser actuatable SMPs can be envisioned to be applicable in versatile fields such as biomedical devices, soft robotics and actuators.
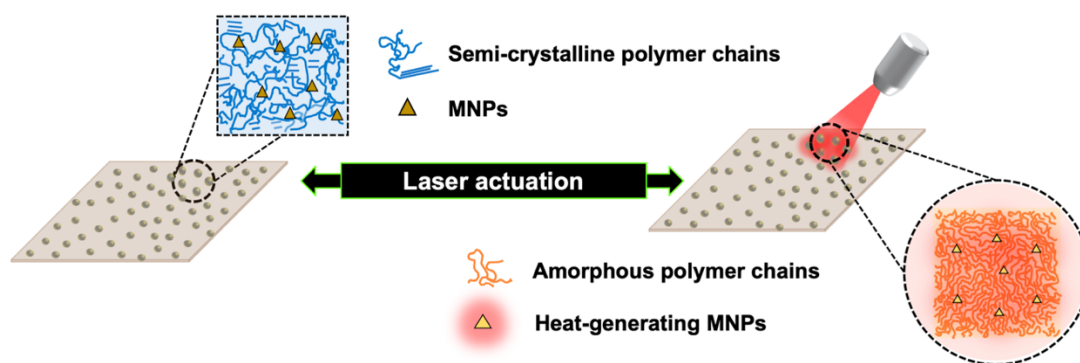
Figure 4.1 Schematic illustrations of shape-memory actuation mechanism for laser actuatable semi-crystalline PCL-based SMP composites with MNPs as photothermal fillers for the heat generation and NIR irradiation as actuation approach.

4.3 Materials and methods

4.3.1 Materials

All reagents were used as received unless otherwise specified. Pentaerythritol, acryloyl chloride, tin (II) 2-ethylhexanoate (Sn(Oct)$_2$), CL, and triethylamine were purchased from Tokyo Chemical Industry Co., Ltd., Tokyo, Japan. Xylene, tetrahydrofuran (THF) (super dehydrated), hexane, acetone, diethyl ether (super dehydrated), methanol, and chloroform-d (CDCl$_3$) with 0.05 v/v% tetramethylsilane (TMS) were purchased from Wako Pure Chemical Industries Ltd., Osaka, Japan. Benzoyl peroxide (BPO) and Iron oxide nanopowder (50-100 nm particles) were purchased from Sigma-Aldrich, MO, USA.[1,26]

4.3.2 SMP synthesis and characterizations

4.3.2.1 Synthesis of 4bPCLs

Initiator, pentaerythritol (1.25 mmol, 168.93 mg) was pre-dried overnight after placing inside a 500mL flask prior to use. Monomer, CL (0.5 mol, 52.84 mL), was then added into the flask with dehydrated initiator under flowing nitrogen atmosphere by a glass syringe with a catalytic level of tin (II) 2-ethylhexanoate. The polymerization was carried out at 120 °C for 12 hours under nitrogen atmosphere. After which, 300 mL of THF was added into the product for dilution. The diluted mixture was then reprecipitated by 1500 mL of hexane/diethyl ether (1:1 v/v%) mixture solvent. The precipitated product was purified by filtration under vacuum and dried overnight under

reduced pressure. The precipitate, 4b100PCL, was purified with the aforementioned mixture solvent repeatedly for 3 to 5 times to wash off the residual unreacted chemicals and dried with the same approach. The dried 4b100PCL (98.2% yield) was collected and stored for further usage.[1,27]

4.3.2.2 Synthesis of 4bPCL macros

The previous obtained 4b100PCL (2.18 mmol, 100.0 g) was dissolved by superdehydrated THF (500mL) in a 500 mL flask by ultrasonication. After it's complete dissolved, an excessive amount of TEA (38.6 mmol, 3.91 mL) and acryloyl chloride (20.6 mmol, 1.862 mL) were added to the flask inside an ice bath and reacted for 12 hours in a shaded environment. The resulted product was reprecipitated against 1500 mL of methanol and filtrated to retrieve the precipitates. Such process was repeated three to five times for purification. Afterwards, the 4b100PCL macro was collected after drying under reduced pressure overnight.[1,27]

4.3.2.3 Characterizations of 4bPCLs and 4bPCL macros

Chemical structures, degrees of polymerizations of 4bPCLs and 4bPCL macros, the end group introduction rate (I.R.) of 4bPCL macros were determined by ^{1}H NMR, JEOL, Tokyo, Japan, in CDCl$_3$ with 0.05 v/v% TMS. Their molecular weights were determined by GPC, JASCO International, Tokyo, Japan using PS as calibration standards and DMF as the elution solvent.[1,26]

4.3.3 Fabrication of PCL/MNPs composite SMP films

PCL/MNPs composite SMP films were fabricated using thermal initiator BPO and the previously synthesized 4bPCL-macros. The 4bPCL-macros (500.0 mg) were dissolved in xylene (40 w.t.%), after which BPO (10.0 mg, 2 w.t.%) and various ratios of MNPs were added under ultrasonication. The mixture was casted with a Teflon spacer (30 mm × 30 mm × 0.3 mm) sandwiched by two glass slides. The reaction was carried out at 80°C for 6 hours. Next, the crosslinked PCL/MNPs composite films were demolded and immersed in acetone for 2 days to remove the unreacted compounds. The obtained films were then washed with methanol for 2h before being dried under reduced pressure overnight. Dried composite films were annealed at 60°C oven for 10 min and collected after cooling down at room temperature.[1,26]

4.3.4 Thermal characterizations

Thermal properties of the SMP strings were characterized using differential scanning calorimetry (DSC) (7000X, Hitachi High-Tech Science, Japan). All specimens were first equilibrated at 100°C and then cooled to -30°C. The DSC curves were obtained in the second heating run at a rate of 5 °C min^{-1} for all runs. The degree of crystallinity (χ_c) was calculated using the enthalpy change (ΔH), according to the equation $\chi_c = \Delta H / \Delta H_m$, where ΔH is the specific melting enthalpy for each SMPB blend films and ΔH_m is the specific melting enthalpy for theoretically 100% crystalline PCL, which is considered as 136 J g^{-1} according to literature.[1,26,28]

4.3.5 Mechanical characterizations

All mechanical properties of the SMPB films were characterized by a uniaxial tensile tester (EZ-S 500N, Shimadzu, Kyoto, Japan) equipped with a heating chamber (M-600FN, TAITEC, Saitama, Japan) for temperature control. All uniaxial tensile tests were conducted at an elongation rate of 5 mm min^{-1} at 25 °C. All specimens had approximately 4.5-mm width, 30.0-mm length, and 0.3-mm thickness. The elastic modulus of the specimen was calculated from the initial slope of its stress–strain curve. The toughness was calculated from the integrated area under the stress-strain curve until break for each specimen. The energy storage capacity at each stretched strain was defined as the corresponding integrated area under the stress-strain curve at 60°C. All data are presented as mean ± SD, n=3.[1,26]

4.3.6 Transmittance of PCL/MNPs composite films

The transmittance of PCL/MNPs composite films were obtained by UV−visible spectra on a V-7200 spectrophotometer (JASCO co.td., Japan).

4.3.7 Laser measurements of PCL/MNPs composite films

The photothermal effect of PCL/MNPs composite films were evaluated by the heated temperature by the irradiation of a picosecond fiber laser (CALMAR Laser, with a wavelength of 780 ± 20 nm) at a distance of 50 cm and an initial energy of (500 mW/cm^2 to 4.5 W/cm^2 respectively) recorded with a thermal camera (FLIR Camera).

The laser actuation tests were measured using PCL/MNPs composite films stretched by 200% strain and added with additional weighs (2, 5, 10, 20g respectively).

Next, the external force was removed. The shape recovery was actuated by laser irradiation with aforementioned laser information at the initial energy density of 4.5W/cm^2. The shape recovery ratios (R_r) of the PCL/MNPs composite films were calculated as $R_r = 100\% \times (\varepsilon - \varepsilon_{rec})/\varepsilon$, where ε_{rec} represents the strain after recovery.[29]

4.4 Results and discussions
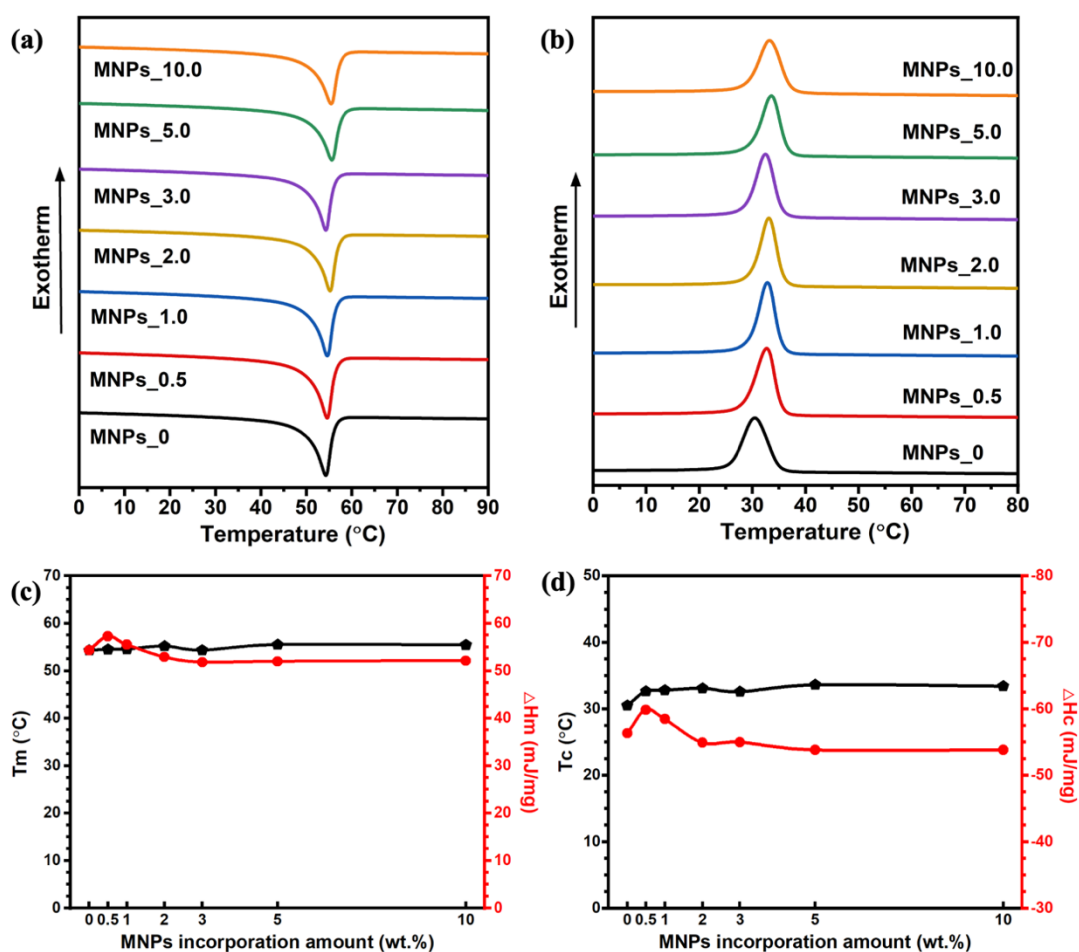
4.4.1 Thermal properties of PCL/MNPs composite SMP films

Figure 4.2 Thermal properties of PCL/MNPs composites prepared with different incorporation amount of MNPs (0.5, 1.0, 2.0, 3.0, 5.0, 10.0 wt.% respectively). **(a)** DSC melting curves, **(b)** DSC crystallization curves, (c) melting temperature and ΔH_m, and (d) crystallization temperature and ΔH_c of the PCL/MNPs composites.

The thermal properties of semicrystalline polymers have been reported to be greatly influenced by their crystallinity. The thermal properties of PCL/MNPs composite SMP films were evaluated by DSC. The endothermic melting peaks of

PCL/MNPs composites in Figure 4.2(a) demonstrated a relatively constant peak positions with the increase of the MNPs incorporation amount. The similar constant peak positions were observed at the exothermic crystallization peaks in Figure 4.2(b) as well. The Tm, Tc, melting enthalpy (ΔH_m) and crystallization enthalpy (ΔH_c) are shown in Figure 4.2 (c) and Figure 4.2(d). The Tm and Tc of the PCL film without incorporation of MNPs were 57.3°C and 27.7°C, respectively. Figure 4.2c and Figure 4.2d demonstrated that the increasing incorporation amounts of MNPs inside the PCL/MNPs composite films can attribute to an almost constant Tm and Tc without elevation.

4.4.2 Mechanical properties of PCL/MNPs composite SMP films

The mechanical properties, particularly elastic modulus and deformability are crucial for the practical application of semicrystalline SMPs in a variety of fields. As compared with aforementioned reports regarding other photothermal fillers, the increase of the incorporation amount of the photothermal fillers could led to the hindrance in forming the crystal region, resulting in the clear decreasing in the deformability.

For the PCL/MNPs composite SMP films, Figure 4.3(a) and Figure 4.3(b) depicted the stretchability and the elastic moduli of the 4 PCL/MNPs composites in the uniaxial tensile test at room temperature. The results revealed a rather drastic decrease in elastic modulus while the value remains to be relatively constant regardless of the incorporation amount of the MNPs. The average elastic modulus is approximately 130MPa, which could still consider as a strong polymeric material. In addition, the stretchability of the PCL/MNPs composite SMP films did not exhibit deterioration, but contrarily showed a slight enhancement, with an average stretchability above 1800%. This excellent stretchability could contribute to an enhanced shape recovery as substantiated by previous reports.[1,30]
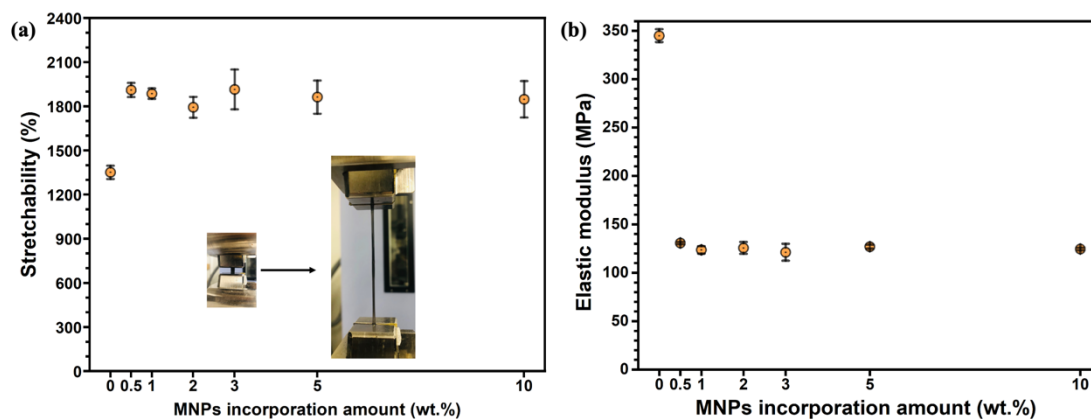
Figure 4.3 Mechanical properties of PCL/MNPs composites prepared with different incorporation amount of MNPs (0.5, 1.0, 2.0, 3.0, 5.0, 10.0 wt.% respectively) at 20°C. (**a**) stretchability, (**b**) elastic modulus of the PCL/MNPs composites.

4.4.3 Photothermal properties of PCL/MNPs composite SMP films

To achieve the laser actuatable shape memory effect, this series of SMP composites need to convert optical energy into heat and increase the temperature above Tm to actuate the shape recovery process. Therefore, the photothermal conversion rates of all SMP composite films were first investigated.

It can be seen from the transmittance results in figure 4.4(a) that even with a minimal incorporation of 0.5 wt.% of the MNPs could greatly enhance the absorbance of the light, to less than 1% transmittance of the SMP composite film. The photothermal heating curves in Figure 4.4(b) and Figure 4.4(c) and d that the PCL/MNPs composites showed a drastic temperature rise after the incorporation of MNPs under NIR irradiation. While the rise of temperature greatly enhanced with the increase of MNPs incorporation amount. Furthermore, the irradiation energy density greatly determines the generated heat as well. For a minimal incorporation amount of 0.5 wt.% MNPs in the SMP composite exhibited elevated temperature to 34.3, 35.3, 57.2, and 83.0 °C by the increase of irradiation energy from 500 mW/cm^2 to 4.5 mW/cm^2 respectively. Therefore, PCL/MNPs composites presented excellent photothermal effect that is adjustable simply by the manipulation of laser energy and the incorporation amount of the MNPs inside the SMP composites.
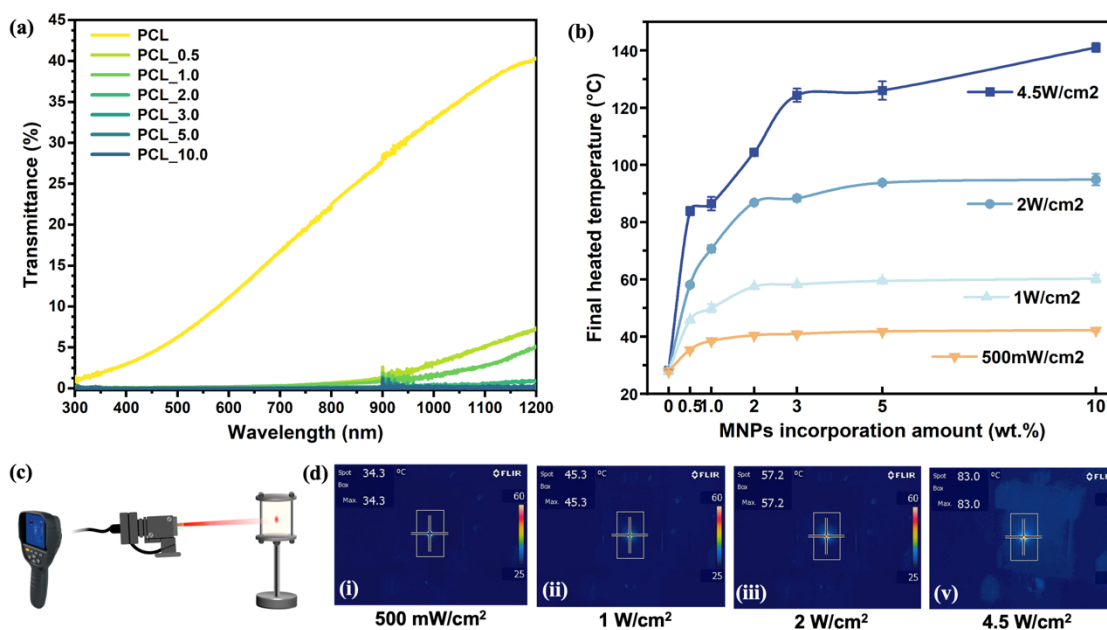
Figure 4.4 Photothermal properties of PCL/MNPs composites. (**a**) Transmittance of PCL/MNPs composites, (**b**) Final heated temperature of PCL/MNPs composites with different laser energy density, (c) schematic illustration of the laser irradiation test setup and (d) Thermal camera images of the PCL/MNPs SMP films with 0.5 wt.% of MPNs at different irradiation energy.

4.4.4 Artificial muscle mimicking weight-lifting tests of PCL/MNPs composite SMP films

For the purpose of evaluating the shape recovery force of PCL/MNPs composite SMP films, an artificial muscle mimicking weight-lifting test was conducted by attaching a weight on PCL/MNPs composite SMP films and measure the shape recovery ratios after the laser irradiation. Figure 4.5(a) demonstrated the Rr of composite SMP films when lifting a weight of 2g, 5g, 10g or 20g respectively. As exhibited from the picture in Figure 4.5(b), the SMP composite films that are stretched to be 200% strains and fixed. The weights were then attached to the end of the SMP films. After which, the laser was irradiated on the SMP composite films to actuate the artificial muscle mimicking lifting motion owning to the shape recovery-induced contraction force. After the complete lifting, the laser was switched off when the specimen were fixed at the contracted state that represented the lifting capability of the composite SMP films.
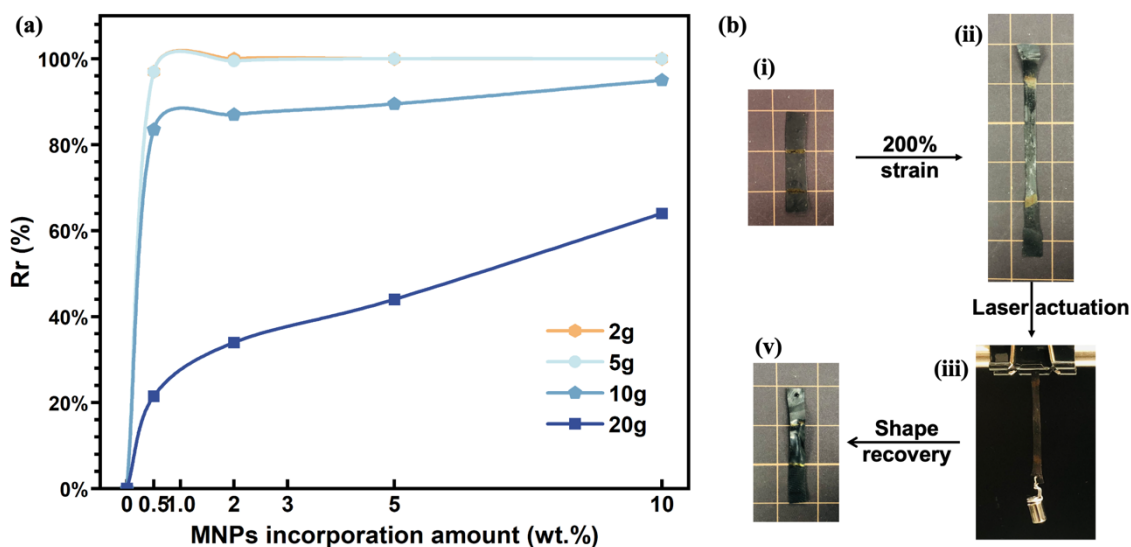
Figure 4.5 Artificial muscle mimicking weight-lifting tests of PCL/MNPs composite films. (**a**) Shape recovery ratio of PCL/MNPs composites bearing different weights, (**b**) Images of the weight-lifting test of the PCL/MNPs SMP films with 2.0 wt.% of MPNs.

Results indicated that SMP composite films with the minimal to maximum MNPs incorporation amounts all exhibited excellent shape recovery ratios, averagely above 98% when lifting weight of 2g and 5g. This indicated that the shape recovery forces of the composite SMP films are sufficient for lifting a weight up to 5g. However, with the increase of the weights, SMP films exhibited a clear deterioration in the lifting abilities with a drastically decreased Rr. With the increased MNPs incorporation amount, there showed a clear elevation in the Rr especially with the maximum weight of 20g. However, even when lifting a heavy weight, MNP_10.0 still managed to maintain a Rr of approximately 63% without further extension of the specimen like other soft elastic materials. This result demonstrated the excellent weight-lifting capabilities of such composite SMP films. This demonstration also proved that this series of SMP composites may be potentially applicable as artificial muscles or medical devices actuatable by laser irradiation.

4.5 Conclusions

In this chapter, we designed and fabricated a series of PCL/MNPs SMP composite films using semicrystalline 4bPCLs that can provide excellent mechanical and shape-memory properties in the previous studies,[1,26] and MNPs as photothermal source for laser actuation. By simple incorporation of different ratios of MNPs inside PCL-based

SMPs, we could obtain a series of laser actuatable SMP composites that possess excellent mechanical properties, shape-memory properties and strong shape recovery force that are selectively actuatable by laser irradiation.

Results indicated that regardless of the incorporation amounts of MNPs inside the PCL/MNPs composite films, their Tm and Tc remained relatively constant without elevation. However, with the incorporation of MNPs, a drastic decrease in elastic modulus is observed. The elastic moduli remained to be approximately 130 MPa regardless of the incorporation amount. Additionally, the stretchability of the PCL/MNPs composite films did not exhibit deterioration and contrarily showed a slight enhancement, averagely above 1800%. In addition, the excellent photothermal effect of the composite SMP films could easily provide an elevation in temperature above Tm. The heated temperature is highly controllable between 27 ℃ to approximately 143 ℃ tunable with different incorporation amount of MNPs and irradiation energy of the laser. This facile and universal design of laser actuatable SMPs can be envisioned to be applicable in various fields such as biomedical fields and soft robotics.

Reference

[1] A. Fulati, K. Uto, M. Iwanaga, M. Watanabe, M. Ebara, Adv. Healthc. Mater. 2022, 11, 2200050.

[2] A. Lendlein, R. Langer, Science (80-.). 2002, 296, 1673.

[3] M. Ebara, K. Uto, N. Idota, J. M. Hoffman, T. Aoyagi, Adv. Mater. 2012, 24, 273.

[4] S. Ouchi, E. Niiyama, K. Sugo, K. Uto, S. Takenaka, A. Kikuchi, M. Ebara, Biomater. Sci. 2021, 9, 6957.

[5] S. Ishii, K. Uto, E. Niiyama, M. Ebara, T. Nagao, ACS Appl. Mater. Interfaces 2016, 8, 5634.

[6] Q. Shou, K. Uto, M. Iwanaga, M. Ebara, T. Aoyagi, Polym. J. 2014, 46, 492.

[7] G. M. Baer, W. Small, T. S. Wilson, W. J. Benett, D. L. Matthews, J. Hartman, D. J. Maitland, Biomed. Eng. Online 2007, 6, 43.

[8] W. Small IV, T. S. Wilson, W. J. Benett, J. M. Loge, D. J. Maitland, Opt. Express 2005, 13, 8204.

[9] K. Uto, M. Ebara, Appl. Sci. 2017, 7, 1203.

[10] R. Mohr, K. Kratz, T. Weigel, M. Lucka-Gabor, M. Moneke, A. Lendlein, Proc.

Natl. Acad. Sci. 2006, 103, 3540.

[11] L. Santo, F. Quadrini, A. Accettura, W. Villadei, Procedia Eng. 2014, 88, 42.

[12] R. Liu, X. Kuang, J. Deng, Y. C. Wang, A. C. Wang, W. Ding, Y. C. Lai, J. Chen, P. Wang, Z. Lin, H. J. Qi, B. Sun, Z. L. Wang, Adv. Mater. 2018, 30, 1.

[13] D. Schönfeld, D. Chalissery, F. Wenz, M. Specht, C. Eberl, T. Pretsch, Molecules 2021, 26, DOI 10.3390/molecules26030522.

[14] Y. S. Wong, A. V. Salvekar, K. Da Zhuang, H. Liu, W. R. Birch, K. H. Tay, W. M. Huang, S. S. Venkatraman, Biomaterials 2016, 102, 98.

[15] B. Liu, Z. Xu, H. Gao, C. Fan, G. Ma, D. Zhang, M. Xiao, B. Zhang, Y. Yang, C. Cui, T. Wu, X. Feng, W. Liu, Adv. Funct. Mater. 2020, 30, 1910197.

[16] T. R. Yeazel, M. L. Becker, Biomacromolecules 2020, 21, 3957.

[17] Y. Zheng, Y. Li, X. Hu, J. Shen, S. Guo, ACS Appl. Mater. Interfaces 2017, 9, 13988.

[18] C. Chu, Z. Xiang, J. Wang, H. Xie, T. Xiang, S. Zhou, J. Mater. Chem. B 2020, 8, 8061.

[19] S. Dai, S. Yue, Z. Ning, N. Jiang, Z. Gan, ACS Appl. Mater. Interfaces 2022, 14, 14668.

[20] C. J. Ward, R. Tonndorf, A. Eustes, M. L. Auad, E. W. Davis, J. Nanomater. 2020, 2020, 1.

[21] H. S. Choi, Y. K. Jo, G. Ahn, K. Il Joo, D. Kim, H. J. Cha, Adv. Funct. Mater. 2021, 31, 2104602.

[22] Y. Kim, M. Ebara, T. Aoyagi, Adv. Funct. Mater. 2013, 23, 5753.

[23] E. Niiyama, K. Uto, C. M. Lee, K. Sakura, M. Ebara, Adv. Healthc. Mater. 2019, 8, 1900102.

[24] J. C. Chacón-Torres, C. Reinoso, D. G. Navas-León, S. Briceño, G. González, Sci. Rep. 2020, 10, 19004.

[25] P. M. Martins, A. C. Lima, S. Ribeiro, S. Lanceros-Mendez, P. Martins, ACS Appl. Bio Mater. 2021, 4, 5839.

[26] A. Fulati, K. Uto, M. Ebara, Polymers (Basel). 2022, 14, 4740.

[27] K. Uto, K. Yamamoto, S. Hirase, T. Aoyagi, J. Control. Release 2006, 110, 408.

[28] B. Lepoittevin, M. Devalckenaere, N. Pantoustier, M. Alexandre, D. Kubies, C.

Calberg, R. Jérôme, P. Dubois, Polymer (Guildf). 2002, 43, 4017.

[29] W. Miao, W. Zou, Y. Luo, N. Zheng, Q. Zhao, T. Xie, Polym. Chem. 2020, 11, 1369.

[30] I. Sedov, T. Magsumov, A. Abdullin, E. Yarko, T. Mukhametzyanov, A. Klimovitsky, C. Schick, Polymers (Basel). 2018, 10, 902.

Chapter 5 Concluding Remarks

In this doctoral dissertation, I have proposed a novel design of a smart shape-memory polymer that simultaneously possessed excellent mechanical properties and shape-memory properties as well as high shape recovery-induced contraction force. Such SMP is intended to be utilized in minimally invasive fetal surgeries to restrict blood inflow to fetal sacrococcygeal teratoma. This work offers a promising avenue for the development of smart functional biomaterials with potential applications in fetal surgical field.

The material-wise objective of this PhD research is to resolve existing dilemmas between the physical and shape-memory properties of shape-memory polymers and to achieve simultaneous realization of strong, ultra-stretchable and tough shape-memory polymers along with excellent shape-memory properties and a robust shape recovery force. Furthermore, the application-wise objective of this PhD research is to design a smart shape-memory polymeric string with aforementioned excellent properties that can effectively occlude the feeding vessel to fetal sacrococcygeal teratoma via minimally invasive fetoscopic surgery using shape recovery-induced contraction motion, to ensure a safe and successful delivery of the fetus.

Chapter 1 of this doctoral dissertation outlined the general research background of this PhD research. The first three sections provided a literature review regarding fetal diseases, fetal surgeries, and fetal sacrococcygeal teratomas. The fourth section introduced shape-memory polymers and provided a literature review regarding the charismatic shape-memory behavior, shape-memory induced motions and the reported applications in this research field. Moreover, this chapter described the current challenges existing in the field. The final section delineated the motivation, objectives, and the outline of this doctoral dissertation.

Chapter 2 described a novel design of shape-memory polymeric string for the contraction of blood vessels in minimally invasive fetoscopic surgery of sacrococcygeal teratoma. This section elucidated the design concept, material selection, synthesis scheme, fabrication approach along with relevant polymer, physical and shape-memory characterizations. Result indicated the successful realization of excellent properties for such shape-memory polymeric strings with customizable physical properties such as ultra-high stretchability (1268% to 1570%); high elastic modulus (102 MPa to 345 MPa); strong toughness (112.6 MJ m^{-3} to 237.9 MJ m^{-3}). As well as excellent shape-memory properties such as high shape fixity ratio and shape recovery ratio both averagely above 99% even at a large deformation rate of 800%. Moreover, the aforementioned shape-memory polymeric strings demonstrated high controllable customizable shape recovery force, tunable from approximately 0.58 N to 7.97 N via a

simple manipulation of the stretched strings and crosslinking thicknesses. In addition, the shape-memory response time is controllable as well, from 0.4 s of instantaneous response to 4.8 s of gradual response. Moreover, they demonstrated excellent shape recovery induced contraction effect on in-vitro simulation models which are proven to be promising for the future application in minimally invasive fetal surgeries for SCTs.

The appealing results achieved in this doctoral dissertation could also be utilized in other shape-memory induced motions and exhibited great promise for diverse future medical applications. In such case, detailed correlations between the appealing shape recovery force and the influential factors that dominates it needed to be understood.

Therefore, Chapter 3 described the investigation of the influences of crystallinity and crosslinking density on the shape recovery force in poly(ε-caprolactone)-based semicrystalline shape-memory polymers. A facile shape-memory polymer blend (SMPB) systems are designed and fabricated through the blending of 4bPCLs with high and low molecular weight. This chapter described the manipulation of a decreasing crystallinity gradient and an increasing crosslinking density gradient in the SMPB systems through the simple tuning of different amorphous component ratios. Result indicated that crystallinity dominates the thermal properties and mechanical properties at room temperature, such as melting temperature, elastic modulus, stretchability, and toughness. On the other hand, crosslinking density dominates the mechanical properties at 60°C and the shape recovery force of SMPs.

Enhanced by the understanding obtained from this chapter, we could achieve a further precise control of a series of physical properties with the manipulation of crystallinity and crosslinking density in the shape-memory polymer network. For instance, stretchability (50.5–1419.5%) and toughness (0.62–130.4 MJ m^{-3}). This could open up broader potentials of SMPs for various future applications such as soft robotics, smart actuators and biomedical devices.

Aside from the design of manipulatable properties, the actuation approach of SMPs is of great significance for the intended application in the minimally invasive fetal surgery of SCTs. Therefore, Chapter 4 described a simple design and fabrication of a laser actuatable SMP composites using aforementioned 4bPCL-based semicrystalline SMP with an incorporation of magnetic nanoparticles (MNPs) into the polymer networks as the photothermal conversion agent. Different incorporation amount of the MNPs in the composite SMP films have been investigated. Results indicated that the incorporation of MNPs inside the PCL/MNPs composite films did not negatively affect the thermal and mechanical properties. In addition, the excellent

photothermal effect of the composite SMP films could easily provide the induction of heat above Tm to successfully actuate the shape recovery of such composite SMP films. The inducted temperature is manipulatable between 27 ºC to 143 ºC by tuning their MNPs incorporation amounts and the irradiation energy of the laser. The facile and universal design of laser actuatable SMPs described in this chapter are envisioned to possess great potentials in various fields.

Above all, the objectives of this PhD research were successfully realized achieving a novel SMPs that are strong, tough, ultra-stretchable and equipped with excellent shape-memory properties and strong shape recovery force. The shape recovery force is tunable with a balanced manipulation of the crystallinity and crosslinking density of the SMP networks. Moreover, such SMPs could be laser actuatable with a simple incorporation of MNPs as photothermal source, while maintaining such excellent properties. The aforementioned appealing characteristics of the SMPs achieved in this research could offer great potential in the minimally invasive fetal surgery of sacrococcygeal teratoma.

List of publications, conferences and awards

Original papers

1. **Ailifeire Fulati**, Koichiro Uto, Masanobu Iwanaga, Miho Watanabe, Mitsuhiro Ebara, Smart shape-memory polymeric string for the contraction of blood vessels in fetal surgery of sacrococcygeal teratoma, Advanced Healthcare Materials, 2022, 11, 2200050.

2. **Ailifeire Fulati**, Koichiro Uto, Mitsuhiro Ebara, Influences of crystallinity and crosslinking density on the shape recovery force in poly(ε-caprolactone)-based shape-memory polymer blends, Polymers, 2022, 14, 21, 4740.

3. Irena Yungerman, Ilya Starodumov, **Ailifeire Fulati**, Koichiro Uto, Mitsuhiro Ebara, Yevgeny Moskovitz, Full-Atomistic optimized potentials for liquid simulations and polymer consistent force field models for biocompatible shape-memory poly(ε-caprolactone), The Journal of Physical Chemistry B, 2022, 126, 21, 3961-3972.

4. Mirei Tsuge, Kanoko Takahashi, Rio Kurimoto, **Ailifeire Fulati**, Koichiro Uto, Akihiko Kikuchi, Mitsuhiro Ebara, Fabrication of water absorbing nanofiber meshes toward an efficient removal of excess water from kidney failure patients, Fibers, 2019, 7, 39.

5. **Ailifeire Fulati**, Koichiro Uto, Masanobu Iwanaga, Mitsuhiro Ebara, Laser actuatable shape-memory polymers with high shape recovery force, ACS Applied Materials and Interfaces, submitted.

Review, Books and Others

Eri. Niiyama, **Ailifeire Fulati**, Mitsuhiro Ebara, Responsive polymers for smart textiles, Smart Textiles: Wearable Nanotechnology, 2018, 111-126.

Conferences

1. **Ailifeire Fulati**, Koichiro Uto, Mitsuhiro Ebara, "Quantifying the contributions of crystallinity and crosslinking density in energy storage density of semi-crystalline shape-memory polymers", The 71st Symposium on Macromolecules, Japan, Sapporo, September 05-07, 2022 (Oral presentation).

2. **Ailifeire Fulati**, Koichiro Uto, Miho Watanabe, Mitsuhiro Ebara, "Design of laser-

actuatable shape-memory polymers for minimally invasive fetoscopic surgery", The 71st Symposium on Macromolecules, Japan, Sapporo, September 05-07, 2022 (Poster presentation).

3. **Ailifeire Fulati**, Koichiro Uto, Miho Watanabe, Mitsuhiro Ebara, "Design of shape-memory polymers for minimally invasive fetal surgery", The 51st Symposium on Biomedical Polymers, Japan, Tokyo, July 25, 2022 (Poster presentation).

4. **Ailifeire Fulati**, Koichiro Uto, Mitsuhiro Ebara, "Quantifying the contributions of crystallinity and crosslinking density in energy storage capacity of shape-memory polymers", The 71st SPSJ Annual Meeting, Online, May 25-27, 2022 (Poster presentation).

5. **Ailifeire Fulati**, Koichiro Uto, Miho Watanabe, Mitsuhiro Ebara, "Design of shape-memory polymeric string for minimally invasive prenatal repair of sacrococcygeal teratoma", Hawaii Joint Symposium of American Society for Biomaterials & Japanese Society for Biomaterials, Online, January 08-10, 2022 (Poster presentation).

6. **Ailifeire Fulati**, Koichiro Uto, Mitsuhiro Ebara, "Design of shape-memory polymeric device for minimally invasive fetal surgery of sacrococcygeal teratoma", Materials Research Meeting 2021, Japan, Yokohama, December 13-17, 2021 (Poster presentation).

7. **Ailifeire Fulati**, Koichiro Uto, Miho Watanabe, Mitsuhiro Ebara, "Design of smart shape-memory polymeric string for fetoscopic surgery of sacrococcygeal teratoma", The 43rd Annual Meeting of the Japanese Society for biomaterials & 8th Asian Biomaterials Congress, Japan, Nagoya, November 28-30, 2021 (Poster presentation).

8. **Ailifeire Fulati**, Koichiro Uto, Mitsuhiro Ebara, "Design and contraction evaluation of smart shape-memory polymers for fetal surgery", The 70th Symposium on Macromolecules, Online, September 06-08, 2021 (Oral presentation).

9. **Ailifeire Fulati**, Koichiro Uto, Mitsuhiro Ebara, "Contraction effect study of shape-memory polymeric device for prenatal repair of sacrococcygeal teratoma", 4th G'Lowing Polymer Symposium in Kanto, Online, July 31, 2021 (Oral presentation).

10. **Ailifeire Fulati**, Koichiro Uto, Mitsuhiro Ebara, "Design of shape-memory

polymeric devices for fetal surgery", The 13th MANA International Symposium, Japan, Online, March 02-03, 2021 (Poster presentation).

11. **<u>Ailifeire Fulati</u>**, Koichiro Uto, Mitsuhiro Ebara, "Design of shape-memory polymeric device for fetoscopic surgery", The 15th Nano-biomedical Conference, Online, November 04-05, 2020 (Oral presentation).

12. **<u>Ailifeire Fulati</u>**, Koichiro Uto, Mitsuhiro Ebara, "Design and mechanical evaluation of smart shape-memory polymers for fetal surgery", The 69th Symposium on Macromolecules, Online, September 16-18, 2020 (Poster presentation).

13. **<u>Ailifeire Fulati</u>**, Koichiro Uto, Mitsuhiro Ebara, "Design of shape-memory polymers for prenatal repair of sacrococcygeal teratoma", Tsukuba Biomedical Engineering Forum 2020, Japan, Tsukuba, January 22, 2020 (Poster presentation).

14. **<u>Ailifeire Fulati</u>**, Koichiro Uto, Mitsuhiro Ebara, "Design of smart shape-memory polymers for biomedical applications", 2nd G'Lowing Polymer Symposium in Kanto, Japan, Tokyo, November 30, 2019 (Oral presentation).

15. **<u>Ailifeire Fulati</u>**, Koichiro Uto, Mitsuhiro Ebara, "Shape-memory polymers for biomedical applications", Annual Meeting for Korean Society of Biomaterials, Korea, Seoul, September 19-20, 2019 (Poster presentation).

Awards

1. **<u>Ailifeire Fulati</u>**, Koichiro Uto, Miho Watanabe, Mitsuhiro Ebara, "Design of laser-actuatable shape-memory polymers for minimally invasive fetoscopic surgery", The 71st Symposium on Macromolecules, Japan, Sapporo, September 05-07, 2022, **Excellent Poster Presentation Award.**

2. **<u>Ailifeire Fulati</u>**, Koichiro Uto, Miho Watanabe, Mitsuhiro Ebara, "Design of shape-memory polymers for minimally invasive fetal surgery", The 51st Symposium on Biomedical Polymers, Japan, Tokyo, July 25, 2022, **Best Presentation Award.**

3. **<u>Ailifeire Fulati</u>**, Koichiro Uto, Miho Watanabe, Mitsuhiro Ebara, "Design of smart shape-memory polymeric string for fetoscopic surgery of sacrococcygeal teratoma", The 43rd Annual Meeting of the Japanese Society for Biomaterials & 8th Asian Biomaterials Congress, Japan, Nagoya, November 28-30, 2021. **Excellent Poster Presentation Award**.

4. **Ailifeire Fulati**, Koichiro Uto, Mitsuhiro Ebara, "Design and contraction evaluation of smart shape-memory polymers for fetal surgery", The 70th Symposium on Macromolecules, Online, September 06-08, 2021, **Publicity Award**.

5. **Ailifeire Fulati**, Koichiro Uto, Mitsuhiro Ebara, "Contraction effect study of shape-memory polymeric device for prenatal repair of sacrococcygeal teratoma", 4th G'Lowing Polymer Symposium in Kanto, Online, July 31, 2021, **Best Presentation Award**.

6. **Ailifeire Fulati**, Koichiro Uto, Mitsuhiro Ebara, "Design of shape-memory polymeric devices for fetal surgery", The 13th MANA International Symposium, Japan, Online, March 02-03, 2021, **L'Oréal Excellent Poster Presentation Award**.

Acknowledgements

Hironaka for their kind support and inspiration. I also appreciate NIMS Namiki Foundry and NIMS Molecule & Material Synthesis Platform for sharing their analysis equipment and expertise.

Additionally, I would like to pay my special thanks to my friend Dr. Chenyu Wang for her support and help throughout this three years of PhD life. My special appreciation also goes to Mrs. Chinami Azechi for her kind support and care for me. Besides, special thanks to my friend Dr. Danni Liu and Mrs. Dilibaier Tayier for their friendship, love and kind support.

Last but not least, I would like to express my deepest love and appreciation to my family, especially my mother Hasiyati Haliding and my father Fulati Abulimiti, whose unconditional love and support helped me through this PhD research. Their love and respect for me and for each other, have always endowed me with so much happiness and power throughout my life. Their dedication and enthusiasm towards work, life and the world, have always been inspiring me to be a better person every single day. For all of that, I am forever grateful.

AILIFEIRE FULATI

(Elfire Polat)

February 2023